

DEPARTAMENTO DE ASTROFISICA

Universidad de La Laguna

DUST AND GAS IN ACTIVE GALAXIES

Memoria que presenta
D. M. Montserrat Villar Martín
para optar al grado de
Doctor en Astrofísica.

A mis queridos padres

Resumen

Existen numerosas evidencias de la presencia de polvo en galaxias activas. Al estudiar la naturaleza del núcleo activo galáctico y las condiciones físicas del medio interestelar de estas galaxias es necesario entender cómo el polvo interactúa con la radiación y las partículas del gas. Si no tenemos en cuenta en nuestro análisis los efectos derivados, posiblemente llegaremos a interpretaciones erróneas. Existen muchas preguntas relacionadas con la existencia de polvo en galaxias activas como: ¿En qué condiciones permite el continuo extremadamente duro del núcleo activo la supervivencia de los granos de polvo? ¿Es la naturaleza del polvo en galaxias activas la misma que en nuestro medio interestelar? ¿Cómo se distribuye el polvo en relación con el gas altamente ionizado por el AGN central? ¿Existe polvo en radio galaxias con desplazamientos al rojo muy altos? El trabajo desarrollado en esta tesis trata de encontrar respuesta a algunas de estas preguntas, mediante un estudio detallado, tanto observacional como teórico, de los mecanismos que controlan la interacción entre el polvo, la radiación y las partículas del gas. Los efectos observables del polvo sobre el espectro de líneas de emisión son también analizados en profundidad. El objetivo es entender cuestiones más generales como el origen del gas emisor, el/los mecanismos de ionización, la geometría, la conexión entre galaxias activas a alto y bajo redshift o la validez del modelo de unificación. En pocas palabras, este trabajo intenta alcanzar una visión más clara del mundo de las galaxias activas.

Summary

There are strong evidences which favour the existence of dust in active galaxies. Understanding the way in which dust interacts with the radiation and influences the physical conditions of the gas is crucial if we want to learn about the nature of the central active nucleus and about the physical conditions of the ISM in such galaxies. Not taking into account such effects may lead us towards misleading interpretations. Many intriguing questions concerns to the nature and the existence of dust in active galaxies: for instance, under which conditions does the very hard ionizing continuum of an AGN allows the survival of dust grains? Is the composition and size distribution of the dust the same as in our local interstellar medium? How is dust distributed compared to the gas which is at least in part highly ionized by the central AGN? Does dust also exist in radio galaxies at very high redshifts? The work developed in this thesis tries to find answers to some of these questions, through a detailed theoretical and observational research of the mechanisms which control the interaction of dust with the radiation and with the ions. The observable effects of the dust on the emission line spectrum are also analyzed in detail. The final goal has been to give clues about more general questions: origin of the emitting gas, ionization mechanisms, geometry, connection between low and high redshift active galaxies or the validity of the unification scenario. This thesis tries, in summary, to provide a clearer understanding of active galaxies in general.

Indice

Resumen	v
1 Introduction	3
1.1 The importance of studying dust in active galaxies.	3
1.2 Evidences of dust in active galaxies.	5
1.2.1 Absorption	5
1.2.2 Scattering and Polarization	6
1.2.3 Thermal emission of warm dust	7
1.2.4 Spectral absorption features	8
1.2.5 Spectral emission features	9
1.2.6 Depletion of heavy elements	10
1.3 The projects developed in this thesis	11
1.3.1 Effects of dust on the Ly α and Balmer decrements in the Narrow Line Region of Seyfert 2 galaxies. (<i>Chapter 2</i>) . . .	11
1.3.2 Does dust exist within the ionized gas of the Extended Emis- sion Line Regions of Radio galaxies? (<i>Chapters 3 and 4</i>) . .	11
1.3.3 Effects of dust and resonant scattering on the UV spectrum of high z radio galaxies. (<i>Chapter 5</i>)	12
Bibliography	13
2 Effects of internal dust on the Narrow-Line region Lyman and Balmer decrements.	15
2.1 Introduction	16
2.2 Computational method	17
2.2.1 The photoionization code	17
2.3 Results	21
2.3.1 Selection of a characteristic cloud density	22
2.3.2 Asymmetric emissivity and internal dust absorption	23
2.3.3 Selection of the ionization parameter U_f	29
2.3.4 Results for a symmetric cloud distribution	30
2.4 Discussion	33
2.4.1 Observational data of KAW3	33
2.4.2 The pure line scattering and the pure dust models	34

2.4.3	The partially covering models	39
2.4.4	Dust and the UV continuum	43

Bibliography **48**

3 Calcium depletion and the presence of dust in large scale nebulosities in radio galaxies (I). **51**

3.1	Introduction	52
3.2	Outline of the method	54
3.2.1	The input parameters	54
3.2.2	How to detect dust	56
3.3	Possible alternative explanations to depletion.	59
3.3.1	Ionization by Ly α and soft continuum photons.	59
3.3.2	Thermal ionization of Ca ⁺	60
3.3.3	Effects on F1 of varying U and the continuum hardness.	60
3.3.4	Effects on F1 of truncating clouds	63
3.4	Conclusions	65

Bibliography **67**

4 Calcium depletion and the presence of dust in large scale nebulosities in radio galaxies (II). **69**

4.1	Introduction	70
4.2	Observations and data reduction	70
4.2.1	Data analysis	75
4.3	Observed and predicted F1 fluxes.	75
4.3.1	Prediction of F1 fluxes	75
4.3.2	Comparison with the observations	76
4.4	Discussion	78
4.4.1	Implications on the origin of the gas	78
4.5	Conclusions.	80

Bibliography **80**

5 Effects of dust and resonant scattering on the UV spectrum of radio galaxies. **83**

5.1	Introduction	84
5.2	Data sample and modeling procedure	86
5.2.1	The data	86
5.2.2	The model and its parameters	86
5.2.3	Adopted physical conditions	86
5.3	Models and comparison with observed UV lines	88

5.3.1	The photoionization assumption at low and high z	88
5.3.2	Effects of viewing direction on the UV lines	89
5.3.3	The effects of internal dust	92
5.3.4	Neutral gas mirrors	95
5.4	Conclusions	99

Bibliography **100**

6 Discussion **103**

6.1	Dust in the ionized regions.	105
6.1.1	Dust at high z	106
6.2	The ionization mechanism.	108
6.2.1	Shocks in active galaxies	109
6.3	Geometry	113
6.4	Our HST project	117

Bibliography **118**

7 Conclusions **121**

Chapter 1

Introduction

1.1 The importance of studying dust in active galaxies.

Dust is an important constituent of active galaxies and must be included in any physical description of them. It is necessary to reach a clear understanding of its influence, not only on the radiation, but also on the physical conditions of dusty nebulae. Ignoring dust in the interpretation of the observations is an oversimplification which may lead us to false conclusions. An example will describe clearly the kind of misunderstandings which can be reached when skipping dust in our interpretations.

High z radio galaxies ($z > 0.5$) show very blue colors and emit a very strong Ly α line. The initial interpretation has been that these objects were galaxies in the process of formation and that the blue young stars could explain the observed properties. In this scenario, the continuum is produced by the stars while Ly α results from recombination of gas from HII nebulosities. Further investigations revealed that the continuum was extended and closely aligned with the radio axis. This indicated a common mechanism for both the radio and the UV continuum emission. Polarization studies (e.g. Tadhunter, Fosbury & di Serego Alighieri 1988; Cimatti et al. 1993) revealed that the continuum was highly polarized and demonstrated that the extended radiation could be scattered nuclear radiation by dust within the interstellar medium. This implies that the star formation rate is lower than previously believed, also lower than we thought if these objects were protogalaxies. There is no clear evidence that these objects are galaxies being born, not even at redshift ~ 4 . Some evidences rather demonstrate the existence of an old stellar population (this will be treated in detail in Chapter 6). The redshift corresponding to galaxy formation seems to be much further back than the currently highest redshift quasar known at $z = 4.9$ (Shneider, Schmidt & Gunn 1991).

The regions responsible for the emission of the narrow lines in active galaxies might well be mixed with dust resulting in selective absorption of the impinging ionizing photons and, therefore, affecting the ionization structure of the gas. The

physical conditions of the gas are also directly influenced: the temperature and the (gas phase) abundances of the heavy elements are sensitive to the presence dust. All these effects will manifest themselves in the emission line spectrum.

In this work we have developed a complete and detailed study (observational and theoretical) of the effects of internal (i.e. mixed with the ionized gas) as well as external (i.e. intervening) dust, on the emission line spectra of narrow line active galaxies. We recall that the emission lines observed in the spectra of this type of objects are not contaminated by a broad component emitted within the so-called Broad Line Region, which makes our study much simpler.

This thesis has consisted of three main projects and attempts to address and solve some of the important problems encountered nowadays in the field of active galaxies. These often involve the presence of dust:

1) Effects of dust on the Ly α and Balmer decrements in the Narrow Line Region of Seyfert 2 galaxies. *What is the proper geometry describing the Narrow Line Region (NLR)?*

2) Does dust exist as a component which is mixed with the ionized gas observed in Extended Emission Line Regions of Radio galaxies? *What is the origin and fate of this extended gas?*

3) Effects of dust and of resonant scattering on the UV spectrum of high z radio galaxies. *Which factor plays a major role on the UV line ratios at high z : geometry or internal dust?*

These specific objectives are quite different in terms of the type of object considered. In effect, we move from low redshift (z) to very high redshift objects (which correspond to much earlier epochs) and consider regions which strongly differ by their physical conditions. However, the goal remains the same: *to understand the nature of active galaxies*. Many researchers are working on this thrilling field, trying to answer many questions which remain open, using different theoretical and observational techniques. In our work, we have modeled the emission line spectra of the regions under study. Starting from a given set of input parameters (some of them well established by the observations), we create theoretical spectra which are then compared with the observations. The discrepancies or agreements resulting from the comparison provide important information about the nature of the regions and objects under study.

1.2 Evidences of dust in active galaxies.

1.2.1 Absorption

Extinction occurs whenever electromagnetic radiation is propagated through a medium containing small dust particles. In general, the transmitted beam is reduced in intensity by two physical processes, absorption and scattering. The energy of an absorbed photon is converted into internal energy of the particle, which is thus heated, while a scattered photon is deflected from the line of sight. There is direct evidence for dust in our Milky Way in the form of dark lanes and rifts that we can see with the unaided eye. Also in some active galaxies, we can detect the presence of dust from the existence of obscured regions, like Cen A (NGC5128), the nearest giant double radio galaxy. In 1847, Sir John Herschel observed for the first time the nowadays familiar dark lane contrasted against the diffuse background of light. Currently, it is known that the galaxy consists of an ellipsoidal stellar component bisected by a dense dusty layer across the apparent minor axis (see Fig. 1) (e.g. Bland et al. 1987; Morganti et al. 1991). Recent HST WFPC2 images of 3CR radio galaxies in the redshift range $0.0 < z < 0.5$, show lanes, patches and wisps that the authors attribute to dust out to a redshift of ~ 0.48 in $\sim 30\text{-}50\%$ of the sample (Baum et al. 1995). At $z > 0.1$, dust is more difficult to detect and one cannot easily separate dust obscuration from emission clumpiness.

Figure 1:

The dusty lane in the active galaxy Centaurus A. A deep (1 hr) image taken at the prime focus of the Anglo-Australian Telescope. (Reproduced from Morganti et al. 1991)

Selective extinction (or reddening) is also evident in the spectra of Narrow

Line Regions (NLR) in Seyfert 2 galaxies. In effect, the $\text{Ly}\alpha/\text{H}\beta$ and $\text{H}\alpha/\text{H}\beta$ ratios indicate a mixture of reddening due to dust *mixed* with the emitting clouds and of resonant scattering of $\text{Ly}\alpha$ by neutral hydrogen (Binette et al. 1993, see also Chapter 2) (some authors propose reddening by *pure* dust (i.e. gas-free dust!), like Ferland and Osterbrock 1986, and Wills et al. 1993).

The narrow emission line profiles provide another indication of dust in the NLRs. Many lines have a noticeable blue asymmetry which is interpreted as a combination of radial motion and dust obscuration (e.g. de Robertis & Osterbrock 1984). The asymmetry parameter (defined by Heckman, Miley & Breugel 1981) measures the asymmetry of the line profiles. Dahari & de Robertis (1988) searched for correlations between this parameter and features attributed to dust such as reddening (measured from the Balmer decrement, $\text{H}\alpha/\text{H}\beta$) far IR luminosity (60-100 μm) and the flux ratio $F(60\mu\text{m})/F(\lambda 5007)$. The results showed a good correlation in Seyfert 2 galaxies between the asymmetry parameter and these three variables. The authors propose that such correlations suggest a direct relation between the asymmetry parameter of the lines and the presence of dust in the NLR.

1.2.2 Scattering and Polarization

The existence of scattered light from the interstellar dust grains was discovered by means of long exposure photographs of systems such as the Pleiades cluster of stars. The associated nebulosity is referred to as reflection nebulosity. The light of the stars in the cluster illuminates the dust grains which then scatter the light, most efficiently at blue wavelengths, explaining the blue colors associated with the nebulosity. The scattering of radiation has a useful observational consequence: the scattered light is polarized. This was first demonstrated by Hall (1949) and Hiltner (1949) who showed that the light of reddened stars is partially plane polarized, typically at the 1-5% level.

Polarization has often been observed in active galaxies and the interpretation generally proposed has been scattering of the radiation by an agent which nature does not reveal clearly: either electrons or dust grains. Antonucci and Miller (1985) discovered that in the Seyfert 2 galaxy NGC1068, both the nonstellar nuclear continuum and the weak broad wings to the Balmer lines and the FeII emission are linearly polarized with the polarization plane perpendicular to the symmetry axis of the nuclear radio morphology. The most plausible interpretation is the existence of a Seyfert 1 type nucleus and of a Broad Line Region hidden from our line of sight by an obscuring torus. The continuum and broad lines which are detected in polarized light, are emitted originally within these hidden regions and later scattered towards the observer. The most plausible scattering agent is, in this case, electrons, although dust could also play a role.

Since Antonucci and Miller's discovery, the number of Seyfert 2 galaxies that harbor hidden BLRs visible only in polarized flux spectra has noticeably increased: Mrk 3, Mrk 48, NGC 7212, etc (e.g. Miller & Goodrich 1990; Tran 1995). The

nature of the scattering material is not clear, dust and/or electrons? But, at least for some objects, scattering by dust seems to be the dominant mechanism (e.g. NGC 7674, Tran 1995). Recently, Inglis et al.(1995) have mapped the polarization of NGC1068 also in regions out of the nucleus. In off-nuclear regions, dust is also responsible for the scattering.

The low redshift radio galaxy PKS2152-69 (see Fig. 2) shows extra nuclear scattering light too. It contains a very blue cloud at 8 kpc from the nucleus which is aligned with the radio axis and emits highly polarized flux. Dust (and electrons) in this cloud could be the scattering agent of the central UV radiation emitted by the nuclear source.

Figure 2:

A WFPC2 UV-continuum (F300W) image of PKS2152-69. The angular separation between the nucleus (lower right) and the jet-cloud interaction front is about 8 arcsec. The interaction site emits X-rays (ROSAT HRI), optical/UV emission lines, a blue/UV continuum as well as radio waves. (Fosbury et al. in prep)

Scattering and polarization (maybe by dust) are also detected at very high redshifts. High redshift radio galaxies ($z > 0.5$) present elongated structures in the UV rest frame, which are aligned with the radio axis. This extended UV radiation is polarized, with the electric vector perpendicular to the axis of the optical structures. The observations indicate that the radiation emitted by a hidden quasar is being scattered by dust and/or cool electrons in the extended ISM. The discovery in several radio galaxies (e.g. di Serego et al. 1996; Dey & Spinrad 1995) of broad polarized MgII λ 2798 emission line (originally emitted in the Broad Line Region which is also hidden from our line of sight), supports this scenario.

1.2.3 Thermal emission of warm dust

Diffuse emission from interstellar dust was predicted by van de Hulst (1946) as a consequence of absorption: the energy absorbed by dust grains must re-emerge

in the infrared. In a typical interstellar environment, a dust particle gains energy mainly from the absorption of ultraviolet photons from the ambient interstellar radiation field. The dust grains will emit in the IR a power equal to that absorbed. These effects are also clearly seen in active and starburst galaxies.

Within the framework of unification theories of AGNs (see Antonucci 1993 for a review), it is believed that a dusty torus surrounds the central accretion disk and the broad line region of active galactic nuclei (AGNs). The main continuum source and the broad lines would be obscured from direct view by a torus in narrow line active galaxies. The dust in the torus should absorb much of the nuclear radiation and re-emit it in the infrared. Measurements by Rieke & Low (1975) and Stein & Weedman (1976) showed already in the 70's that many Seyfert galaxies have large infrared excesses. In fact, the overall characteristics of the spectra of AGN show a certain gross uniformity with much of the energy emitted in the IR. This emission is attributed to warm dust, heated either by the central AGN or by recently formed stars, or both. At very high z , the dust thermal emission is redshifted to the far IR and the submm waveband, depending on z . Several high redshift radio galaxies have been detected with excesses in these spectral ranges, which indicates the existence of warm dust also at much earlier epochs of the Universe (e.g. Downes et al. 1992; Isaak et al. 1994).

The unified models of AGNs propose that the diversity of AGNs is smaller than believed and that many of the observed differences are due to orientation effects: the obscuring torus determines a radically different appearance of the AGN at different viewing angles, AGNs of different orientation will be assigned to different classes. This scenario has been tested by studying dust emission from the torus (Hess 1995): for instance, if radio galaxies and quasars are intrinsically the same objects, the torus should intercept the same amount of ultra-violet photons in both types of objects and we would expect that they emit similar output of reprocessed infrared emission. IRAS data indicate that quasars are brighter at $60\mu\text{m}$ than narrow line radio galaxies, which contradicts the unified models. This could be explained if the obscuring circumnuclear torus is still optically thick at $60\mu\text{m}$. Other mechanisms dependent on orientation could explain the differences if for instance the IR emission was not only due to thermal dust emission but also due to a non thermal component. In this case, relativistic beaming of the core component might influence the 60μ emission.

1.2.4 Spectral absorption features

Interstellar absorption features in the spectra of reddened stars and infrared sources are attributed to solid particles on the basis of position, width, shape and continuity of profile. The absorption lines due to gas phase atomic or molecular species in the interstellar medium are, in general, extremely sharp (FWHM of 1 km s^{-1} or less), reflecting the conditions of low temperature and pressure in which they are formed. Solid state spectral features are intrinsically broad and continuous and cannot be resolved into discrete lines, in contrast to the vibration-rotation bands of many

gas phase molecules. Of the observed absorption features attributed to interstellar dust, the $\lambda 1275$ feature in the mid-ultraviolet is the strongest and, in frequency units, the broadest, forming a prominent peak in the interstellar extinction curve. In principle, dust-related spectral features provide a direct means of identifying the chemical composition of interstellar grains.

Active galaxies also show absorption features due to dust. Mrk 231 is a Seyfert 1 galaxy with very strong IR emission. Its optical spectrum is very heavily reddened. Relatively high resolution infrared measurements by Rieke (1976) show the redshifted interstellar absorption feature due to silicates at $10 \mu\text{m}$, which means absorption certainly arises in Mrk 231.

However, the absence of spectral features which are customarily attributed to dust in our galaxy should not be interpreted necessarily as indicating the absence of dust. The dust in external galaxies might not have exactly the same extinction properties as in our interstellar medium. Even in our own Galaxy, there are regional variations in the optical properties of the interstellar dust. Already in 1937, Baade and Minkowsky found that the extinction curves for stars in the Orion Nebula differ from the “mean” galactic extinction curve. Selective removal of the small particles is the reason. Environmental influences (grain growth by coagulation, size dependent destruction, etc) can strongly influence the composition and size distribution of the dust grains and, therefore, the extinction properties. Dust in active galaxies may exist under very different conditions than in the ISM of our galaxy.

1.2.5 Spectral emission features

The principal emission signatures attributed to cosmic dust arise in silicates and hydrocarbons. The PAH spectrum is a series of narrow emission features with principal wavelengths at 3.3, 6.2, 7.7, 8.6 and $11.3 \mu\text{m}$. They are now widely attributed to polycyclic aromatic hydrocarbons, a class of organic molecules composed of benzene rings. Their infrared spectra are characterized by a number of resonances, excited by absorption of ultraviolet photons (Duley and Williams 1981; Léger and Puget 1984). The PAH features are commonly observed in the lines of sight to planetary nebulae, HII regions and reflection nebulae.

PAH features are observed in the nuclei of many external galaxies. They are particularly prominent in systems with nuclear HII regions and are therefore indicative of recent OB star formation in which an intense ultraviolet radiation field very soft beyond the Lyman limit can excite the different transitions. Indeed, the occurrence of PAH features appears to be a useful discriminator between starburst galaxies (dominated by rapid star formation) and active galaxies (dominated by compact, energetic nuclei). PAH emission occurs in the spectra of starburst galaxies because many luminous HII region are included in a resolution element. In contrast, PAH features are generally absent from the spectra of active galaxies, suggesting that the carriers are destroyed by hard UV radiation in the vicinity of the nuclear source (Aitken & Roche 1985; Désert & Deneffeld 1988).

1.2.6 Depletion of heavy elements

The term depletion refers to the underabundance of gas phase elements with respect to the solar standard as a result of their presence in the dust grains. Ultraviolet spectroscopy of interstellar gas indicates a depletion in the abundances of many of the heavy elements with respect to solar values, which is most readily explained if the missing atoms are tied up in solid particles.

Ferland (1993) demonstrated the presence of dust grains in the narrow line region gas. He showed that in the absence of dust the [CaII] near infrared forbidden lines ($\lambda\lambda 7291, 7324$) would be among the strongest lines in the optical to infrared spectrum of the NLR, assuming cosmic Ca abundance. He interpreted the non detection of these lines as due to the depletion of calcium in the NLR, showing that grains must be present, mixed with the ionized gas.

1.3 The projects developed in this thesis

1.3.1 Effects of dust on the Ly α and Balmer decrements in the Narrow Line Region of Seyfert 2 galaxies. (*Chapter 2*)

Despite its simple atomic configuration, the hydrogen line spectrum of AGNs is not well understood. In 1984, Gaskell and Ferland showed that the theoretical spectra of many NLR models of Seyfert 2 define a narrow band in the Ly α /H β vs. H α /H β diagnostic diagram named the intrinsic band. The displacement inside this band is explained by variations in metallicity, hardness of the ionizing continuum and electronic density. However, the observed data locate many Seyfert 2 galaxies outside the theoretical band, sometimes quite far away from it, being Ly α much fainter than expected with respect H α and H β . Previous studies (e.g. Ferland & Osterbrock 1986; Wills et al. 1993) propose a combination of atomic processes and dust absorption to explain the observations.

In this work we propose a new scenario that solve the discrepancies between the HI observed and predicted ratios of the NLR, a scenario where dust plays an important role, but also geometry, a factor which has not been considered before and which strongly influences the line emission, specially the resonant line Ly α .

1.3.2 Does dust exist within the ionized gas of the Extended Emission Line Regions of Radio galaxies? (*Chapters 3 and 4*)

The main goal of this project has been to investigate the origin of the gas which forms the extended emission line regions (EELRs) and which is observed to extend up to several hundreds of kpc in powerful radiogalaxies. In some cases, morphological similarities with filamentary systems surrounding galaxies near the centers of rich clusters suggest that the origin of the EELR consist of gas cooling from the hotter phase, similar to the X-ray emitting corona which surround many cD galaxies in clusters. In other cases, morphological and kinematical studies of the gas often suggest the existence of a collision or merger in the recent past.

The existence or not of dust in such regions has important consequences for the origin of the gas: if the gas had cooled from a hotter X-ray phase, any dust introduced in the intracluster medium would have been sputtered and rapidly destroyed. In the cooling process there would have been not enough time for the dust to form. On the other hand, if the gas consists of galactic debris, the gas/dust ratio is expected to have a value appropriate to the chemical composition of a normal galaxy.

We have investigated the existence of dust in the EELRs of a sample of low z radio galaxies in order to discriminate between these two main theories relative to the origin of the gas.

1.3.3 Effects of dust and resonant scattering on the UV spectrum of high z radio galaxies. (*Chapter 5*)

Radio galaxies at very high z ($z > 2$) have been until very recently the youngest galaxies we know of and, therefore, good laboratories to study galaxies at early epochs. In order to determine correctly the epoch when they were formed, we need to establish the age of the oldest stars in such systems. However, we don't have yet a clear picture of the processes which are going on in these special objects. The presence of an active (very powerful) nucleus influences strongly the ISM of the galaxy and it is difficult to separate the different components (including stars) which contribute to the observed radiation. We need, therefore, a clear understanding of the physical processes involved in the formation of the various lines and of the continuum in order to be able to disentangle the stellar from the AGN-related sources.

In our work we interpret the UV (rest-frame) emission line spectrum of a sample of high redshift radio galaxies. Due to the short wavelengths and the presence of several resonant lines, this spectral range is very sensitive to geometry and dust. Comparing our photoionization models with the observed line ratios, we study in detail the effects that both, dust and geometry have on the UV line ratios. Our study provides results about the presence of dust and the 3-dimensional structure of these galaxies, which can be very useful for understanding the nature of such extreme objects.

Figure 3:

A composite radio galaxy spectrum in the UV rest-frame constructed from observations of $0.1 < z < 3$ galaxies (from McCarthy 1993).

References

- Aitken D.K., Roche P.F., 1985, *Mon. Not. Roy Astr. Soc.*, 213, 777
- Antonucci R.R.J., Miller J.S., 1985, *Astrophys. J.*, 297, 621
- Antonucci R.R.J., 1993, *ARA&A* 31, 473
- Baade W., Minkowsky R., 1937, *Astrophys. J.*, 86, 123
- Baum S., de Koff S., Sparks W., Miley G., Biretta J., Golombek D., Macchetto D., McCarthy P., poster contribution for the meeting “Cold Gas at high z”, Hoogeveen, August 1995 (in press)
- Binette L., Wang J., Villar-Martín M., Martin P.G., Magris C.M., 1993, *Astrophys. J.*, 414, 535
- Bland J., Taylor K. & Atherton P.D., 1987, *Mon. Not. Roy Astr. Soc.*, 228, 595
- Cimatti A., di Serego Alighieri S., Fosbury R.A.E., Salvati M., Taylor D., 1993, *Mon. Not. Roy Astr. Soc.*, 264, 421
- Cimatti A., Freudling W., 1995, *A&A*, 300, 366
- Dahari O., De Robertis M.M., 1988, *Astrophys. J.*, 331, 727
- de Robertis M.M., Osterbrock D.E., 1984, *Astrophys. J.*, 286, 171
- Désert F.X., Dennefeld M., 1988, *A&A*, 206, 227
- Dey A., Spinrad H., 1995, *Astrophys. J.*, in press
- di Serego Alighieri S., Cimatti A., Fosbury R.A.E., 1994, *Astrophys. J.*, 431, 123
- di Serego Alighieri S., Cimatti A., Fosbury R.A.E., Pérez-Fournon, 1996, *Mon. Not. Roy Astr. Soc.*, submitted
- Downes D., Radford S.J.E., Greve A., Thum C., Solomon P.M., Wink J.E., 1992, *Astrophys. J.*, 398, L25
- Duley W.W., Williams D.A., 1981, *Mon. Not. Roy Astr. Soc.*, 196, 269
- Ferland G.J., Osterbrock D.E., 1986, *Astrophys. J.*, 300, 658
- Ferland G.J., 1993, in Proc. Madrid Meeting on The Nearest Active Galaxies, ed. J.E. Beckman, H. Netzer & L. Colina, p. 75
- Hall J.A., 1949, *Science*, 109, 166
- Heckman T.M., Miley G.K., Breugel W.J.M., 1981, *Astrophys. J.*, 247, 403
- Hess R., 1995, Ph.D. Thesis, University of Groningen
- Hiltner W.A., 1949, *Science*, 109, 165
- Inglis M.D., Young S., Hough J.H., Gledhill T., Axon D., Bailey J.A., Ward M.J., 1995, *Mon. Not. Roy Astr. Soc.*, 275, 398
- Isaak K.G., McMahan R.G., Hills R.E., Withington S., 1994, *Mon. Not. Roy Astr.*

- Soc.*, 269, L28
- Léger A., Puget J.L., 1984, *A&A*, 137, L5
- McCarthy P.J., 1993, *ARA&A* 31, 639
- Miller J.S., Goodrich B.F., 1990, *Astrophys. J.*, 335, 456
- Morganti R., Robinson A., Fosbury R.A.E., di Serego Alighieri S., Tadhunter C.N., Mailn D.F., 1991, *Mon. Not. Roy Astr. Soc.*, 249, 91
- Rieke G.H., Low F.J., 1975, *Astrophys. J.*, 200, L67
- Rieke G.H., 1976, *Astrophys. J.*, 210, 5
- Schneider D.P., Schmidt M., Gunn J.E., 1991, *Astron. J.* 102, 837
- Stein W.A., Weedman D.W., 1976, *Astrophys. J.*, 205
- Tadhunter C.N., Fosbury R.A.E., di Serego Alighieri S., 1988, in Maraschi L., Maccacaro T. & Ulrich M.H., eds., "BL Lac Objects", Springer-Verlag, Berlin, p.79
- Tran H.D., 1995, *Astrophys. J.*, 440, 565 (I, II & III)
- van de Hulst H.C., 1946, *Rech. Astron. Obs. Utrecht*, 11, 1
- Wills B.J., Netzer H., Brotherson M.S., Han M., Wills D., Baldwin J.A., Ferland G.J., Browne I.W.A., 1993, *Astrophys. J.*, 410, 534

Chapter 2

Effects of internal dust on the Narrow-Line region Lyman and Balmer decrements.

Binette, Wang, Villar-Martín, Martín & Magris 1993, ApJ, 414, 535

Abstract

We present detailed calculations on the effects of internal dust on the Balmer and Lyman decrements for a spherically symmetric distribution of low covering factor clouds represented as slabs and consider the effects of Ly α resonance and absorption by dust. We consider the important effects of perspective on the emergent fluxes, which in our simplified scheme present either the photoionized face to the observer (“f”) or the back (“b”) face. We adopt canonical values for the gas excitation (U_f) and for the ionizing energy distribution ($\alpha = -1.4$, $F_\nu \sim \nu^{+\alpha}$) and compute sequences of photoionization models in which the relative internal dust content by mass (μ) is progressively increased to values comparable to the local ISM (i.e., $\mu=1$). We find that for moderate amounts of internal dust $\mu=0.2-0.3$, radiation-bounded clouds result in Lyman and Balmer decrements in the range 32-37 and 3.0-3.1, respectively. Our main result, valid for the calculations with standard NLR input parameters and for an open geometry in which multiple cloud covering is negligible, is that even with internal dust, while $H\alpha/H\beta$ is reddened, $Ly\alpha/H\beta$ turns out not very different from recombination case B. The Seyfert 2 observations show much lower Lyman decrements than predicted from the spherically symmetric model and a critical study is made of various explanations: dust-or line scattering screens, a semiopen geometry can span the region covered by the Seyfert 2 observations. We also study the possibility that dust reddening of the *continuum* may account for the apparent deficit of ionizing photons seen in many Seyfert 2’s. This reddening may be present in addition to, or in place of, the anisotropic beaming/occultation of ionized radiation (cf. “occultation/reflection

picture”) that is generally invoked to explain the deficit.

2.1 Introduction

The calculation of the intrinsic Balmer decrement emitted by the narrow-line region (NLR) of Seyferts has attracted much interest in the past (e.g., Gaskell 1984; Malkan 1983; Halpern & Steiner 1983; and Ferland & Netzer 1983) because it is the most direct means of determining how much (intervening) extinction the observed emission-line spectrum has undergone. This information can be used to deredden the whole line spectrum for the effect of external dust along the line of sight. It has been recognized early on by Halpern & Steiner (1983) and Ferland & Netzer (1983) that the NLR intrinsic Balmer decrement was likely to be higher than that of recombination case B as a result of collisional excitation within the partially ionized zone. The resolution of the problem of intrinsic HI line ratios was further advanced by combining the information provided by the Lyman decrement with that of the Balmer decrement (e.g., Ferland & Osterbrock 1985). Gaskell & Ferland (1984) studied in details how the NLR metallicity, density, and hardness of the ionizing continuum affected both decrements. The most probable range for the NLR decrements which these authors favor is $H\alpha/H\beta=2.8-3.1$ and $Ly\alpha/H\beta=30-50$ (similar to values determined earlier by Ferland & Osterbrock 1985). The observational determination of the intrinsic HI line ratios is facilitated in Seyfert 2 galaxies since one need not decompose the line profiles into BLR and NLR components. However, Seyfert 2's are on average significantly more reddened than Seyfert 1's (Gaskell 1984). De Zotti & Gaskell (1985) concluded that the dust was probably associated with the NLR clouds or filaments owing to the extremely weak correlation of the extinction with disk inclination angle and also due to the significantly lower extinction found in Seyfert 1.5.

If there is so much dust associated with the nuclear emission region, we might expect some dust to be associated with the photoionized gas itself. The effect of internal dust mixed with ionized gas for physical conditions pertaining to the broad-line region (BLR) has been investigated by Ferland & Netzer (1979). More recently, however, Netzer (1993) concluded that the BLR was devoid of dust (but see Crosas & Weisheit 1993). From considering the ratios $H\alpha/H\beta$ vs. $H\gamma/H\beta$ in Seyfert 2's, Binette et al. (1990) suggested the possibility of an intrinsic (NLR) Balmer decrement as high as $H\alpha/H\beta \approx 3.4$, which they modeled using photoionization calculations with dust internally mixed with the ionized gas.

Internal dust results not only in somewhat higher Balmer decrements but can furthermore increase the equilibrium temperature of the ionized gas. This property was used by Magris, Binette, & Martin (1993) to solve the problem of the high electronic temperature (based on [OIII] lines) observed in the extended ionized nebulosities of powerful radio galaxies (cf. Tadhunter, Robinson & Morganti 1989). Furthermore dust can reflect towards the observer a nonnegligible fraction of the

impinging optical radiation, an interesting property which appears to explain quite well the extended blue polarized continuum observed in distant radio galaxies (cf. Fosbury 1993; Cimatti et al. 1993; Binette et al. 1993a). Dust may also explain the absence of any intermediate region between the BLR and the NLR according to Netzer & Laor (1993), not to mention its relation with the infrared emission (Clavel, Wamsteker, & Glass 1989; Barvainis 1992; Sanders et al. 1989; Pier & Krolik 1992).

In this work, we expand upon the calculations of Binette et al. (1990) and study the effects of internal dust on the intrinsic $H\alpha/H\beta$ by taking into account the observer's perspective of the emitting clouds. In addition, we consider the effects of dust on the Lyman decrement. Kwan & Krolik (1981) and Puetter & Hubbard (1987) have shown using dust-free BLR calculations how significant is the effect of perspective on resonant $Ly\alpha$. With dust mixed in, it becomes essential to take into account satisfactorily the cloud's perspective and the global NLR geometry when deriving the intrinsic decrements, as described in §2.2. We first investigate in §2.3 the magnitude of the $Ly\alpha$ destruction due to internal dust in photoionization calculations and compare in §2.4 our calculations with the Seyfert 2 data of Kinney et al. (1991) (hereafter KAW3).

2.2 Computational method

We describe the photoionization code and the line transfer of $Ly\alpha$, $H\alpha$, and $H\beta$ across the dusty medium and review the input parameters that enter our calculations.

2.2.1 The photoionization code

To compute HI lines we have employed the multipurpose photoionization-shock code MAPPINGS (cf. Binette, Dopita, & Tuohy 1985). To compute the hydrogen lines, we treat the hydrogen atom as a six-level system ($1s$, $2s$, $2p$, 3 , 4 and 5) plus continuum. The hydrogen levels are populated through direct recombination (followed by cascade) as well as by collisional excitation either by thermal electrons (using Johnson 1972 rate coefficients) or by suprathermal electrons (adopting the method developed by Shull & Van Steenberg 1985) as earlier described in Binette et al. (1993b, hereafter BWZM).

In the computation of the ionization structure, we adopt a simple-plane-parallel geometry whereby our putative thick gas cloud is represented by a radiation-bounded slab of gas containing interstellar dust. The ionized slab is subdivided into many small layers in which the equations of photoionization and thermal equilibrium are solved by standard methods.

The escape probability formalism is used to solve for the transfer of the resonance lines. The effects of dust on the ionization structure as well as on the thermal balance of the plasma are considered in detail by implementing the physical processes relevant to dust mixed with emission plasma as described in Appendix C of Baldwin et al. (1991). For instance, heating of the plasma by dust photoelectric emission is considered. The dust grain charge is calculated self-consistently and the formula describing the photoelectron energy distribution and the yield are from Draine (1978), but with a cap of 0.2 for the yield at high photon energies as in Baldwin et al. (1991).

One interesting aspect of the new code MAPPINGS is that the effect of dust scattering on the line transfer is explicitly solved using the numerical solution of Bruzual, Magris & Calvet (1988). This aspect of the transfer is particularly relevant to the “open geometry” adopted for most of the calculations presented in this thesis. Destruction of the resonant line by dust absorption is taken into account using the results of Hummer & Kunasz (1980). We describe in more details in Appendix A of BWZM the method implemented in MAPPINGS for solving the line transfer of emission plasma with internally mixed dust.

Trace elements and dust content

Even though this work only addresses the intensities of hydrogen lines, the abundance of trace elements remains an important factor since they affect directly the thermal balance of the photoionized plasma. Abundance gradients observed in spiral galaxies point towards a metallicity even higher than solar for the nuclear region. Many models of the NLR on the other hand have favored more often than not the exploration of abundances lower than or equal to solar (e.g., Gaskell & Ferland 1984; Ferland & Netzer 1983). As this work emphasizes the role of internal dust, for definiteness we will assume that the abundances of metals appropriate to the NLR are close to solar and adopt the solar system abundances of Anders & Grevesse (1989) (see list in Table 4 of Appendix A). We define Z as the total (gas+dust phases) metallicity relative to solar which implies $Z \equiv 1$ for this work.

The absorption and scattering cross sections of dust (from the infrared to the soft X-rays) were computed by Peter Martin (the curves are displayed in Fig.6 of Martin & Rouleau 1991) and corresponds to a dust models of the extinction curve of the solar neighborhood interstellar medium. In MAPPINGS, we scale the scattering and absorption cross sections (and, therefore, the dust content) by a dimensionless factor μ . The grain model of Martin & Rouleau (1991) results in a dust-to-gas *mass* ratio of 0.0064μ ($\rho_{dust}/\rho_{gas} \cong 0.71\rho_{dust}/\rho_H$) and to an extinction opacity at 5500 \AA $\tau_V (=0.921A_V) = 4.8 \times 10^{-22} \mu N_H \text{ cm}^2$, where $N_H(\text{cm}^{-2})$ is the *total* hydrogen column density. When $\mu \equiv 1$, these quantities are all consistent with the standard extinction curve of the local ISM (interstellar medium).

To be consistent with the depletion of metals unto dust grains, we deplete the abundances of metals in the *gas* phase, Z_{gas} , according to the dust content

μ . The adopted scheme described in Appendix A uses the depletion indices listed in Whittet (1992) and if necessary scales them with μ/Z . Renormalization of the derived gas phase abundances is performed until the mass locked into dust grains becomes consistent with the dust-to-gas mass ratio implied by μ . For instance, when $\mu=1$, $Z_{gas} = 0.6$ as a result of depletion. In this work, the *total* metal abundances are always solar and, therefore, $Z = Z_{gas} + Z_{dust} \equiv 1$

The slab geometry and the input parameters

All our calculations assume the same standard values for the input parameters, that is: an isobaric density behaviour, a power law ionizing continuum of index $\alpha = -1.4$ ($F_\nu \propto \nu^{+\alpha}$) and solar *total* abundances (but depleted gas abundances: $Z_{gas} = Z - Z_{dust} = 1 - Z_{dust}$). Our constant pressure models are parameterized in terms of the so-called ionization parameter, that is, the ratio of the density of ionizing photons impinging on the slab to the density of the outermost gas layer of the slab:

$$U_f = \frac{1}{cn_H^f} \int \frac{\phi_\nu^f}{h\nu} d\nu = \frac{\phi_\nu^f}{cn_H^f} \quad [1]$$

where c is the speed of light and ν_0 is the Lyman limit frequency, ϕ_ν^f is the ionizing photon flux (in photons $\text{cm}^{-2} \text{s}^{-1}$) impinging on the slab (quantities with superscripts f or b refer to their values at the front or at the back of the slab, respectively). For the reference dust-free model (*filled star* in the figures) which is referred below, we adopted $n_H^f=5000 \text{ cm}^{-3}$ and $U_f=0.0015$ as justified in §§ 2.3.1 and 2.3.3.

Using the code MAPPINGS, the calculation of the ionization and emissivity structure is carried inward in the slab either up to a column depth (i.e., $\int N_H dx$) $N_H^{slab} < N_{H^*}$ in the case of matter-bounded calculations or, in the case of radiation-bounded calculations, up to N_{H^*} . The column density N_{H^*} gives the depth of the complete “photoexcited” region, that is, the depth at which the incoming ionizing flux is exhausted. The operative definition of the boundary of the photoexcited region (at depth N_{H^*}) is defined as the depth where the following two conditions are simultaneously satisfied: (1) the inabsorbed ionizing flux $\phi_\nu^f < 1 \%$, of the impinging flux ϕ_ν^f , and (2) the ionized fraction $n_{H^+}^b/n_H^b \leq 1\%$. The code computes successively the emergent flux seen directly from the photoionized face (perspective “f”; see Fig.4) as well as seen from the back (perspective “b”). The transfer solution used across the dusty medium not only considers absorption but dust scattering as well (see BWZM).

Because the harder photons of the power-law ionizing continuum (with $\alpha = -1.4$) creates quite a large partially ionized region (hereafter PIZ) in which the ionized gas very gradually becomes neutral, N_{H^*} is a factor ~ 10 higher than the Strömgen depth (in cm^{-2}) which is technically defined as

Figure 4:

Adopted slab geometry for the constant pressure photoionization calculations. The slab comprises a fully ionized zone and a partially ionized zone (PIZ) which adds up to the column density of the photoexcited zone N_{H^*} . Beyond the photoexcited regions a zone of neutral gas may exist of column density N_{H^0} . Perspective “f” considers the emergent line fluxes seen from the side which is photoionized (front), while perspective “b” corresponds to the opposite back side. The dust extinction opacity of any zone is proportional to its relative dust content μ and total hydrogen column density N_H .

$$N_{H^+}^S = cU_f/\alpha_B \approx 10^{23}U_f \text{ cm}^{-2} \quad (T_e = 10^4 \text{ K}) \quad [2]$$

where α_B is the recombination coefficient to excited states of hydrogen. In an HII region, because of the softness of the ionizing continuum, the PIZ is negligible and $N_{H^*} \simeq N_{H^+}^S$. For radiation-bounded clouds, equation (2) entails that the fully ionized zone [$N_{H^+}(n_{H^+}/n_{H^0} \geq 10) \approx 0.8N_{H^+}^S$] which contributes most of the line luminosity nevertheless contributes only a small fraction of the dust opacity inside N_{H^*} and, therefore, the spectrum seen from perspective “b” is more reddened than the one emerging from perspective “f”.

By portraying the emitting NLR cloud as a slab, a determinant parameter with which the dust opacity scales is the total column density $N_{H^+}^{slab}(= N_{H^0}^{slab} + N_H^{slab})$ of the slab. In this work, in most instances, we assume the slab to be not only radiation-bounded but in some cases to exceed N_{H^*} due to a neutral H^0 zone of column density $N_{H^0}^0$ (beyond the PIZ) as depicted in Figure 4. The dust inside this region can play a determinant role in reducing the emergent line fluxes seen from perspective “b”. Apart from absorption of the lines by dust, the neutral zone also is assumed isothermal with a temperature taken to be equal to the temperature at the last computed ionized layer. Changing this temperature even arbitrarily has practically no effect on the zone’s reflectivity to $\text{Ly}\alpha$ since even without such a zone the already huge $\text{Ly}\alpha$ line opacity within the PIZ would cause most of the $\text{Ly}\alpha$ to emerge from perspective “f” rather than from “b” (cf.2.3.2).

In our nomenclature, the total column density of the slab is given by $N_H^{slab} = N_{H^*} + N_{H^0}^0$ (see Fig.4) if the slab is radiation-bounded (otherwise, $N_H^{slab} < N_{H^*}$ if the slab is matter-bounded). We assume that dust-to-gas ratio μ is uniform within each zone but may take different values in the photoexcited zone from that in the neutral zone. Assuming that the same dust size distribution and composition applies to the different zones (that is, the shape of the extinction curve remains constant), we obtain that the total slab opacity in the V band (5500 Å) is given by

$$\begin{aligned} \tau_V^{slab} &= \tau_V(N_{H^*}) + \tau_V(N_{H^0}^0) = \\ &= 4.8 \times 10^{-22} [\mu(H^*)N_{H^*} + \mu(H^0)N_{H^0}^0] \quad [3] \end{aligned}$$

Due to the high reflectivity of Ly α by the H 0 zone as well as by substantial amount of H 0 inside the transition zone, the emergent Ly α originating from perspective “b” is generally negligible. The Balmer lines are generated isotropically but are absorbed differently when emerging from perspective “b” or “f” because of the asymmetry in dust opacity introduced by the $N_{H^0}^0$ zone and the PIZ. If we picture the NLR as an ensemble of clouds with very low covering factor symmetrically distributed around a nuclear ionizing source, the *number* of cloud seen from the back can be postulated to be equal statistically to that of clouds seen from the front. To a first order the resulting line ratios for such an “open” geometry is obtained by adding first with equal weight the line fluxed from the “f” and “b” perspectives and then taking the ratios of the summed fluxes.

In § 2.3, we will first explore the effect of varying the internal dust-to-gas ratio μ on the Ly α /H β and H α /H β line ratios emerging from a symmetric distribution of clouds (i.e., the case represented by “f” + “b”). After comparing models (§2.4.1) with Seyfert 2 data of Kinney et al. (1991) and after discussing the pure dust hypothesis (§2.4.2), we will look into the possibility of having more clouds seen from perspective “b” as well as the limiting case of a spherically closed geometry (§2.4.3).

2.3 Results

Our main purpose is to explore the effect of internal dust on the HI line ratios in the context of the standard photoionization model of the NLR. For this reason, we have limited the scope of the calculations to restricted plausible values of input parameters; we consider, for instance only solar abundances (but with progressive

depletion of gas phase metallicity Z_{gas} with increasing dust content μ) and canonical $\alpha = -1.4$ ionizing power law ¹ (cf. Ferland & Osterbrock 1986; Kinney et al. 1991). The choice and role of the gas density is first discussed (§2.3.1) as well as that of incomplete opacity to ionizing photons (§ 2.3.2) and the selection of the ionization parameter (§2.3.3). We then discuss the results of nebular models with internal dust §2.3.4.

2.3.1 Selection of a characteristic cloud density

The choice of a representative cloud density in the calculations is much more problematic than the selection of other parameters. There is evidence of a wide distribution of cloud densities in the NLR following the work of DeRobertis & Osterbrock (1984,1986) who have shown in many Seyferts the tendency of the forbidden line profile widths to correlate with the respective deexcitation critical density of the transition involved. This lends support to the picture of a wide gradient in cloud densities ($10^3 \leq n_e \leq 10^6 \text{ cm}^{-3}$) as well as in velocity dispersion as a function of distance from the nucleus. In this picture, the bulk of a line luminosity would be contributed by clouds of density approaching the line's critical density. The few available direct measurement of the NLR electron densities have been mostly provided by the ratio of the [SII] $\lambda\lambda 6716,6731$ density-sensitive doublet (Osterbrock 1989) which show densities which are relatively low (200-2000 cm^{-3}). These low densities do not necessarily contradict a wide range of cloud densities within the NLR because the critical density of [SII] red lines is relatively low and moreover the S^+ zone coincides with the partially ionized zone of the emitting cloud where the electron density can be expected to be lower than in the fully ionized zone. This can be demonstrated with constant pressure photoionization calculations with densities covering the range $80 < n_H^f < 6000 \text{ cm}^{-3}$ which show that the electronic density inferred from the [SII] line ratio is a factor 4-5 smaller than the mean $\langle n_e \rangle$ of the fully ionized zone. Finally, there also exists a significant fraction of Seyferts in which line widths correlate with line excitation (cf. Pelat, Alloin, & Fosbury 1981; Filippenko 1985; DeRobertis & Osterbrock 1984,1986) which could indicate that the density range within these objects is narrower.

Following the indications given by the [SII] densities and given that we will not integrate the line contribution of clouds over different densities, we opt for a single density of $n_H^f=5000 \text{ cm}^{-3}$ which we expect to characterize the NLR gas that emits the bulk of the HI lines. Before discussing models with dust we first summarize the dependence of HI lines on density.

The direct dependence of $H\alpha$ and $H\beta$ intensities on the gas density is very weak when the line is produced by recombination alone (Hummer & Storey 1987). However, in a power law photoionized plasma, both lines become indirectly coupled

¹A much harder distribution (flatter power law) would give a rather poor fit to the low excitation lines assuming the photoionized clouds are radiation bounded.

to density when substantial collisional excitation takes place within the PIZ. The reason is that increasing the density reduces the effectiveness of cooling of many important forbidden lines as a result of collisional deexcitation, thereby increasing the equilibrium plasma temperature which in turn increases the rate of collisional excitation of HI in the PIZ. In the fully ionized zone, there is too little HI to excite and the Balmer lines are produced only by recombination independent of the plasma temperature. In the case of Ly α , the dependence of the line intensity on the electron density is much more direct. When the density is increased much above 10^3 cm^{-3} , there is an increasing conversion of the level 2s population otherwise responsible for the 2q continuum emission into Ly α emission by excitation into the 2p level (see Osterbrock 1989; Gaskell & Ferland 1984). In the low density regime case B in the absence of the Ly α sinks (e.g., dust absorption), the fraction of energy emitted as Ly α versus 2q emission from recombination alone is $\alpha_{2p}^{eff} / \alpha_B \approx 0.67(T_e/10^4 K)^{-0.054}$ and tends toward unity for densities above 10^5 cm^{-3} .

To illustrate quantitatively the effect of density, we have calculated a sequence of constant pressure models covering the range $50 < n_H^f < 2 \times 10^6 \text{ cm}^{-3}$. The results of integrated nebulae calculations as function of the mean slab electron density are presented in Figure 5. The case of a pure recombination-dominated HII region model (*dotted line*) is also shown for comparison with the power-law model (*solid line*). In Figure 5a, it is evident that both ionizing energy distributions result in a qualitatively similar functional dependence of Ly α /H β on $\langle n_e \rangle$, except that Ly α /H β is consistently higher for the power law due to collisional excitation within the PIZ. For the Balmer decrement (Fig. 5b), at low densities ($\langle n_e \rangle \ll 5 \times 10^4 \text{ cm}^{-3}$), however there is a sharp increase in H α /H β owing to the enhancement of collisional excitation that occurs when the gas temperature increases due to gradual suppression of the forbidden lines.

Subsequent models with internal dust have all been calculated with the single representative density of $n_H^f = 5000 \text{ cm}^{-3}$. This reference density coupled with the adopted U_f introduced below provides us with a comparative zero point (i.e., dust-free case) in our Ly α /H β versus H α /H β diagrams (as represented by the filled star). If one is interested in estimating the line ratios different zero point in density space, Figure 5 can be used to determine very approximately the differential change in the ratios due to density alone and apply it to the models which contain dust.

2.3.2 Asymmetric emissivity and internal dust absorption

Because line scattering increases the path length of Ly α photons, the efficiency of internal dust to absorb line photons is drastically higher for the optically thick resonant Ly α line than for the optically thin Balmer lines. Hummer & Kunasz (1980) have derived scaling laws for the energy loss, the mean path length, and the mean number of scattering suffered by resonant line photons in the presence of continuous absorption (by dust and/or photoelectric absorption). (See Neufeld 1990 for a discussion of these scaling laws using analytical methods). The fraction

Figure 5:

Sequences of dust-free solar metallicity photoionization calculations with varying gas density n_H^f . Results for two different energy distributions of the ionizing continuum are represented: the power law with $\alpha = -1.4$ (*solid line*) adopted in this work and a black body of 40,000 K (*dotted line*) for which recombination is the only process generating HI lines. The ionization parameter U_f is constant along both sequences and takes on the values of 0.0015 and 0.010 for the power law and for the blackbody sequences, respectively. Panel (a) shows the Ly α /H β ratio (“f”+“b”) as a function of the mean electron density $\langle n_e \rangle$ characterizing the isobaric photoexcited zone, while panel (b) shows the corresponding behavior of H α /H β . The star represents the standard model ($U_f=0.0015$, $n_H^f= 5000 \text{ cm}^{-3}$) discussed in §2.3.

of energy from a resonant line generated within a midplane layer which escapes unabsorbed from a slab of total line opacity Γ depends essentially on the parameter $\beta \equiv k_c/k_L$ which is the ratio of continuous opacity to line opacity. The results of Hummer & Kunasz (1980) concerning the transfer as well as the interplay between escape probability and dust absorption have been incorporated in MAPPINGS as described in detail in Appendix of BWZM.

One aspect of the transfer particularly relevant to thick nebulae is the asymmetry which characterized the Ly α flux emerging from the front or from the back of the ionized slab. This is taken into account in the code through the definition of an emissivity whose asymmetry depends on the local two-sided escape probability. The asymmetry factor A^f ($0 \leq A^f \leq 2$) in our transfer solution is defined as follows

$$A^f = 2\epsilon(\tau, \beta) / [\epsilon(\tau, \beta) + \epsilon(\Gamma - \tau, \beta')] \quad [4]$$

where τ is line opacity of the layer under consideration, $\Gamma (= \int d\tau)$ is the line opacity of the whole slab, $\epsilon(\tau, \beta)$ is the escape probability from the back. (See Appendix A in BWZM for further details on the escape asymmetry). The implication of the two-escape scheme is that the emissivity of the resonant line is asymmetric with the forward emissivity given by $j_L^b = j_L(2 - A^f)$. The observer, in this simple two-stream transfer scheme, is placed either in front of the slab or behind it and the emergent line flux from either perspective “f” or “b” is obtained by integrating the appropriate emissivity (j_L^f or j_L^b).

An important consequence of using equation (4) in integrating the line emissivity is that for a slab illuminated on only one side by the ionizing radiation, the Ly α intensity emerging from perspective “f” is much higher than that from “b” whenever the line is reasonably thick ($\tau > 10$), a condition almost always satisfied except for extremely low column density matter-bounded slabs. For a slab of total line opacity Γ , the depth N_H at which line photons have equal probability of escaping from the front (“f”) as from the back (“b”) occurs at the depth $N_H(\tau = \Gamma/2)$, i.e., $N_H = N_H(\tau = \Gamma/2)$. Since $d\tau/dN_H \propto n_{H^0}/n_H$ is a monotonically increasing function of N_H , the depth $N_H(\tau = \Gamma/2)$ is quite generally located much deeper than the depth that divides equal Ly α production. As a result, Ly α photons preferentially escape from the front (“f”). This is true even for soft impinging ionizing continua as occurs, for instance, in HII regions. For a power-law ionizing continuum, to the extent that recombination still dominates Ly α production, most of Ly α is produced within the fully ionized zone, i.e., at $N_H \leq 0.8N_{H+}^S$ which is much less than $N_H(\tau = \Gamma/2) \sim N_H H^*$ owing to the extended PIZ (cf. § 2.2.3). In the opposite case of the extremely low column density nebulae, the neutral fraction $n_{H^0}/n_H \approx \text{constant}$ so that $N_H(\tau = \Gamma/2) \approx N_H^{slab}/2$, which coincides approximately with the depth dividing equal Ly α production. In this case, the Ly α flux emerges symmetrically from the front (“f”) and the back (“b”).

To illustrate how one progressively goes from symmetrically emerging Ly α

in the very thin slab case to the opposite asymmetric situation in the radiation-bounded slab case, we have computed a sequence of matter-bounded models in which N_H^{slab} is gradually increased in lock steps. Figure 6 gives the fraction of Ly α which escapes from perspective “b” as a function of the matter bounded slab’s thickness (expressed in a different way in each panel). Note that internal dust has been included in these models, but it does not affect significantly the degree of asymmetry except when N_H^{slab} approaches N_{H^*} , the radiation-bounded case. Two of the sequences correspond to $U_f=0.015$ with $\mu=1.0$. The results indicate that the fraction of Ly α which escapes from the back is close to half only when the matter-bounded slab is indeed very thin (i.e., for $\tau_{H^0}^c(912\text{\AA}) < 10$ or $N_H^{slab}/N_{H^+}^S < 0.5 - 0.8$).

The effect of perspective need not be considered in previous work on the intrinsic NLR Ly α /H β and H α /H β line ratios since it was implicitly assumed that perspective effects averaged out due to the geometry of the ensemble of NLR clouds. This might be a valid assumption in the dust-free case where no Ly α destruction takes place despite the high number of scatterings. When dust is present, however, the effect of perspective cannot be ignored since the Ly α transfer with internal dust present is nonconservative with respect to perspective with most of the surviving Ly α photons escaping from the front.

Perspective can also affect significantly the integrated Balmer lines of a system of clouds with internal dust because the dust within the extensive PIZ significantly absorbs the Balmer lines which emerges from the back (producing at the same time the steeper Balmer decrement). This effect is particularly important in understanding the results presented in § 2.3.4. To illustrate the dominant effects of both perspective and dust, we picture a thin fully ionized region which generates the bulk of Ly α , and, depending on how opaque the region is to dust [$\tau_V(H^+)$], a substantial fraction of the resonant Ly α escapes from the front while half of the Balmer lines’ flux is required to transfer across the larger and dustier PIZ before escaping from the back (the other half emerges from the front after suffering little extinction).

To illustrate the role of internal dust on the total emerging Ly α and Balmer lines, we present in Figure 7 the line ratios resulting from adding together the fluxes from perspective “f” and “b” (before taking the ratio) as a function of the Ly α limit opacity $\tau_{H^0}^c(912\text{\AA})$ for the matter bounded sequences presented in Figure 6. The larger destruction rate of Ly α for the high-ionization parameter (*dotted line*) model is apparent and is the result of a higher value of β throughout the nebula (cf. § 2.3.3). We also find for all three sequences that for $\tau_{H^0}^c(912\text{\AA}) > 100$, because dust in the PIZ starts absorbing much of the H β flux escaping from the back, the “f+b” Ly α /H β ratio rebounds up (the Ly α flux actually remains steady). The somewhat higher Balmer decrement in the matter-bounded regime in the higher U_f model is generally caused by reddening [larger $\tau_V(H^+)$]. When $\tau_{H^0}^c(912\text{\AA}) < 10$, then in addition to reddening, for β sufficiently high, the normal conversion of the higher Lyman lines into Balmer or higher series is reduced because of dust absorption of

Figure 6:

Matter-bounded calculations in which the ordinate represents the fraction of Ly α flux which escapes from the back (perspective “b”) as a function of different quantities which measures the ionized slab’s thickness. The abscissae represent, panel by panel, the following: panel (a): the fraction of unabsorbed ionizing photons which leaks out from the back ϕ_H^b/ϕ_H^f ; panel (b): the slab’s column density to that of the Strömngren depth $N_{H^+}^S = cU_f/\bar{\alpha}_B$, where $\bar{\alpha}_B$ is evaluated at the slab *mean* electronic temperature; panel (c): the hydrogen ionized fraction within the last layer at the back; panel (d): the slab Lyman-limit continuum opacity. The solid and short dash curves were both calculated using the reference value of $U_f = 0.0015$ (and $n_H^f = 5000 \text{ cm}^{-3}$; see §§ 2.3.2 and 2.3.3) but with an internal dust content of $\mu = 1.0$ and 0.2 respectively. The dotted line corresponds to calculations with $U_f=0.015$ and $\mu=1.0$

Figure 7:

In panel (a), $\text{Ly}\alpha/\text{H}\beta$ as a function of the Lyman-limit opacity of the matter-bounded photoionized slabs. As in Fig.6, the solid and short dashed curves were calculated with $U_f=0.0015$ and an internal dust content of $\mu=1.0$ and 0.2 respectively. The dotted line corresponds to calculations with $U_f=0.0015$ and $\mu = 1.0$. Panel (b) plots the Balmer decrement as a function of the Lyman-limit opacity.

these Lyman line (this effect simulates something resembling case A).

2.3.3 Selection of the ionization parameter U_f

The most simple geometrical model of the narrow-line region consists of a symmetric distribution of ionized clouds surrounding the ionizing source. Any reasonable assumed electron densities leads us to infer a very small *volume* filling factor for the emitting gas. The ionization parameter which is inferred from the line ratios is surprisingly uniform within a given class of AGN.

To determine U_f , we have simply required the radiation-bounded calculations to approximately fit the "mean" optical Seyfert 2 line spectrum derived by Ferland & Osterbrock (1986, hereafter FO86) in which a ratio of $[\text{OIII}]\lambda 5007/\text{H}\beta$ of ~ 10 is observed. With the other parameters specified above, this leads us to adopt $U_f=0.0015$ for the reference ionization parameter.

The choice of the ionization parameter affects strongly the role played by dust. For instance, internal dust can absorb a fraction of the ionizing radiation and therefore shrink the Strömgren depth due to competitive absorption with H^0 . In the case of our reference model with $U_f=0.0015$, only 3% of ϕ_H^f is lost to dust absorption when $\mu = 1$. However, with an ionization parameter 10 times larger [recall that $\tau_V(\text{H}^+)$ scales with $N_{\text{H}^+}^S$, we find that as much as 24 % of ϕ_H^f is absorbed by dust when $\mu=1$. This effect can be seen in the $U_f=0.015$ sequence shown in Figure 6b where the dotted line curve is shifted to the left because scaling is relative to the dust-free value of $N_{\text{H}^+}^S$.

Another aspect where U_f is important is the amount of destruction of resonant $\text{Ly}\alpha$ by dust. To show this, let us define using equation (2) the pure absorption opacity by dust at depth half way within the fully ionized zone:

$$\tau_{dust}^{abs}(1216\text{\AA} \frac{1}{2} N_{\text{H}^+}^S) \cong 2.2\tau_V^{ext} \cong 60\mu U_f \quad [5]$$

The justification for choosing this position is that most of the $\text{Ly}\alpha$ is generated as well as destroyed within the fully ionized region. Assuming $U_f = 0.0015$ and $\mu = 1.0$, we obtain $\tau_{dust}^{abs}(1216\text{\AA}) \approx 0.1$. As a crude estimate to illustrate the effect of dust on $\text{Ly}\alpha$, at this depth, the line (scattering) opacity is $\sim 10^5$ which allows us to estimate $\beta \sim 10^{-6}$ and derive the fraction of $\text{Ly}\alpha$ which escapes unabsorbed from this layer at $\sim 50\%$ by using the scaled results of Hummer & Kunasz (1980). On the other hand, for the higher value of $U_f=0.015$, the line opacity at a similar relative position corresponding to $\tau_{dust}^{abs}(1216\text{\AA}) \approx 1$ ($\mu=1$) is higher ($\sim 3 \times 10^6$), and we estimate that with $\beta \sim 3 \times 10^{-7}$, only 2% of $\text{Ly}\alpha$ escapes the layer. For calculations with the adopted ionization parameter $U_f=0.0015$, we see that $\text{Ly}\alpha$ destruction due to dust should be moderate.

2.3.4 Results for a symmetric cloud distribution

We approximate the typical NLR emission cloud as a slab of gas of constant internal pressure with an outer density of $n_H^f = 5000 \text{ cm}^{-3}$ (cf. § 2.3.1). Using MAPPINGS, we compute the line spectrum from photoionization calculations using the ionization parameter $U_f = 0.0015$ (cf. § 2.3.3) and an ionizing power-law of index $\alpha = -1.4$. In all the calculations, the gas phase abundances are modified consistently with the dust content μ in such a way that the total metallicity (gas+dust) remains always solar: $Z = Z_{gas} + Z_{dust} = 1$ (cf. § 2.2.2 and Appendix A). The assumed symmetric distribution of the clouds is taken into account in the calculated spectrum by adding together spectral “f” and “b” of MAPPINGS calculations which is equivalent to supposing that there are as many clouds seen face-on as are seen from the back.

Using this procedure, we have computed three sequences of models with the dust content μ covering the range $0 \leq \mu \leq 1.25$. These three sequences are presented in Figure 8 (*solid lines*) and correspond to three different total slab column densities N_H^{slab} . The intermediate sequence corresponds to the radiation-bounded case $N_H^{slab} = N_{H^*}$ (see § 2.3.3 for the operative definition of the depth of the photoexcited region N_{H^*}), a second sequence represents the matter-bounded case in which N_H^{slab} corresponds to the depth where hydrogen is 10% ionized (i.e., $N_H^{slab} \simeq 2.4 \times 10^{20} \text{ cm}^{-2}$), a third one is the case in which the NLR clouds are more massive than the radiation-bounded case and has $N_H^{slab} \equiv N_{H^*} + N_{H^0}^0 = 5 \times 10^{21} \text{ cm}^{-2}$, which is about 6 times the N_{H^*} of the dust-free case². The zero-point dust-free reference model with $U_f = 0.0015$ is represented in all figures by the filled star. We emphasize that our simple geometry assumes a very low volume filling factor of the emitting clouds so that as many “f” clouds as “b” clouds are seen by the observer without any intervening obscuration.

The most important result of the calculations shown in Figure 8 is to prove that despite large amounts of internal dust, the $\text{Ly}\alpha/\text{H}\beta$ calculated using canonical input parameters is not radically different from recombination case B, and, if anything, it can even be larger when $\mu \rightarrow 1$. The expected range for $\text{Ly}\alpha/\text{H}\beta$ in the dust-free recombination case B is between 23 and 34 depending on the gas density. If, in addition, collisional excitation is present due to the hardness of the continuum or to low gas metallicity, both the Balmer and the Lyman decrement become larger (see Gaskell & Ferland 1984), a situation not unlike that shown in Figure 8 except that here it is the result of internal dust.

The two main factors explaining the relatively high $\text{Ly}\alpha/\text{H}\beta$ are that, first, with $U_f = 0.0015$, $\text{Ly}\alpha$ destruction is modest in the clouds since the column density

²Note that N_{H^*} progressively increases with μ , from $8 \times 10^{20} \text{ cm}^{-2}$ when $\mu = 0$ to $2.6 \times 10^{21} \text{ cm}^{-2}$ when $\mu = 1.25$. The main reason has to do with the criterion requiring that hydrogen be only 1% ionized at the inner boundary of the photoexcited region. Because the recombination coefficient depends on T_e , N_{H^*} becomes larger when the temperature of the PIZ increases as a result of depletion of the gas phase with increasing μ . We have found that T_e increases from 1200 K in the dust-free case to 3300 K at $\mu = 1.25$

Figure 8:

$\text{Ly}\alpha/\text{H}\beta$ as a function of the Balmer decrement for the three sequences with $U_f=0.0015$ in which μ is monotonically increasing ($0 \leq \mu \leq 1.25$). Tick marks from left to right along the solid lines indicate values of μ of 0.1, 0.2, 0.4, 0.6, and 1.0, respectively. The three sequences (*solid lines*) differ only by the total column density of the slab N_H^{slab} . The lowermost sequence is matter-bounded using the criterion that the hydrogen ionized fraction is 10% at the back layer. The intermediate sequence corresponds to the radiation-bounded case without any additional neutral gas zone at the back. The uppermost sequence includes a neutral back zone such that the *total* column density of the slab is constant at $5 \times 10^{21} \text{ cm}^{-2}$. The neutral and photoexcited zones are assumed to have the same dust content [$\mu(\text{H}^0) = \mu(\text{H}^*)$]. The filled star represents the reference dust-free case ($\mu=0$). Also shown in the figure is an ionization parameter sequence (*dotted line*) for radiation-bounded slabs (with $N_{\text{H}^0}^0 = 0$) of constant dust content $\mu = 1.0$ and covering the range $10^{-4} \leq U_f \leq 10^{-2}$. In all above calculations, the ionizing energy distribution is a power law with index $\alpha = -1.4$, the gas density is $n_H^f = 5000 \text{ cm}^{-3}$ at the face of the cloud, the metals are depleted from the gas phase in accordance with the dust content μ , and the line intensities are given by the sum of the “f” and “b” perspective.

of ionized gas and therefore $\tau_V(H^+)$ is not large, and second, the portion of the Balmer lines' flux which escape from the back is subject to considerable absorption by the dust inside the PIZ or within the neutral core of the cloud. It is therefore not surprising that the models which depart most from case B $\text{Ly}\alpha/\text{H}\beta$ are those of the matter-bounded sequence, comparatively little absorption occurs for the Balmer lines while destruction of $\text{Ly}\alpha$ photons (which occurs mostly in the fully ionized zone) remains significant (cf. § 2.3.2). To illustrate to what extent much higher values of U_f would be catastrophic to the escape of $\text{Ly}\alpha$ photons, the dotted line in Figure 8 represents an ionization parameter sequence with models of constant dust content ($\mu=0.1$). Of course, these models are of limited relevance since they result in a forbidden-line spectrum incompatible with observed optical line ratios.

Since in the dust-free case we used solar metallicity for the gas, little collisional excitation takes place within the PIZ and the resultant Balmer decrement is not significantly above that of a dust content of $\mu=1$, however, the Balmer decrement in the radiation-bounded case is shown in Figure 8 to approach 3.3. On the other hand, moderate amounts of internal dust $\mu \sim 0.2 - 0.4$ would favor an intrinsic Balmer decrement in the range 3.0-3.1 assuming the clouds are radiation-bounded (the corresponding range the Lyman decrement is 32-37). This range (3.0-3.1) corresponds to that proposed by various authors (Gaskell & Ferland 1984; Halpern & Steiner 1983) for the intrinsic NLR Balmer decrement except that it is here more the result of the presence of internal dust rather than of a hard ionizing continuum or of deficiencies in the gas metallicity relative to solar. Binette et al. (1990) pointed out the apparent lack of Seyfert 2 with $\text{H}\alpha/\text{H}\beta < 3.4$ if one considers only objects with good S/N in the $\text{H}\gamma$ line. If this high value of 3.4 was exclusively caused by internal dust present in all Seyfert 2's, then large values of μ (~ 1) are implied from Figure 8. Alternatively, a portion of the extinction may be the result of *intervening* gas containing dust, in which case the amount of *internal* dust implied is lower. There are two possibilities for how this intervening gas/dust may arise. In one case this dust is contained in a detached screen. Such models, however, may not be physically plausible as discussed in §4.2. Another possibility is that the intervening dust+gas arises from a large covering factor of the NLR clouds themselves. This case is presented in §2.4.3.

Radiation-bounded calculations with our selected parameters are known to over predict by a factor ≈ 2 the $[\text{OI}]\lambda 6300/\text{H}\beta$ ratio. Using a moderately matter-bounded cloud such as the one shown in Figure 8, one can resolve this discrepancy by cutting the cloud at some depth to make the $[\text{OI}]$ fit the observed value. As previously shown in Figure 7, the matter-bounded model $\mu=1$ results in a lower $\text{Ly}\alpha/\text{H}\beta$ (than radiation-bounded calculations) somewhat below case B and in a moderately reddened Balmer decrement. The procedure of cutting the clouds to adjust $[\text{OI}]$ to the observed value is, however, quite arbitrary. A more realistic approach is the dual gas components model of Viegas & Prieto (1992) which was proposed as a solution to explain the observed high $\text{HeII}/\text{H}\beta$ ratio observed in the

spatially extended NLR (ENLR) (see also Morganti et al. 1991). This model consists of a matter-bounded (MB) and a radiation-bounded (RB) component. The MB component has a higher volume filling factor (to compensate for its much lower emission measure) and a higher ionization parameter ($U_f > 0.0015$). Although we did not consider this level of complication in our modeling, we can still establish some of its general properties in relation to dust using the results of §§ 2.3.2 and 2.3.3. Under most instances, the effects of dust on the HI lines cannot be larger in the case of the dual-component model than with our simpler single RB component because the MB component, despite its higher U_f , is nevertheless extremely thin in column density and therefore generally results in little Ly α destruction³. Furthermore, the RB component should have $U^{RB} < 0.0015$ (Viegas & Prieto suggest $U^{RB} < 0.0006$) and therefore much lower τ_V than in our single RB component. In conclusion, a working dual-component model would in all likelihood be characterized by *smaller* line absorption effects due to dust at equal values of μ than in our simplified single component model.

2.4 Discussion

After comparing calculations with internal dust with recent Ly α /H β data on Seyfert 2's (§2.4.1), we discuss various interpretations of the low values observed. We look at the possibility of pure line scattering or pure dust absorption (§2.4.2) as well as that of mutual covering of Ly α clouds (§2.4.3). On §2.4.4, we consider the possibility of dust absorption of the UV continuum for explaining the apparent deficit of ionizing photons.

2.4.1 Observational data of KAW3

The available data on the NLR Lyman decrement is still rather limited. The most reliable information on the NLR comes from Seyfert 2's since, as pointed out by FO86, only for these objects can one deduce an optical to ultraviolet line spectrum which is totally free of contamination by BLR components. It is likely, however, that the physical information gathered from the NLR of Seyfert 2 is relevant to that of Seyfert 1 and quasars. One of the motivations of the current work was the recent publication by Kinney et al. (1991) of a Seyfert 2 data set for which the optical spectra were taken through an aperture which matched the large IUE satellite aperture. The matching of aperture size for the different lines is a crucial point in the study of the NLR Lyman decrement because the emitting line region is spatially extended and in the likely event that Ly α , H α , H β present

³The dual component model of Viegas & Prieto (1992) suggest a MB component with opacity $\tau_{H\alpha}^c(912 \text{ \AA}) < 1$. Adopting $\tau_{H\alpha}^c(912 \text{ \AA}) = 0.55$ and a similar $U^{MB} = 0.01$ to what they use, we obtain $N_H^{slab} \cong 0.067 \mu$. Even with high dust content $\mu=1$, our calculations indicate a Ly α destruction of only 0.13 dex with a difference in flux between “f” and “b” perspectives of 15%.

a different spatial distribution in surface brightness, the interpretation of ratios of lines derived from different apertures becomes very complicated, if not impossible. By comparing for instance objects common to both the KAW3 and FO86 data set, one finds many objects with significantly different line ratios between the two data sets presumably as a result of the much smaller aperture of the FO86 optical observations. For this reason we have limited our analysis to the data set of KAW3 which are presumed free of this problem.

In Figure 9 (which is an expanded scale version of Fig.8), we present the data of KAW3 (*filled squares*) with their estimated error bars. The earlier model sequences of Figure 8 now appear as broken dash lines in the upper left. What is immediately striking is that internal dust absorption for an isotropic distribution of emitting clouds does not account for the low $\text{Ly}\alpha/\text{H}\beta$ ratio which is significantly below case B.

In order to explain the overall low $\text{Ly}\alpha/\text{H}\beta$ ratio in Seyfert 2's, either an intervening absorption/scattering screen is required or we must modify our simple NLR geometry. The first possibility, discussed in detail in §4.2, would require pure line scattering from the screen to explain the near-case B $\text{H}\alpha/\text{H}\beta$ objects. The second possibility is that the covering factor of the emission clouds is not small as was assumed so far. This idea is explored in §2.4.3 along with the possibility that if the covering is extreme, a closed spherical geometry might be preferable to that of an isotropic distribution of slab-approximated clouds.

2.4.2 The pure line scattering and the pure dust models

There are broadly two types of Seyfert 2 objects in the KAW3 data: the objects with near-case B $\text{H}\alpha/\text{H}\beta$ and the objects with reddened $\text{H}\alpha/\text{H}\beta$. The first category might be explained by pure $\text{Ly}\alpha$ scattering due to an intervening screen of H^0 which is supposed to be covering only the observer's view of the NLR but not the complete sky as seen from the NLR. Assume a slab geometry for the screen. Then for a pure scattering screen of thickness $\tau_{\text{H}^0\text{scat}}$, where $\tau_{\text{H}^0\text{scat}} = 5.9 \times 10^{-14} N_{\text{HI}}^{\text{screen}} (T_{\text{HI}}/10^4\text{K})^{-1/2}$ is the $\text{Ly}\alpha$ resonant scattering optical depth at line center, the fraction of photons impinging on the screen from the side facing the source which penetrates to the opposite side (the side facing the observer) is $\propto \tau_{\text{H}^0\text{scat}}^{-1/2}$ for $\tau_{\text{H}^0\text{scat}} \gg 1$ (Slater, Salpeter, & Wasserman 1982). Owing to the large magnitude of $\tau_{\text{H}^0\text{scat}}$, only modest values of $N_{\text{HI}}^{\text{screen}}$ are required to efficiently suppress the $\text{Ly}\alpha$ flux reaching the observer. Thus, for instance, for $N_{\text{HI}}^{\text{screen}} \sim 10^{15} \text{cm}^{-2}$ (10^{17}cm^{-2}), only 10% (1%) of the incident $\text{Ly}\alpha$ photons reaches the observer; the rest are reflected back toward the source. At such column depths, the dust opacity within the screen is entirely negligible, and so the extinction vector+ shown in Figure 9 is purely vertical.

The lack of objects with near-case B $\text{H}\alpha/\text{H}\beta$ in the FO86 sample has led these authors to propose pure dust absorption (ignoring the destruction of $\text{Ly}\alpha$

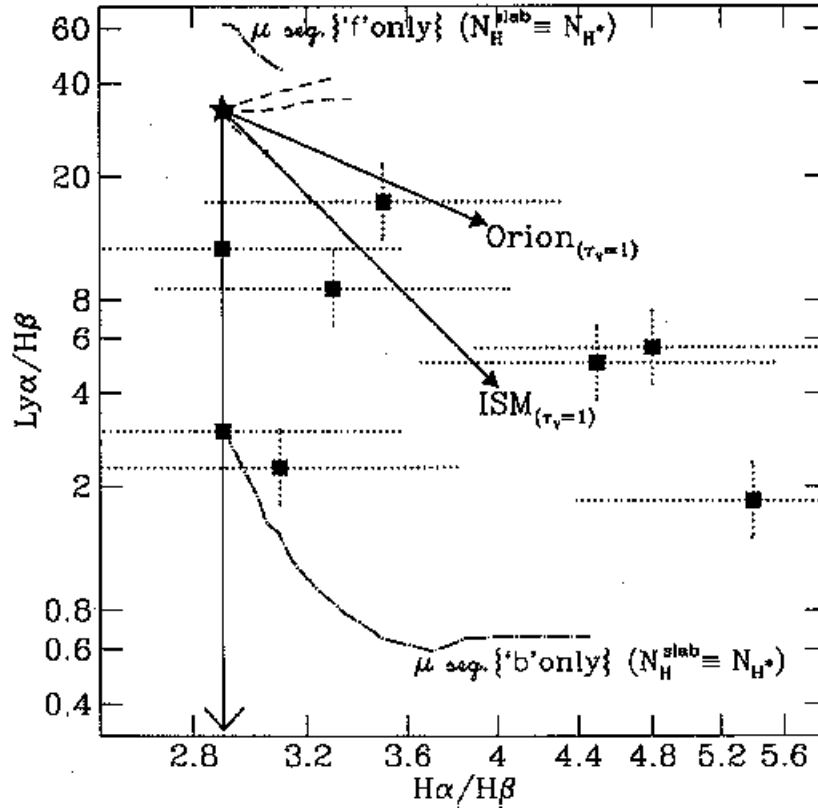


Figure 9:

The squares represent the homogeneous data set of Seyfert 2 observations of $Ly\alpha/H\beta$ vs. $H\alpha/H\beta$ by Kinney et al. (1991) in which the aperture in the optical closely matches the large-aperture IUE $Ly\alpha$ observations. Two reddening vectors corresponding to the ISM and the Orion extinction curve, respectively, are drawn to indicate the expected displacement due to foreground *pure* dust. The vectors' length correspond to an extinction $\tau = 1$ in the visible (5500 \AA). The vertical solid line represents the effect of scattering of $Ly\alpha$ by a foreground neutral hydrogen screen at the same redshift as the NLR (see § 4.2). The dash-dotted lines represents the μ sequence with $U_f=10^{-2.8}$ and $N_{H^0}^0 = 0$ but as seen *separately* from perspective "f" and "b". The three dash lines correspond to the same μ sequences of Fig. 8 (i.e., with "f" + "b")

after multiple resonant scatters) since their objects all broadly lie along the ISM reddening vector (see Fig.6 FO86). Within the sample of KAW3, many objects still lie in the general direction of the ISM reddening vector. The pure dust screen (without any line scattering; otherwise, the reddening vector would be steeper than shown above) remains a possible interpretation for the observed ratios, but only for the reddened $H\alpha/H\beta$ objects. Several limitations exist, however with the picture of the pure dust screen which we now proceed to analyze.

In the pure dust screen model, a layer of dust and gas is presumed to lie outside the NLR toward the line of sight to the observer. Photons that pass through this layer are assumed to suffer solely absorption by the dust, that is, interaction between the photons and the gas are ignored. While this is a good approximation for non resonant line photons such as $H\alpha$ and $H\beta$, it is a poor approximation for resonant line photons such as $Ly\alpha$. Owing to the large resonant scattering cross section of $Ly\alpha$ photons, resonant scattering by these photons with neutral hydrogen atoms as they traverse the layer cannot be ignored in general. For example, to obtain a reddening of $A_V = 1$ require $N_H = 2 \times 10^{21} \text{ cm}^{-2}$ for $\mu = 1$. For a gas at $T_e=10^4$ K, this corresponds roughly to $N_{HI} \sim 10^{20} \text{ cm}^{-2}$, which implies a line center resonant scattering optical depth for $Ly\alpha$ photons of $\tau_{H^0_{scat}} \sim 6 \times 10^6$.

One possible way to avoid resonant scattering so that only pure dust absorption is operative is to have the layer move with sufficiently large bulk velocity so that the line is shifted out of the Doppler core. How large a column density in neutral hydrogen can be tolerated without significant resonant scattering then depends on how fast the layer is moving away from the line source. We plot in figure 7 this critical neutral hydrogen column density, N_{HI}^{critic} , against the layer bulk velocity for gas at $T_e = 10^2, 10^4, \text{ and } 10^6$ K where N_{HI}^{critic} is defined as the N_{HI} (measured in the comoving frame) that gives $\tau_{H^0_{scat}}=1$ (see Appendix B, § 1). Thus, resonant scattering may be ignored for layers with a neutral hydrogen column density lying below the curves. The "steps" in the curves correspond to where the line is shifted from the core into the wings. It is evident that N_{HI}^{critic} is very low ($< 10^{14} \text{ cm}^{-2}$) unless the bulk velocity is very high. In order to have $A_V \geq 1$, we require $N_{HI} \geq 10^{20} \text{ cm}^{-2}$ (assuming $T_e = 10^4$ K and $\mu \approx 1$), which requires $V \geq 500 \text{ km s}^{-1}$) from figure 7. Aside from the issue of how to accelerate the layers to such high bulk velocities, there remains the problem that these clouds must be constantly replenished from some unknown source. This replenishing must be very efficient and continuous because the narrow-line gas in the dust screen is at $T_e=10^4$ K) and has $N_{HI} \geq 10^{20} \text{ cm}^{-2}$, the screen itself should have significant emissivity in lines such as $H\alpha$ and $H\beta$, unless the screen is placed sufficiently far outside the NLR so that geometric dilution reduces the impinging ionizing flux to insignificant levels. Otherwise, one should see highly blueshifted lines (from the screen) in addition to the usual lines from the NLR. This is not observed.

Without invoking bulk motion, another way to make the pure dust screen viable is to make the gas in the dust screen very cold relative to the width of

Figure 10:

The critical neutral hydrogen column density, N_{HI}^{crit} , of the dust screen vs. the screen's bulk velocity, V . The quantity N_{HI}^{crit} is defined as the column density (measured in the comoving frame) giving Ly α resonant scattering optical depth of unity ($\tau_{H^0_{scat}} = 1$). The region below the curves have $\tau_{H^0_{scat}} < 1$. The curves correspond to a dust screen gas temperature of 10^2 K (*dashed*), 10^4 K (*solid*), and 10^6 K (*dot-dashed*). The "step" in each of these curves correspond to where the line is shifted from the core into the wings. The impinging Ly α line is assumed to be monochromatic at the line center (as measured in the line source frame).

Figure 11:

The fraction of energy, f , in the Ly α line impinging on the dust screen that suffers interactions with the screen's gas vs. the neutral hydrogen column density, N_{HI} , of the screen. The horizontal dotted line corresponds to $f=0.01$. The curves correspond to $\kappa = \delta V_S/\delta V_a = 10$ (*solid*), 10^2 (*dashed*), and 10^3 (*dot-dashed*), where δV_S is the width (in velocity units) of the impinging Ly α line and δV_a is the width of the Ly α resonant scattering line profile for the gas in the dust screen.

the line impinging on the screen. In this manner, only a very narrow band about line center will suffer resonant scattering within the screen. In Figure 11 we plot the fraction of the impinging energy in the Ly α line (assumed to have a gaussian profile) that suffers interactions with neutral gas atoms in the screen as a function of the neutral hydrogen column density of the screen (see Appendix B, § 2). The horizontal line shows where 1% of the incoming line energy suffers interactions. The curves are labeled by the width of the impinging line (expressed in velocity units) relative to the width (in velocity units) across which the line will interact with the gas in the screen. Typical line widths for the NLR Ly α emission line is $\sim 10^3 \text{ km s}^{-1}$. It is evident from Figure 11 that even for (screen) gas at $T_e=10^2 \text{ K}$ so that $\kappa = \delta v_s/\delta v_a = 10^3$, the critical neutral hydrogen column density (to have 1% interaction or less) is only $\sim 10^{16} \text{ cm}^{-2} \sim N_H$, corresponding to $A_V \sim 5 \times 10^{-6} \mu$. Thus, a cold screen is unfeasible because the low hydrogen column densities it requires (to avoid resonant scattering) imply negligible absorption by dust internal to the screen.

We conclude that either with bulk motion or with a very cold cloud, the pure dust screen model is not physically plausible. The only scenario we can conceive of where a pure dust screen might work is a "coronal" model wherein the dust is

embedded in a *very* highly ionized, and hence very hot ($T_e \sim 10^6$ K), and tenuous ($n_e \sim 10 \text{ cm}^{-3}$) medium. Assume for now that dust can exist in significant quantities in this coronal gas. To have $A_V \sim 1$ require $N_H \sim 10^{21} \text{ cm}^{-2}$ for $\mu=1$, or $N_H \sim 10^{22} \text{ cm}^{-2}$ for $\mu=0.1$. With $n_e \sim 10 \text{ cm}^{-3}$, this corresponds to a coronal region with linear size $L \sim 10^2 \text{ pc}$ ($\mu=1$) or $L \sim 10^3 \text{ pc}$ ($\mu = 0.1$). In the former case, the size is comparable to the size of the NLR. While the existence of such a region external to the NLR cannot be ruled out, it is somewhat ad hoc. In the latter case, the large volume required for the coronal region almost surely implies that the corona would cover the whole NLR. In this case, one would expect the same dust in the coronal gas that affects the narrow lines to redden the starlight from the central galactic buldge. This reddening is generally not observed.

The properties of the coronal gas is probably not all that different from those of the intercloud medium in the NLR, if we assume a two phase medium for the NLR with the two phases (cloud and interclouds) being in pressure equilibrium. If so, then postulating a separate corona outside the NLR seems superfluous; it would be more natural to assume dust to be present in the NLR intercloud medium itself. If, however, one is to consider dust in the intercloud medium, then one should also consider dust in the clouds themselves. The narrow lines produced within the NLR cloud would then be affected in general by dust in both the cloud and intercloud medium. With regard to dust survival, it is likely that both evaporation (owing to the high gas temperature) and sputtering will render the dust life-times to be shorter in the coronal-like intercloud medium than in the clouds. The main dust destruction process inside the clouds is sputtering which gives a dust lifetime of $\sim 10^5 \text{ yr}$ (assuming $n_e \sim 10^3 \text{ cm}^{-3}$ and $T_e \sim 10^4 \text{ K}$). In the NLR model we adopt, we assume that dust is able to be replenished on such time scales inside the clouds to enable a significant dynamic steady state abundance of dust to be present. This replenishment is probably more difficult to achieve in the coronal-like intercloud medium and in our model, we assume that dust is not present in any significant quantities in the intercloud medium.

2.4.3 The partially covering models

One obvious advantage of a simple interpretation for the position of all the objects in Figure 9 rather than the two separate pure dust and pure line scattering interpretations is that it might be more informative of the NLR geometry. Although the $\text{Ly}\alpha/\text{H}\beta$ observed is much below that predicted by the “f” + “b” models, some of the objects are not that far from the pure perspective “b” models (see dot-dash line in Fig. 9). This naively suggests a nonnegligible covering factor for the emission region in which individual clouds partly cover one another in the line of sight to the external observer. Although plane-parallel calculations do not allow us to replicate very accurately such a geometry, a first order estimate of the effects involved can nevertheless be arrived at. For instance, we can safely expect the $\text{Ly}\alpha$ luminosity to be dominated by the few uncovered clouds which are directly

seen from the front (i.e., “f” clouds). The Balmer lines in our simplified scheme would essentially come from three different components: the few “f” clouds seen directly, the many “b” clouds seen from the back, and finally the “f” clouds seen through other clouds and which we postulate are seen through a depth statistically equivalent to a single cloud (we neglect multiple cloud covering). By assuming that the transmitted spectrum of each covered “f” cloud is approximately equivalent to that of a “b” cloud ⁴, we can readily estimate the main effects of a partially covered geometry by simply giving more weight to the “b” clouds, i.e., “f”+ γ “b”.

In Figure 12, we present the loci of “f”+“b” calculations in which the weight γ takes on the values of 1, 3, 10, 30, 100, and 300 using photoionization calculations in which the dust content $\mu(H^*)=0.2$. For a given value of γ , the solid line tracks result from varying the depth of neutral gas $N_{H^0}^0$ (beyond the PIZ). Since the dust content within the neutral zone $\mu(H^0)$ (see eq.[3]) might be plausibly be different from $\mu(H^*)$, we specify $N_{H^0}^0$ in Figure 12 in terms of the dust opacity in the visible, $\tau_V(H^0)$ [leaving $\mu(H^0)$ unspecified; see tick marks]. Considering the size of error bars (*dotted lines*) which characterizes the data, we find very encouraging that the tracks pretty much cover the whole region occupied by all the Seyfert 2 observations.

Even if the tracks are only crude estimates and are not unique in terms of the parameter $\mu(H^*)$, they succeed in illustrating that a very simple and self-consistent mixture of internal line scattering and dust absorption can explain the observed ratios without the need for ad hoc intervening screens. We infer from this exercise that the NLR HI line ratios points toward a significantly self-covered distribution of gas which is very patchy and where all the Ly α originates from ionized gas in direct view of the observer.

If this conclusion is valid, it is possible to study one limiting case of this picture by supposing the covering factor to be so high that spherical geometry becomes a preferable representation of the NLR (and which at least addresses the effects of multiple scattering inside the geometry, a possibility excluded when considering only independent slabs).

Adopting spherical geometry, we will represent the NLR as a Strömberg sphere uniformly surrounded by a layer of neutral gas of opacity $\tau_V(H^0)$ except for a small area where the ionized sphere is not covered as depicted in Figure 13. As in the simple partial covering model discussed above, Ly α escapes exclusively from the region which is uncovered. The Balmer lines, on the other hand, emerge through both the uncovered area and the neutral dust outer layer.

To compute in spherical geometry and yet retain an adequate treatment of the transfer through dust, we integrate the emissivity of volume cells within either the near-side hemisphere “b” or the far-side hemisphere “f”. For the line transfer we

⁴A zero-order approximation based on the fact that the fully ionized zone is only a small fraction of the whole cloud and therefore any “b” spectrum is really seen through a screen of dust of depth comparable to that given by the whole slab.

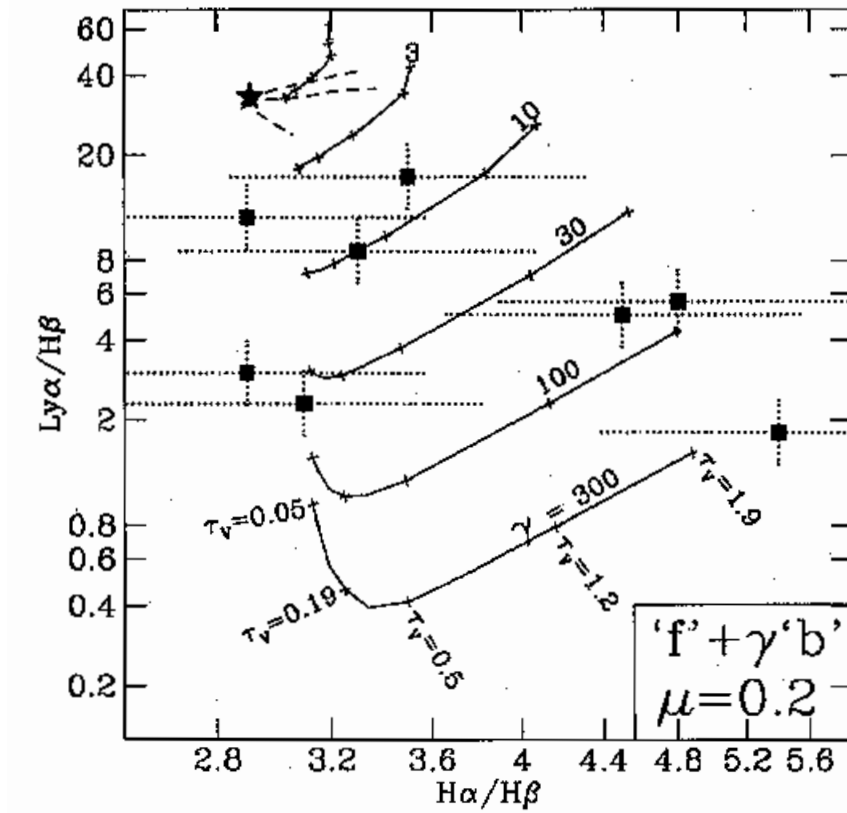


Figure 12:

Same observations as in Fig. 9 but compared with the partially covering model using $\mu(H^*) = 0.2$ (see eq.[3]) and with the line fluxes obtained by giving a higher weight γ to perspective “b” (“f” + γ “b”). For a given value of γ , the solid line illustrates the effect of increasing the neutral zone depth, $N_{H^0}^0$, characterized by a dust content $\mu(H^0) = 1.0$. The tick marks from left to right correspond to opacities of the $N_{H^0}^0$ zone of $\tau_V = 0.05, 0.19, 0.5, 1.2$ and 1.9 [for example, with $\mu(H^0) = 1.0$ these correspond to $N_{H^0}^0 = 10^{20}, 4 \times 10^{20}, 2.5 \times 10^{21}$ and $4 \times 10^{21} \text{ cm}^{-2}$, respectively]. The three dash lines correspond to the same μ sequences drawn in Fig. 8 (“f”+“b”)

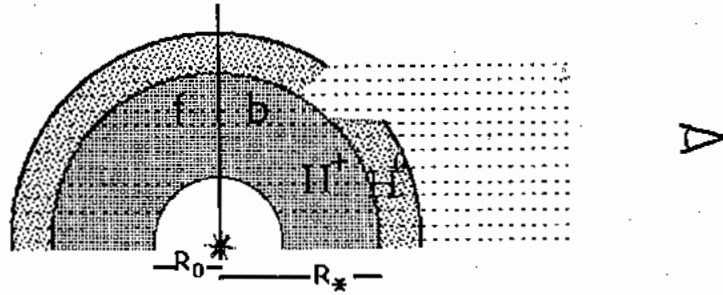


Figure 13:

Schematic depiction of the spherical geometry assumed for the NLR. The photoexcited sphere of radius R_* and dust content $\mu(H^*)$ is divided into two hemispheres “f” and “b”. The integral of the emissivity of each hemisphere is integrated along 10 concentric cylinders whose axis defines the observer’s perspective. The photoexcited sphere is surrounded by a neutral shell of gas of dust content $\mu(H^0)$ and opacity $\tau_v(N_{H^0}^0)$. A small area of the sphere is uncovered from which some Ly α escape probability is determined radially starting from the inner gas radius R_0 .

use the dust opacity occurring between each cell and the surface of the sphere along the direction of the observer’s line of sight. The ionization and thermal structure are calculated, as usual, radially from the inner gas radius R_0 up to the limit of the photoexcited region R_* . For the line opacity, the integral extends out to include the outer neutral layer. The line emissivity cells are defined by the intersection of the photoionized spherical layers (used in the calculation of the radial ionization structure) of either hemisphere : “f” or “b” with concentric cylinders oriented along the lines of sight to the observer. In this scheme, we are in effect simulating the use of 10 concentric ring apertures of an observer which is looking at the spherical NLR. The global model is the sum of 10 “f” + “b” cylindrically integrated contributions.

Supposing no external neutral gas layer, we find that for the same amount of dust $\mu(H^*)$ and column density of ionized gas $N_{H^+}^S$, the spherical geometry results in a reduced Ly α /H β compared to the slab “f” + “b” case, resembling in fact more the “b” perspective of the slab case. This is understandable given that the direction of the gradient ionization structure (n_{H^0}/n_H increasing with radius) seen by an observer external to the H $^+$ sphere is similar to that of a slab looked up from perspective “b”. We emphasize that the effect of clumpiness of the ionized gas (which we do not consider in the transfer) would be more consistent with the geometry of a large number of clouds superposed along the line of sight. This would allow a larger fraction of Ly α to escape the ionized region as argued by Neufeld (1991), although the implementation of such effects is beyond the scope of this work.

To derive the emergent spectrum for the partially uncovered case, we simply combine the spectra of the fully covered sphere -excluding the contribution of a

certain number of aperture rings- with the corresponding missing aperture rings of a spherical model calculated without any external gas layer covering the “b” hemisphere. Note that in the dust-free case, such procedure would underestimate the emerging Ly α by a factor of 2. With the presence of internal dust, the treatment is only approximate and rests on the reasonable assumption that most of the Ly α scattering is local to the point of emission an approximation which is increasingly valid as μ increases since a photon which would scatter too many times over a length scale of order R_* will likely be destroyed. Furthermore, the resonant photon does not know a priori where the hole in the outer layer is and will likely be absorbed in the much larger neutral outer zone which covers the ionized sphere.

The results are presented in Figure 14 where the amount of uncovered area is expressed as a fraction of the total projected emitting area πR_*^2 . The parameters of the models were derived as follows. As for the slab case, we adjusted the ionization parameter of the spherical radiation-bounded models until $[\text{OIII}]\lambda 5007/\text{H}\beta \sim 10$ (by varying the source luminosity in the center and/or the volume filling factor of the infinitesimal gas filaments). The ionizing continuum is the same as before, the density at R_0 is 5000 cm^{-3} and the gas pressure is maintained constant with radius. The resulting photoexcited sphere in our calculations has $R_*/R_0 \sim 2.4$ and $N_{H^*} \sim 6.3 \times 10^{20} \text{ cm}^{-2}$. The electron column density in $N_e = 2.1 \times 10^{20} \text{ cm}^{-2}$ which is exactly the same as for the reference slab model $\bar{U} = 0.0013$. Because more Ly α is destroyed in spherical geometry, we have assumed smaller values for $(\mu(H^*))$, [See, for instance, the long dash line in Fig. 14 which corresponds to models with $\mu(H^*) = 0.4$, a clearly excessive value.]

The solid lines in Figure 14 correspond to models with a small internal dust content ($\mu(H^*) = 0.1$). The dust opacity of the external layer takes on the values of $\tau_V(H^0) = 0.5$ (*leftmost solid line*) and $\tau_V(H^0) = 2.4$ (*rightmost solid line*). From the position of the near-case B objects on the left, we infer that their NLR is probably less deeply embedded in dust [$\tau_V(H^0) \sim 2-3$]. The fraction of the uncovered area runs from 30% to as little as 3.0%-0.3%. Overall, the models bracket quite well the region occupied by the Seyfert 2 observations.

2.4.4 Dust and the UV continuum

It is not clear how representative of Seyfert 2 the sample of KAW3 is since as many as five objects of the 12 objects in Figure 9 show evidence of properties assigned to Seyfert 1. These include either a very weak BLR either seen directly as in Mrk 348 and NGC4388, or seen in polarized light as in Mrk 348, Mrk 3, and Mrk463 (also NGC4388), or variability of the featureless continuum as in Mrk 477. Unification models of Seyferts have been proposed in which Seyfert 2's present a very thick torus which hides direct view of the BLR as a result of its inclination (see, for instance, Antonucci & Miller 1985; Krolik & Begelman 1988). Our conclusion from §2.4.3 is that the ionized gas regions responsible for the emission lines are at least partly covered by large amounts of gas and dust with Ly α emerging from

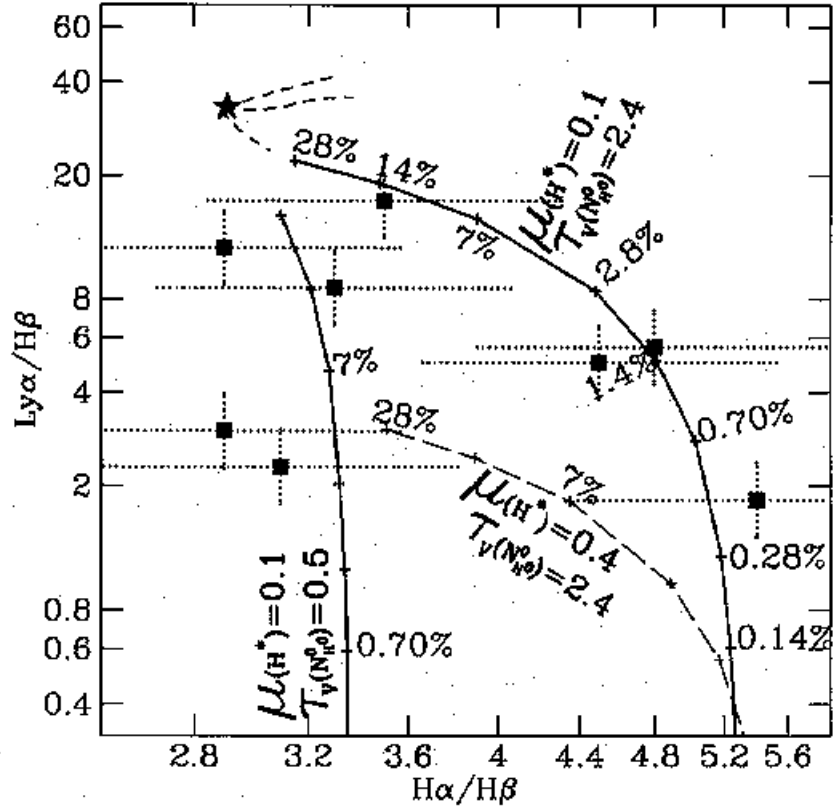


Figure 14:

Same observations as in Fig.9 but compared with the spherically closed geometry calculations. The ionized sphere is surrounded by an outer shell of neutral gas $N_{H^0}^0$ [with dust content $\mu(H^0)$; see eq.[3]) which we express in terms of dust opacity $\tau_V(H^0)$. The curves represent the effect of having a hole in this shell which directly exposes part of the Strömgen sphere and allow some Ly α to escape out. Models with internal dust content $\mu(H^*)=0.1$ and either $\tau_V(H^0) = 0.5$ or 2.5 are shown as solid lines. The long dash line corresponds to a model with a higher internal dust content in the ionized region with $\mu(H^*)=0.4$. Tick marks along each curve represent the percentage of the uncovered area relative to the sphere's projected emitting area (πR_*^2).

the least covered regions. According to this picture, we would expect the nuclear continuum to be reddened as well. We will present briefly some arguments which favor continuum reddening, a possibility earlier studied by Boisson & Durret (1986) (see also Carleton et al. 1987), although the idea of an extinction free continuum is more commonly accepted (e.g., FO86, KAW3).

KAW3 performed an important test on the photon budget of the nuclear engine by extrapolating the power laws which they had fitted to their IUE spectra and deriving the number of ionizing photons N_{ion}^{obs} which originates from the nucleus (assuming an isotropic source). After comparing with the number of recombination photons deduced from the $H\beta$ luminosity N_{rec}^{der} (using the *dereddened* $H\beta$ flux and assuming a covering factor of unity), they found that most objects showed a clear deficit of ionizing photons ($N_{rec}^{der}/N_{ion}^{obs} > 1$), which they concluded as favoring the “occultation/reflection picture” of Antonucci & Miller (1985). According to this picture, the ionizing photons stream out freely only along the axis of the torus axis and are sufficiently numerous to account for the luminosity of the HI recombination lines (although the continuum observed in our direction [off-axis] is too weak to account for them).

Although the “occultation/reflection picture” is supported by other independent arguments, there remains, however, an unresolved paradox (see Binette, Fosbury & Parker 1993): if $H\beta$ of the large NLR is so much reddened (and considering a closed geometry for the NLR), why is the nuclear continuum of comparatively pointlike size not reddened at all? Interestingly, using other IUE Seyfert observations, Boisson & Durret (1986) as well as Carleton et al. (1987) concluded that there is no deficit of ionizing photons if dereddening of the nuclear continuum is taken into account. The important argument against continuum reddening given by KAW3 is that the 2175 Å ($10^{15.14}$ Hz) dust absorption feature was not present in their featureless continua. Although this seems to be clearly the case for objects like NGC 1068, we are not strongly convinced that this feature is totally absent from some of their spectra given the noise level present. In particular, objects like Mrk 3 and possibly NGC 4388 show plausible hints of such a feature. Furthermore, the absence of the 2175 Å feature is not so compelling if we consider the possibility that the properties of the dust in AGNs might differ from that in the Galaxy. After all, we know that dust grain properties depend strongly upon the environment in which they form (Whittet 1992).

One way of addressing the issue of extinction of the nuclear “nonstellar” continuum is to look at possible hints of correlation of the inferred deficit of ionizing photons with the IUE spectral index as well as with the amount of reddening inferred from the Balmer decrement. We present in Figure 15 the results of such an attempt based upon the KAW3 data set. Note that we plotted in abscissa the quotient $N_{rec}^{der}/N_{ion}^{obs}$ which differ from KAW3 in that it is based on the observed $H\beta$ *not* corrected for reddening (since we want to model all the observed quantities as a function of extinction). Although the correlations of Figures 15a and 15b are

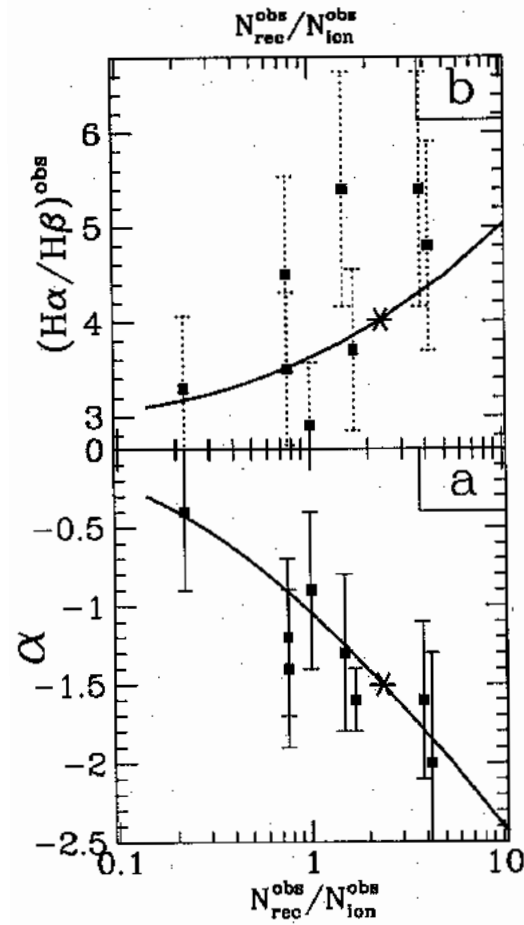


Figure 15:

In panel (a), the power-law index α vs. the ratio $N_{rec}^{obs}/N_{ion}^{obs}$. The spectral index α corresponds to the power-law fit by KAW3 of the observed continuum energy distribution between 2600 Å and 1300 Å. In panel (b), the observed Balmer decrement is plotted as a function of $N_{rec}^{obs}/N_{ion}^{obs}$. The ratio $N_{rec}^{obs}/N_{ion}^{obs}$ differs from KAW3 in that the *observed* value of the H β flux is used to derive the number of recombination photons instead of using the reddening-corrected H β flux. The solid line is a model representing the effect of increasing dust extinction on an intrinsic power-law ionizing continuum of index $\alpha = -0.3$ assuming a covering factor of 15% (panel [a]) and an intrinsic Balmer decrement of 3.1 (panel [b]). The apparent index α of the calculated transmitted spectrum is derived by simply using the flux ratios at 2450 Å and 1310 Å. The star represents the locus of a model with a shell dust extinction of $\tau_V=1.3$.

not statistically significant, given the magnitude of the errors, the data is not inconsistent with a simple reddening model (*solid line*) described below and applied to an intrinsic power law of index $\alpha = -0.3$ (assuming the gas covering factor and the continuum's shape to be intrinsically the same in *all* the objects).

To obtain the theoretical results represented by the solid line in Figure 15, we illuminate isotropically a slab of dust with opacity τ_V with an $\alpha=-0.3$ power-law continuum and a one-parameter sequence of slab models in τ_V . For each model, we compute the emergent reddened α (defined by the flux ratios at 2450 Å and 1310 Å) in the calculated transmitted dust extinction (τ_V on the observed $N_{rec}^{der}/N_{ion}^{obs}$ starting with an unreddened value $(N_{rec}^{der}/N_{ion}^{obs})_0=0.15$, corresponding to a gas covering factor of 15% (varying the covering factor simply slides the curve horizontally). In figure 12b we present the intrinsic ratio of 3.1. The standard extinction curve has been assumed in our model. Details on the transfer solution for the continuum and for the lines are given in Appendix C.

We have assumed the impinging flux to be isotropic in order to approximate a shell layer of dust illuminated by a pointlike central source; a more appropriate treatment which distinguishes the isotropic optical lines from the radio continuum flux will be the subject of subsequent work. Because both the continuum and H β are reddened by the same amount of dust, the equivalent width of H β is independent of τ_V in our slab treatment. Although the index $\alpha = -0.3$ is rather flat, it is not at odds with the range -0.08 to +0.11 denoted by Shuder (1981) (for the case of a covering factor of 10%) in his study of the proportionality between continuum and H α luminosity in various classes of AGNs (see also Binette, Fosbury & Parker 1993).

Comparing Figures 15a and 15b, the slope of the model in the case of the Balmer decrement panel seems too low. This could be a consequence of an inhomogeneous covering of the nuclear dust as proposed in §2.4.3 for the HI lines (Figs. 13 and 14). Since $N_{rec}^{der}/N_{ion}^{obs}$ and α depend mostly on the UV part of the spectrum which is very sensitive to small amounts of dust, these quantities are expected to be strongly weighted towards the least obscured regions, while the optical Balmer lines may merge from more obscured regions.

Despite the recognized validity of the “occultation/reflection picture” in explaining cones of ionization and hidden polarized BLR in some Seyfert 2's, it remains important to test further whether the nuclear continuum is as reddening free as generally assumed and, therefore, whether part of the apparent deficit in the ionizing radiation does not simply result from dust extinction.

References

- Anders E., Grevesse N., 1989, *Geochim. Cosmochim. Acta*, 53, 197
- Antonucci R.R., Miller J.S., 1985, *Astrophys. J.*, 297, 621
- Baldwin J.A., Ferland G.J., Martin P.G., Corbin M.R., Cota S.A., Peterson B.M., Slettebak A., 1991, *Astrophys. J.*, 374, 580
- Barvainis, R., 1992, *Astrophys. J.*, 400, 502
- Binette L., Dopita M.A., Tuothy I.R., 1985, *Astrophys. J.*, 297, 476
- Binette L., Robinson A., Courvoisier T.J.L., 1988, *A&A*, 194, 65
- Binette L., Calvet N., Cantó J., Raga A.C., 1990, *Pub. Astr. Soc. Pac.*, 102, 273
- Binette L., Magris C.M., Martin P.G., 1993a, *Ap&SS*, 205, 141
- Binette L., Wang J.C.L., Zuo L., Magris C.M., 1993b, *Astron. J.* 105, 797 (BWZM)
- Binette L., Fosbury R.A.E., Parker D., 1993, *Pub. Astr. Soc. Pac.*, 105 1550
- Boisson C., Durret F., 1986, *A&A*, 168, 32
- Bruzual A., Magris C.M., Calvet N., 1988, *Astrophys. J.*, 333, 673
- Carleton N.P., Elvis M., Fabbiano G., Willner S.P., Lawrence A., Ward M., 1987, *Astrophys. J.*, 318, 395
- Chandrasekhar S., 1960, *Radiative Transfer* (New York: Dover)
- Cimatti A., di Serego Alighieri S., Fosbury R.A.E., Salvati M., Taylor D., 1993, *Mon. Not. Roy Astr. Soc.*, 264, 421
- Clavel J., Wamsteker W., Glass I.S., 1989, *Astrophys. J.*, 337, 236
- Cohen R.D., 1983, *Astrophys. J.*, 273, 489
- Crosas M., Weisheit J.C., 1993, *Mon. Not. Roy Astr. Soc.*, , 262, 359
- De Zotti G., Gaskell C.M., 1985, *A&A*, 147, 1
- DeRobertis M.M. & Osterbrock D.E., 1984, *Astrophys. J.*, 286, 171
- DeRobertis M.M. & Osterbrock D.E., 1986, *Astrophys. J.*, 301, 727
- Draine B.T., 1978, *ApJS*, 36, 595
- Ferland G.J., Netzer H., 1979, *Astrophys. J.*, 229, 274
- Ferland G.J., Netzer H., 1983, *Astrophys. J.*, 264, 105
- Ferland G.J., Osterbrock D.E., 1985, *Astrophys. J.*, 289, 105
- Ferland G.J., Osterbrock D.E., 1986, *Astrophys. J.*, 300, 658
- Filippenko A.V., 1985, *Astrophys. J.*, 289, 475
- Fosbury R.A.E., 1993, in *The Nature of Compact Objects in AGN*, ed. A. Robinson & R.J. Terlevich (Cambridge: Cambridge Univ. Press)

- Gaskell C.M., 1984, *Ap.Letters*, 24, 43
- Gaskell C.M., Ferland G.J., 1984, *Pub. Astr. Soc. Pac.*, , 96, 393
- Halpern J.P., Steiner J.E., 1983, *Astrophys. J.*, 269, L37
- Hummer D.G., Kunasz P.B., 1980, *Astrophys. J.*, 236, 609
- Hummer D.G., Storey P.J., 1987, *Mon. Not. Roy Astr. Soc.*, 224, 801
- Johnson L.C., 1972, *Astrophys. J.*, 174, 227
- Kinney A.L., Antonucci R.R.J., Ward M.J., Wilson A.S., Whittle M., 1991, *Astrophys. J.*, 377, 100
- Krolik J.H., Begelman M.C., 1988, *Astrophys. J.*, 329, 702
- Kwan J., Krolik J.H., 1981, *Astrophys. J.*, 250, 478
- Lilly S.J., 1988, *Astrophys. J.*, 333, 161
- Magris C.G, 1985, in senior physics thesis, Universidad Simón Bolívar and CIDA, Venezuela
- Magris C., G., Binette L., & Martin. P. G., 1993, in proc. The Nearest Active Galaxies, ed. J. Beckman; Astrophysics and Space Science, 205, p. 141
- Malkan M.A., 1983, *Astrophys. J.*, 264, L1
- Martin P.G., Rouleau F., 1991, in Extreme Ultraviolet Astronomy, ed. R.F. Malina & S. Bowyer (Oxford: Pergamon), 341
- Morganti R., Robinson A., Fosbury R.A.E., di Serego Alighieri S., Tadhunter C.N. Malin D.F., 1991, *Mon. Not. Roy Astr. Soc.*, 249, 91
- Netzer H., ., 1993, in Proc. Madrid Meeting on The Nearest Active Galaxies, ed. J.E. Beckman, H. Netzer & L. Colina, 219
- Netzer H., Laor A., 1993, *Astrophys. J.*, 404, L51
- Neufeld D.A., 1990, *Astrophys. J.*, 350, 216
- Neufeld D.A., 1991, *Astrophys. J.*, 370, L85
- Osterbrock D.E., 1989, *Astrophysics of Gaseous Nebulae and Active Galactic Nuclei* (Mill Valley: University Science Books)
- Pelat D., Alloin D., Fosbury R.A.E., 1981, *Mon. Not. Roy Astr. Soc.*, 195, 787
- Pier E.A., Krolik J.H., 1992, *Astrophys. J.*, 401, 99
- Puetter R.C., Hubbard E.N., 1987, *Astrophys. J.*, 320, 85
- Sanders D.B., et al. 1989, *Astrophys. J.*, 347, 29
- Shuder J.M., 1981, *Astrophys. J.*, 244, 12
- Shull J.M. & van Steenberg M., 1985, *Astrophys. J.*, 298, 268
- Slater G., Salpeter E.E., Wasserman I., 1982, *Astrophys. J.*, 255, 293

Tadhunter C.N., Robinson A., Morganti R., 1989, in ESO Workshop on "Extranuclear Activity in Galaxies", ed. E.J.A. Meurs, Fosbury R.A.E. Fosbury, ESO Conf. and Workshop Proc. No.32, Garching, p.293

Viegas S.M., Prieto A., 1992, *Mon. Not. Roy Astr. Soc.*, 258, 483

Whittet D.C.B., 1992, *Dust in the Galactic Environment* (Bristol:IOP)

Chapter 3

Calcium depletion and the presence of dust in large scale nebulosities in radio galaxies (I).

Villar-Martín & Binette 1995, A&A, in press

Abstract

We show that the study of the Calcium depletion is a valid and highly sensitive method for investigating the chemical and physical history of the very extended ionized nebulae seen around radio galaxies (EELR), massive ellipticals and ‘cooling flow’ galaxies. By observing the near IR spectrum of nebular regions characterized by low excitation emission lines (LINER-like), we can use the intensity of the [CaII] $\lambda\lambda 7291, 7324\text{\AA}$ doublet –relative to other lines, like H α – to infer the amount of Calcium depletion onto dust grains. The presence of dust in these objects – which does not necessarily result in a measurable level of extinction– would favour a ‘galactic debris’ rather than a ‘cooling flow’ origin for the emitting gas. Before applying such test to our data, we study four possible alternative mechanisms to dust depletion and which could have explained the absence of the [CaII] lines: a) ionization of Ca⁺ from its metastable level, b) thermal ionization of Ca⁺, c) a high ionization parameter and/or a harder ionizing continuum than usually assumed and d) matter bounded models associated to a hard ionizing continuum. We show that none of these alternative mechanisms explain the absence of the [CaII] lines, except possibly for the highly ionized EELR where a high ionization parameter is required combined with a soft power law. We thus conclude that for the other low excitation emission regions (cooling flows, liners, low excitation EELR), the absence of the CaII lines *must* be due to the depletion of Calcium onto dust grains.

3.1 Introduction

The study of the interstellar medium (ISM) of external galaxies provides important information about the global kinematic (inflow, outflow) of such gas, its chemical composition and the implied star formation history, its mass distribution, etc. This gas forms a vital part of the record of the formation of the parent galaxy, and the evolutionary processes involved.

How can this material be studied in details? One way is to have it illuminated or excited by a powerful AGN, giving rise to the phenomenon of extended emission line region (EELR). The drawback of course is that it only allows us to look at a restricted class of galaxy. The large scale EELR phenomenon is observed in a majority of the most powerful radiogalaxies with EELR extending to radial distances of up to 100 kpc from the nuclei (Tadhunter 1986; Baum et al. 1988), much larger radii than the stellar population distribution of the parent galaxy. The morphologies and kinematics of such regions cover the full range from regular disc/ring systems to chaotic systems for which no pattern can be discerned. Their spectra show strong emission lines, covering a wide range in ionization. It is generally accepted that the EELR are ionized by some mechanism connected with the nuclear activity, but there is no full consensus on the excitation mechanism. Some objects show evidences for an interaction between the radio jets, which transport energy to the outer radio lobes, and the gas in the outer region. Maybe this interaction is responsible of the excitation of the gas through some kind of shocks (Sutherland, Bicknell & Dopita 1993). For other objects, that do not show evident spatial coincidence between the radio structures and the EELR, the excitation might be due to direct photoionization by the nuclear ionizing radiation field (Robinson et al. 1987: hereafter RBFT87). A reduced scale version of the EELR is the one observed in many Seyfert galaxies (Haniff, Ward & Wilson 1988) where the ionized gas may extend up to a few kpc although it is brightest within the central 100–300pc. The EELR morphology tends to be conical (Wilson & Tsvetanov 1994). Its detailed observation is complicated by the presence of the very luminous stellar background of the bulge. In normal bright ellipticals, quite weak extended nebulosities of low excitation are a common phenomenon (Buson et al. 1993, Goodfroid 1994). The very large scale gas around radio-galaxies, on which we focus here, presents the advantage that the lines are observed against the sky background rather than against the bright parent galaxy bulge.

The origin of the gas making up these *large scale* extended nebulosities remains unknown. Furthermore, the distinction between these and the filamentary nebulae seen in some clusters and around some massive ellipticals and often identified with cooling flows, is unclear. We do know, however, that this gas in every case is chemically enriched as compared to primordial gas. Emission line analyses (RBFT87) show common element abundances to be within a factor of a few (\leq) of Solar and also to be rather uniform over all the objects observed.

The two most likely explanations for the origin of the material are:

a) debris from recent tidal interactions and mergers

b) gas cooling from the hot (\sim virial) phase which from X-ray observations (Forman, Jones & Tucker 1985) has been shown to exist around massive ellipticals and inside galaxy clusters

The main arguments behind these explanations are the following:

a) Heckman et al. (1986) showed that a large fraction of powerful radiogalaxies have morphological features –shells, tails, loops, etc– similar to those produced in numerical simulations of galaxy interactions (*e.g.* Toomre and Toomre 1972, Quinn 1984). This could indicate that the activity has been triggered either because fresh gas has been accreted from outside or because preexisting gas in the galaxy has been caused to collapse to the core as a result of the interaction. This interaction scenario is also supported by observations of a few nearby radio galaxies which, apart from morphological peculiarities, show large misalignments between the stellar and the gaseous rotation axes, indicative of an external origin for the gas.

b) Hot X-ray corona ($T \geq 10^4\text{K}$) are a common feature of bright early-type galaxies. Within some critical radius, radiative cooling becomes important, leading to the development of the so-called ‘cooling flow’ hypothesis (Nulsen, Stewart & Fabian 1984, Thomas et al. 1986) Eventually, condensations or filaments could be formed, dense and cool enough to radiate detectable optical emission lines. Most powerful radio galaxies are too distant for the characteristic X-ray emission to be currently detectable, but it is quite plausible that the EELR gas has condensed out of a surrounding cooling flow.

Distinguishing between these alternative hypotheses has been attempted using gas kinematic measurements (Tadhunter, Fosbury & Quinn 1989) which show that the radio galaxy EELR generally have a high specific angular momentum which is difficult to reconcile with the cooling flow picture. An alternative approach is to look for the presence of dust associated with the EELR gas. If the gas has cooled directly from a hot phase, there will have been no opportunity for dust to form, according to the standard cooling flow theory. Any dust introduced from galaxies into the hot intracluster medium will be rapidly destroyed (Draine & Salpeter 1979). We would need a mechanism to produce this dust once the gas has cooled down (Fabian, Johnstone & Daines 1994). If, on the other hand, the material has fallen in during a merger, the dust/gas ratio is expected to have a value appropriate to the gas chemical composition found in normal galaxies.

Determining the presence or absence of dust is important because:

-of its relevance in deriving chemical composition which takes into account the effects of depletion of metals onto dust grains

-of the implication for the star formation history and the ISM evolution: when does dust form? (and so stars?)

-of the effects of dust on the apparent morphology of continuum and line

features: pure absorption (reddening) and/or scattering (blueing/polarization)

We discuss below how the absence of the forbidden [CaII] lines can be used to infer the presence of dust mixed in with the emission gas. We assess in detail all the most plausible *alternative* explanations to that of internal dust for explaining the absence of [CaII] lines. As no acceptable alternative solution is found, we conclude in favour of the validity of the method initially proposed by Ferland (1993). We however adapt and optimize the [CaII] dust detection technique to the context of the EELR studies in which we are involved. The observational results and their interpretation will be presented in a subsequent paper.

3.2 Outline of the method

To investigate how the forbidden Calcium doublet of [CaII] in the infrared is affected by the physical condition encountered in photoionized plasma, we outline first the computer code which we used and then proceed to illustrate how the [CaII] lines might be used to infer dust in the ISM of galaxies and thus our interest in securing these conclusions by closing up the possibility of alternative interpretations.

To compute the emission lines used in our study, we have used the multipurpose photoionization–shock code MAPPINGS described in Chapter 2. The Ca⁺ ion is considered as a five level atom. Its structure is shown in Fig. 16.

3.2.1 The input parameters

We now proceed to define the parameters employed in the calculations. Most of these are derived from our observational knowledge of EELR although we recognize that it is incomplete and can be biased by particular diagnostic tools which are employed.

Metallicity

For definiteness, we adopt a set of solar abundances (Anders & Grevesse 1989) for the trace elements, in line with the finding of RBFT87 who indicated values for the EELR not radically different from solar. The solar abundance of (*not* depleted) atomic Calcium is 2.2×10^{-6} by number relative to hydrogen. Depletion into interstellar dust grains is known to reduce this abundance in the local ISM by a factor of ~ 5000 (Whittet 1992) so that if depletion was taking place in the partially ionized EELR plasma, even a small dust-to-gas ratio might be sufficient to eliminate any detectable trace of atomic Calcium.

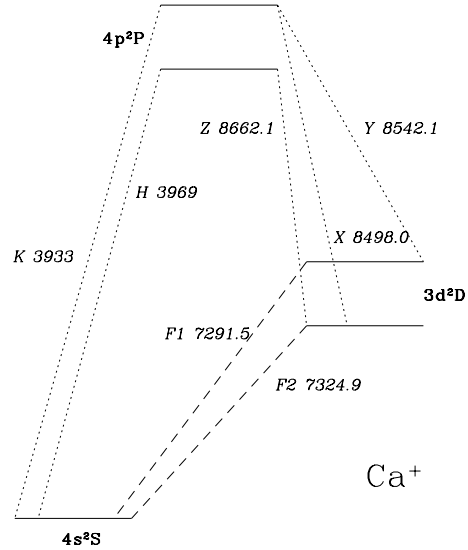


Figure 16:

Energy level diagram for CaII showing the radiative transitions among the five levels considered here. Permitted transitions are represented with dotted lines and forbidden transitions with dashed lines. F1 and F2 are the forbidden doublet lines considered in this work.

Geometry

It's been accepted for a long time that the EELR is formed by individual clouds that are ionized by the central source. In most models presented here, each emitting cloud is considered (see section 2.2.1) like a radiation bounded slab (optically thick to the Lyman continuum) which comprises a fully ionized region, closer to the illuminated face and responsible for the high ionization lines and a partially ionized zone (PIZ), where the low ionization lines like CaII are emitted. Matter bounded clouds will be considered in Sect. 3.3.4. As we want to concentrate on the depletion phenomena, we will simplify the calculations by not considering any neutral region (see Fig. 4, Chapter 2) beyond the PIZ which would contain dust, the effect of which would be to cause additional extinction for an hypothetical and unfavorably placed observer looking from the back of the slab. We have verified that the results reached here using line ratios of similar wavelengths are not altered by the presence or not of this neutral absorbing zone.

Gas density

We adopt a representative density for the EELR clouds of 300 cm^{-3} . Typical electron densities values measured vary between a few tens (or less) to a few hundreds. The densities derived from forbidden line ratios might not apply to every subregion, but they are sufficiently low to consider the low density limit as a generally

valid and very good approximation to the physical conditions affecting the CaII lines of large scale EELR. In the low density regime, the effects of density variations on the emission line ratios which are considered in this paper are very small by comparison to the effects of other parameters like the ionization parameter or the hardness of the ionizing continuum.

The calculations consider the gas pressure to be constant within the cloud (isobaric models) with the density behaviour modulated with depth into the cloud by the behaviour of the temperature and by the ionization fraction of the gas.

The ionizing continuum and the ionization parameter U

We implicitly assume that the dominant ionization mechanism of the ionized gas in radio galaxies is photoionization. It has been shown by RBFT87 that a hard continuum extending well down into the soft X-ray region, despite some discrepancies with the observed spectra, can be considered to reproduce generally well the measured line ratios. This continuum can take its source in the active nucleus or be locally generated (*e.g.* fast shocks: Binette, Dopita, Tuohy 1985). We have considered power law (PL) distributions of various values of α ($F_\nu \propto \nu^{+\alpha}$) as well as hot blackbodies (BB) of temperature $T_{bb} \approx 10^5 K$ in order to study the effects that hardness has on our conclusions.

The ionization parameter, a measure of the excitation level of the ionized gas, was defined in section 2.2.1.

$$U_f = \frac{1}{cn_H^f} \int \frac{\phi_\nu^f}{h\nu} d\nu = \frac{\phi_\nu^f}{cn_H^f},$$

quotient between the density of impinging ionizing photons and the density of the gas cloud.

We find that the parameters having the strongest effect on the line spectrum are the ionization parameter U and the mean ionizing photon energy (*i.e.*, hardness of the continuum).

3.2.2 How to detect dust

How can we detect dust within the gas associated with EELR? We here summarize different techniques and compare their sensitivities.

a) Reddening: given the nature of the gas distribution and the fact that it is ionized externally (unlike HII regions which are internally excited), the extinction may not necessarily be sufficiently high to be easily detected using optical observations. Indeed, the EELR ratios studied by RBFT87 show little or no reddening. Furthermore a small enhancement of the Balmer decrement over recombination

case B might be interpreted as resulting from collisional excitation rather than from reddening.

b) Scattering: polarization measurements of high redshift radio galaxies (di Serego Alighieri et al. 1989, Januzi & Elston 1991, Tadhunter et al. 1992) show conclusive evidence for scattered nuclear light over large volumes and, although there are reasons to believe that the scattering medium is dust, it is difficult to rule out entirely Thomson scattering by electrons. Detailed studies of the low redshift galaxy PKS2152-69 do, however, show polarized continuum radiation from highly excited extranuclear gas cloud with an energy distribution which is so blue that it must arise from dust scattering (Fosbury et al. 1990).

c) Infra-red thermal dust emission: the IRAS satellite has shown that many galaxies radiate significant fractions of their energy in the far infrared spectral region. Significant masses of dust at temperatures of around 40K are responsible for this radiation at wavelengths of $60\mu\text{m}$ and beyond. In many cases the FIR spectral energy distributions is still rising at $100\mu\text{m}$, out of the spectral range detectable by IRAS. The cool dust can only be detected at millimetre and submillimetre wavelengths. A strong limitation of this technique is the very poor spatial resolution of the IRAS satellite. Groundbased studies of the far IR emission of galaxies in the sub-mm range also exist (*e.g.* Clements, Andreani & Chase 1993), but still with poor spatial resolution. Although it is possible to infer masses and temperatures of the warm and cool dust components (dependent on models), the spatial distribution of the dust is not known.

d) Indirect effects on the line spectrum. There are several ways this can happen: effects of dust on the gas temperature (photoionization of dust grains may raise the temperature of the plasma), effects of dust on the ionization structure (dust grains selectively absorb ionizing photons of lower energies), and influence on apparent chemical composition via the depletion of refractory elements onto dust grains. The first effect does not provide a unique interpretation for the unusually high temperatures seen in some EELR (Tadhunter, Robinson & Morganti 1989) while the second effect cannot be discriminated against reliably since even dust-free photoionization models are still too uncertain to be used as absolute reference point. For these reasons, the last effect is the only clearly promising one and is looked into details below.

Calcium is very sensitive to the presence of dust as it is always found to be depleted in the interstellar medium (*e.g.* Crinklaw, Federman & Joseph 1994). Photoionization calculations appropriate to LINERS –a hard ionizing spectrum with a relatively low ionization parameter– invariably predict the [CaII] $\lambda\lambda 7291, 7324\text{\AA}$ doublet ($4s^2S-3d^2D$) to be very strong (Ferland 1993). These two forbidden lines (hereafter F1 $\equiv \lambda 7291\text{\AA}$ F2 $\equiv \lambda 7324\text{\AA}$) have a high critical density $\sim 10^6 \text{ cm}^{-3}$. The latter line, 7324\AA is the weakest of the doublet and is furthermore blended with the [OII] $\lambda 7325\text{\AA}$ multiplet. The other line, $\lambda 7291\text{\AA}$ lies some 30\AA shortward of [OII] and is therefore straightforward to isolate given reasonable spectral resolution. The fact that any of these doublet lines are generally not seen in LINERS

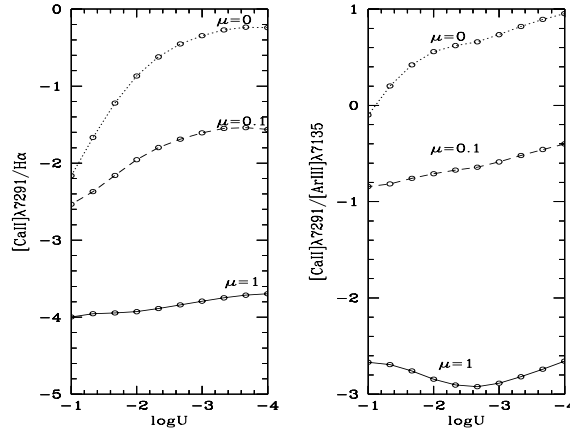


Figure 17:

MAPPINGS photoionization models showing the strength of $[\text{CaII}]\lambda 7291$ relative to $\text{H}\alpha$ (left panel) and $[\text{ArIII}]\lambda 7135$ (right panel) as a function of the ionization parameter U . The models assume solar abundances but with different amounts of dust-to-gas ratios μ expressed in solar neighborhood units. The gas phase abundances of Ca/H for the $\mu = 0, 0.1$ and 1.0 models are 2.2×10^{-6} (no depletion), 9.2×10^{-8} and 4.4×10^{-10} (Whittet 1992), respectively, after taking into account depletion. The hydrogen density is 300 cm^{-3} and the ionizing power law index is $\alpha = -1.4$

but are so in some novae when their envelopes have reached the appropriate ionization level can be interpreted as evidence of Calcium depletion onto dust grains in the former objects. Since EELR which are the subject of our investigation are often seen in the ionization parameter region of the line ratio diagnostic diagrams occupied by LINERS ($10^{-4} \leq U \leq 10^{-3}$), we can similarly use the $[\text{CaII}]$ doublet measurements to infer whether or not there is depletion taking place in EELRs and thus conclude whether dust is also mixed with the gas as is thought to be the case in LINERS.

The above arguments have already been used for several objects with ‘cooling flow’ filaments by Donahue & Voit (1993) to infer the presence of dust mixed with the ionized gas. Ferland (1993) has shown the great sensitivity of this method to the presence of dust under NLR conditions. We now show it to be also the case under EELR conditions. We present two diagnostic diagrams in Fig. 17, the ratio $[\text{CaII}]/\text{H}\alpha$ (7291/6563) and the ratio $[\text{CaII}]/[\text{ArIII}]$ (7291/7135) as a function of the ionization parameter U . The variable parameter distinguishing the three different sequences in U is μ , the dust-to-gas ratio of the plasma expressed in units of the solar neighborhood dust-to-gas ratio. The dramatic difference in line ratios between the grain depleted Ca/H ($\mu > 0$) and the undepleted case ($\mu = 0$), shows the sensitivity of this method, particularly for low values of U .

3.3 Possible alternative explanations to depletion.

Before we carry the conclusions of the current analysis to the interpretation of our observations (Chapter 4), we report first on our effort in investigating other possible alternative mechanisms to dust depletion. If the warm Ca^+ region predicted by standard models does exist, then Calcium depletion becomes the only reasonable explanation for the non detection of the doublet lines. What we consider in this section is the possible NON EXISTENCE of the emitting [CaII] region by investigating different mechanisms which could eliminate it. During our investigation, we require however that successful models do not result in important discrepancies with other observed line ratios. The mechanisms we have considered to eliminate the [CaII] region are

- Ionization of Ca^{+*} by $\text{Ly}\alpha$ and soft continuum photons from the metastable level of Ca^+
- Thermal (collisional) ionization of Ca^+
- Photoionization with a much harder continuum or a much higher U than usually assumed

3.3.1 Ionization by $\text{Ly}\alpha$ and soft continuum photons.

Wyse (1941) proposed that the ionization of CaII from the metastable level by $\text{Ly}\alpha$ photons, could explain the fact that the IR lines of CaII at 8498, 8542 and 8662Å appear in emission near the maximum phase of Me variables, whereas the H and K lines only occur in absorption. Trapped $\text{Ly}\alpha$ photons could also play a part in ionizing metastable Ca^{+*} as suggested by Wallerstein et al. (1986).

We investigate here if this process is important under the conditions found in EELR clouds. In order to do this, we add two terms to the ionization equilibrium equation of CaII. One which considers photoionization of excited Ca^{+*} by the impinging UV continuum. The other is photoionization of excited Ca^{+*} by the nebular $\text{Ly}\alpha$ photons. The statistical equilibrium equations give the relative population of the metastable level, which turns out to be, under EELR conditions, $\frac{n_{3d}}{n_{4s}} \sim 10^{-7}$, being n_{4s} the density of Ca^+ ions in the ground level. With such a negligible population, the density of ionizing photons must be very high to increase the ionization rate to a non negligible level as compared to the ground state ionization rate. A simple estimate presented in Appendix D demonstrates this level to be out of reach.

In summary, the very diluted radiation fields and the low densities appropriate to the EELR implies an extremely small population for the excited levels which prevents the ionization of Ca^{+*} by $\text{Ly}\alpha$ and soft continuum photons from being of any significance.

3.3.2 Thermal ionization of Ca^+ .

We investigate here the possibility of collisional ionization by thermal electrons of Ca^+ to Ca^{++} , a process which is important when the electronic temperature becomes higher than 20000K (Jordan 1969). In order to establish a comparison in U , we have considered two extreme cases in our calculations, $\log U = -4$ & -2 . To illustrate how a much harder continuum will result in much higher gas temperatures, we also use two different PL of index $\alpha = -1.4$ and -0.4 . Note that such a hard continuum as $\alpha = -0.4$ is probably quite unrealistic. However, our intention here is simply to test whether very high temperatures can be achieved with photoionization models and specifically near the Ca^+ region. The results are shown in Fig. 18 as a function of depth in the photoionized slab. Of the eight plots, the four upper ones correspond to $\alpha = -1.4$ while the four at the bottom to $\alpha = -0.4$. The four plots on the right, have $\log U = -2$, and the four on the left, $\log U = -4$. Two plots therefore are shown for each pair of $[U, \alpha]$ values: one is the the temperature T_4 in units of 10000K and the one immediately underneath is the intensity of F1 ($\text{erg.s}^{-1}.\text{cm}^{-2}$), both as a function of the depth in units of 10^{20}cm into the slab. These plots allow us to see the corresponding electron temperature to the position where the bulk of the $[\text{CaII}]F1$ emission takes place.

For the traditional PL of index $\alpha = -1.4$, the electron temperatures are not anywhere near high enough for the process of thermal ionization to be relevant. Harder continua and increasing U values do produce higher temperatures, but, unless U are unrealistically high (even $\log U = -2$ is not enough), the gas is never hot enough. Thus, realistic photoionization models are *not* able to heat the gas sufficiently to thermally ionize Ca^+ . We might conjecture that there could be an additional heating source like shocks which could raise the temperature of the gas. This would be an interesting point for further investigation.

3.3.3 Effects on F1 of varying U and the continuum hardness.

We now investigate how the F1 line might become undetectable by simply varying arbitrarily the ionization parameter U or the continuum hardness. Fig. 19 shows six diagnostic diagrams with the abscissae always representing the line ratio $[\text{OI}]\lambda 6300/[\text{OIII}]\lambda 5007$. The $[\text{OI}]/[\text{OIII}]$ ratio monotonically increases with decreasing gas excitation (i.e., with decreasing U) and is therefore a good measure of the excitation level of the gas. Each diagram shows in the ordinate a different line ratio which can be related to a given gas property. $[\text{OI}]\lambda 6300/\text{H}\alpha$, for instance, might measure the hardness of the continuum. In the last diagram, the ordinate corresponds to the quotient $F1/[\text{OI}]\lambda 6300$. The three sequences of models shown in each diagram differ by the slope of the power law which takes on the values of $\alpha = -1.4, -1$ and -0.4 . The values of $\text{Log } U$ covered by each curve is in the range -4 to -1 . Our aim is to look for models which can decrease the F1 intensity below

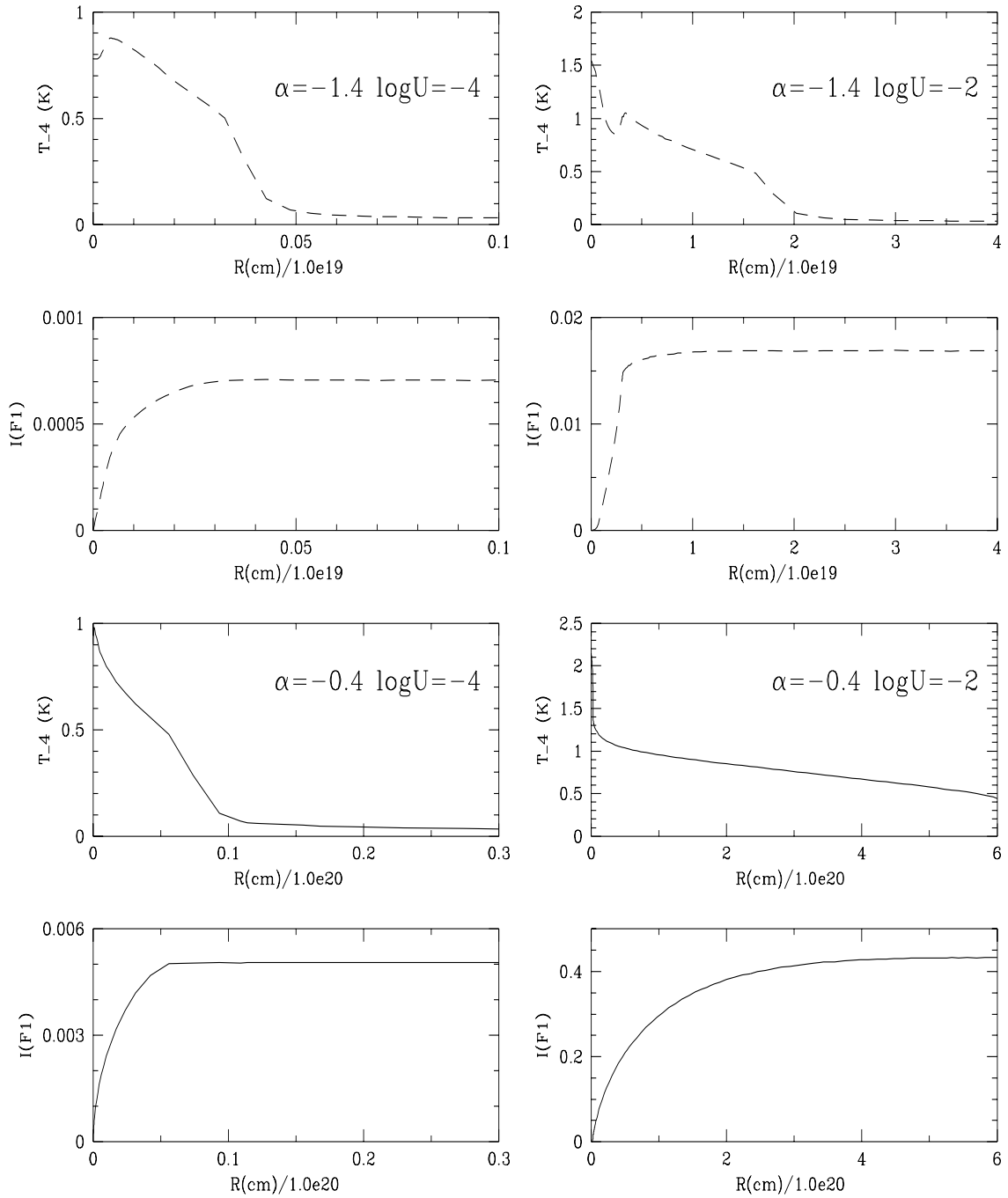


Figure 18:

Distribution of temperature and integrated intensity of F1 (in $\text{ergs s}^{-1} \text{cm}^{-2}$) line across an EELR cloud. Dotted lines (top diagrams) correspond to a power law of index -1.4 ; solid lines (bottom diagrams) to a power law of index -0.4 . Each temperature diagram must be compared with the one just below, to see the temperature that correspond to each point in the nebula.

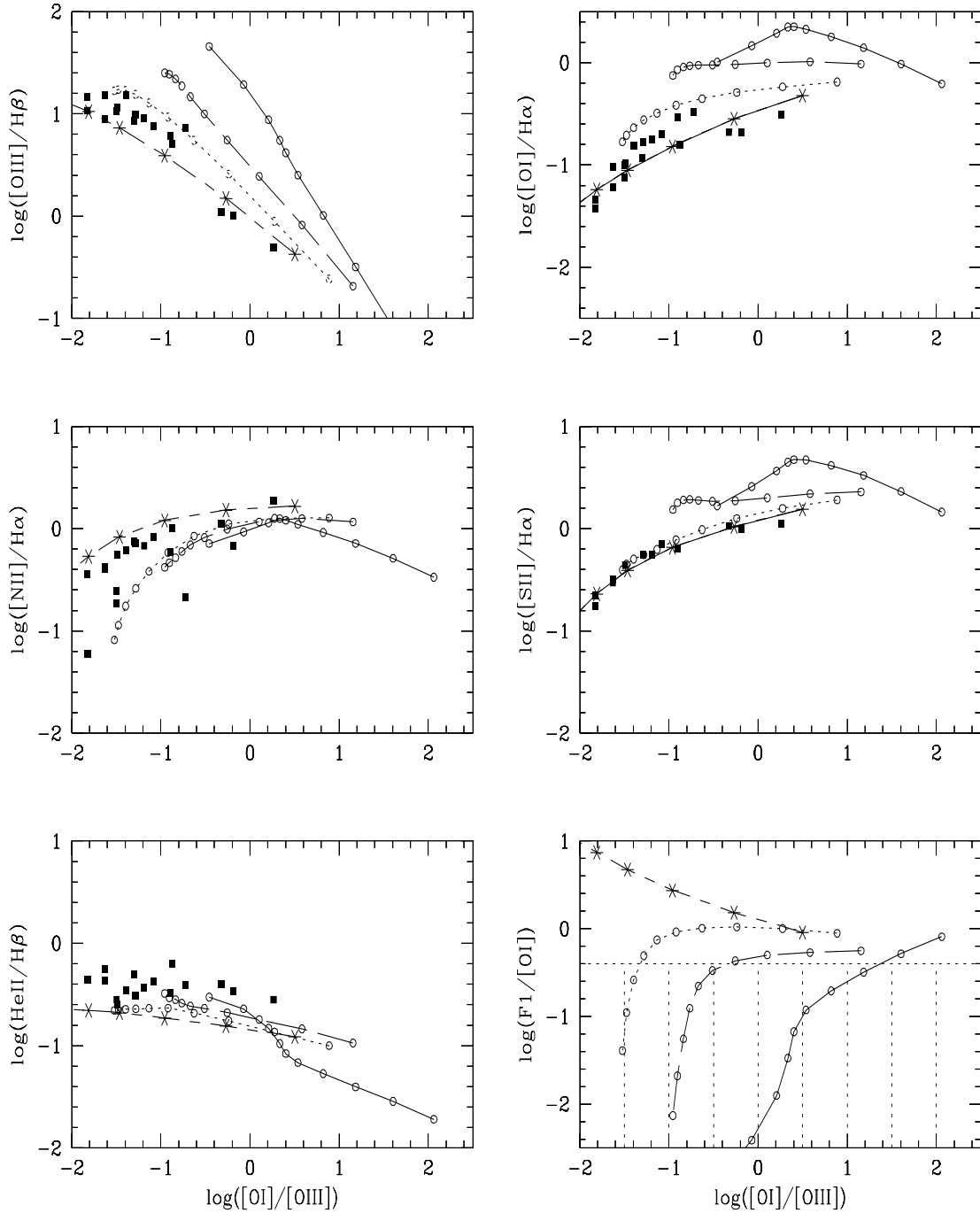


Figure 19:

The curves correspond to ionization parameter U model sequences for different ionizing continua: power laws (small circles used as fiducial marks) of index $\alpha = -1.4$ (.....), -1 (— —), -0.4 (- - - -) and a black body continuum of $T_{bb} = 1.2 \times 10^5 K$ (*-*-*). The region represented by vertical dotted lines in the last diagram shows the area where F1 would fall under the detection limit defined in Sect. 3.3.3. All the models within this region are successful in accounting for the absence of the [CaII] lines without requiring depletion by dust. Line ratios of extended emission line regions observed by RBFT87 (uncorrected for reddening) are shown with solid squares.

the detection limit. Let's look at how we might define a practical detection limit. The open squares in the diagrams of Fig. 19 represent line ratios measured by RBFT87 in several EELR. The faintest line they measure is typically HeII λ 4686. The mean ratio of HeII λ 4686/[OI] λ 6300 observed is $10^{-0.4} = 0.4$ for the large scale nebulosities. We establish our 'artificial' detection limit in the following way: since HeII is one of the weakest line successfully measured by RBFT87, we will assume that any line fainter than 0.4 below the [OI] λ 6300 flux is not detectable. In the last diagram, the region where F1 falls below this detection limit is shown by a dash line grid. Any model found in this area is deemed successful in explaining the non-detection of F1 without requiring depletion.

We see that for the standard PL ($\alpha = -1.4$), only models with high U ($\log U > -2$) decrease $\log(F1/[OI])$ below -0.4 . These models, as we can see in the diagrams, would therefore be valid only for the high excitation EELR, but not for LINERs, cooling flow filaments, or EELR of low and intermediate excitation. On the other hand, increasing the hardness of the continuum (flatter power laws), helps F1 to get fainter with respect to [OI] λ 6300, but the discrepancies with observed line ratios in other diagrams become totally unacceptable (see top two diagrams of Fig. 19).

It is interesting to compare a BB sequence (1.2×10^5 K) with the canonical PL sequence $\alpha = -1.4$. We see that both ionizing continua reproduce rather well the observed line ratios as was earlier shown by RBFT87. From these line ratios alone, there are no reasons to favour power laws over hot blackbodies. A similar conclusion was reached by Binette, Robinson and Courvoisier (1988) for the mean NLR spectrum of Seyferts.

A BB produces a much stronger F1 compared to [OI] λ 6300 than any of the power laws considered. One reason for this is that the fraction O^0/O^+ in the PIZ is completely controlled by the charge exchange reactions of O^0 and O^+ with H^+ and H^0 , respectively, and not by direct photoionization of O^0 . This is not so for Ca^+/Ca^0 which is free to respond to the different amount of hard photons (the only one to make it to the PIZ) available in a PL or a BB. We conclude from the last diagnostic diagram that the BB models could not explain the absence of F1 from the observed spectra without invoking depletion.

3.3.4 Effects on F1 of truncating clouds

We showed in the previous section that a harder continuum can potentially bring F1 under the detection limit but results in important discrepancies with the low excitation lines. The reason is that the partially ionized zone (PIZ) where most of the low excitation lines are generated gets larger and larger with increasing hardness of the continuum. If the clouds were truncated, the smaller PIZ would generate weaker low ionization lines, thus improving the overall fit.

We have investigated models with $\alpha = -0.4$ which were truncated at a depth

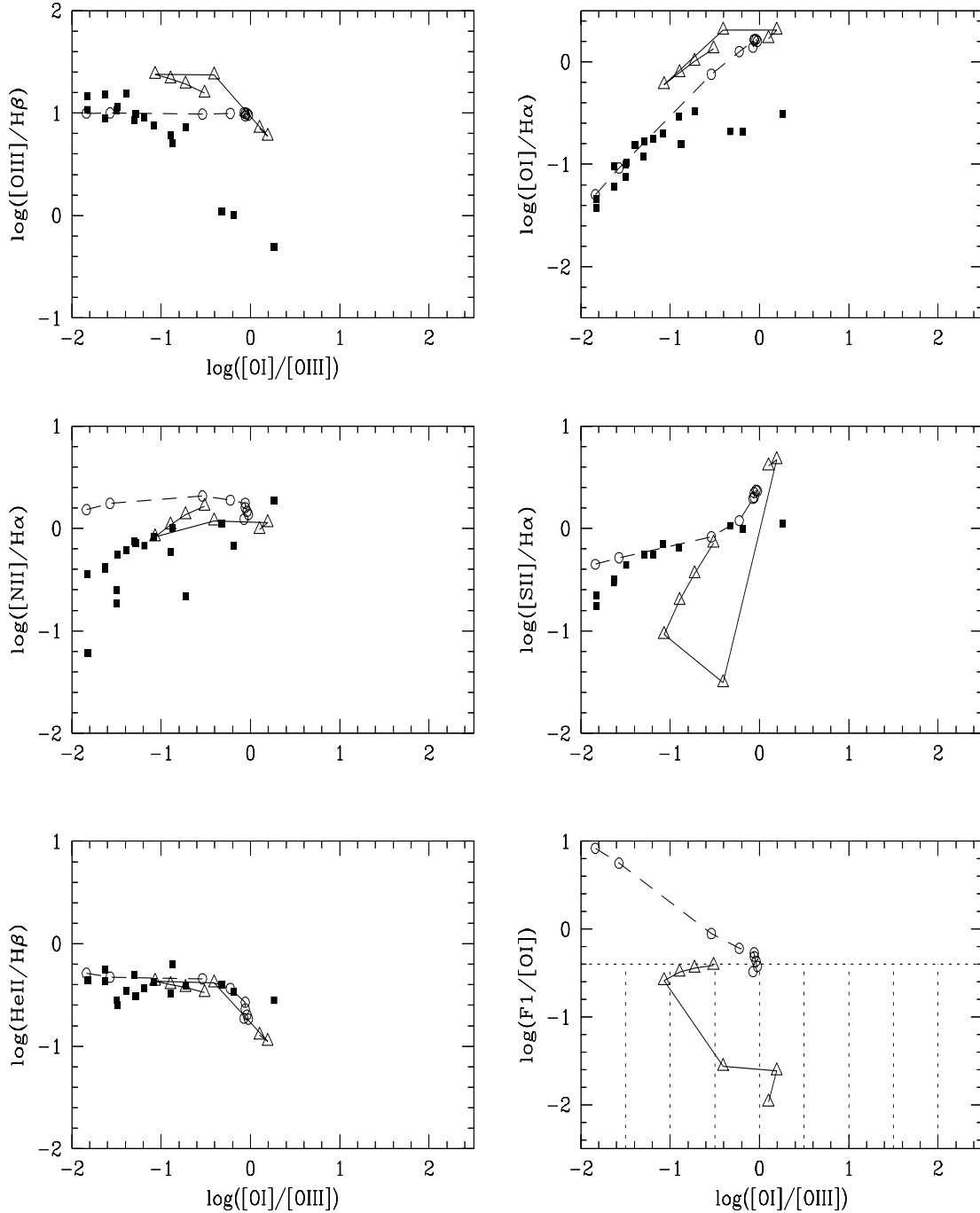


Figure 20:

Same diagrams as in Fig. 19 but for truncated gas clouds and only for hard power laws ($\alpha = -0.4$). The open circles (connected by the dashed line) correspond to matter bounded clouds ($5.2 \times 10^{-5} \leq U \leq 5.2 \times 10^{-4}$) truncated at a depth which produce $[OIII]/H\beta = 10$ (see text). The open triangles (connected by the solid line) are similar models truncated at a depth such that $F1/[OI] \leq 0.4$ ($3.7 \times 10^{-3} \leq U \leq 2.7 \times 10^{-2}$).

which satisfies a given criterion based on a specific line ratio. This has been done in two ways:

1) The criterion in this case is to truncate the calculations when $\text{OIII}/\text{H}\beta$ has reached a value of 10 which is the typical ratio for the high excitation EELR.

The sequence of models shown in Fig. 20 are separated by a factor of 0.14dex in U . Although there are still discrepancies, there is a notable improvement compared to the radiation bounded models of Fig. 19. The predicted line ratios are now located closer to the observed data (same scale as in Fig. 19). We conclude that models with a hard ionizing continuum must be matter bounded in order to fit acceptably most observed ratios.

What happens now with $\text{F1}/[\text{OI}]$? In the last diagram of Fig 20, we see that all these models produce F1 above the detection limits and cannot therefore explain the non detection of Calcium.

2) The second method consists on imposing that the models produce F1 under the chosen detection limit ($\text{F1}/[\text{OI}]=0.4$) and check if such models agree with the position of the observed line ratios in the rest of the diagrams.

The models in the sequence which satisfy this criterion are found in the range $3.7 \times 10^{-3} \leq U \leq 2.7 \times 10^{-2}$. They are represented in Fig. 20 as open triangles connected by a solid line. As we see in the top left diagram, the ratio $[\text{OIII}]/\text{H}\beta$ is not any more defining a simple trend with excitation (which is represented by the ratio $[\text{OI}]/[\text{OIII}]$). Furthermore $[\text{OI}]/\text{H}\alpha$ remains a discrepant ratio as in Fig. 19. So although it is in principle possible to satisfy the $\text{F1}/[\text{OI}]=0.4$ criterion with a hard power law, the truncation must be done at a specific yet *ad hoc* depth and furthermore the previous trend of excitation with U has disappeared.

Without rejecting the possibility of a more complicate mixture of matter and radiation bounded models, we believe that simply truncating clouds does not convincingly solve the problem of the weakness of the CaII doublet and dust depletion remains the most likely interpretation.

It is interesting to note that truncated clouds adjust better the $\text{HeII}/\text{H}\beta$ ratio (bottom left diagram) as proposed before by Morganti et al. (1991) and Viegas and Prieto (1992).

3.4 Conclusions

This work is based on the method proposed by Ferland (1993) to investigate the presence of dust mixed with the gas of the Narrow Line Region of active galaxies. Because photoionization models predict remarkably strong forbidden lines $[\text{CaII}]\lambda\lambda 7291, 7324\text{\AA}$ assuming reasonable abundances of atomic Ca, the basic idea is to infer a systematic depletion of Calcium onto dust grains whenever the infrared $[\text{CaII}]$ lines are observed very weak or undetected. This test of the dust content

was applied to cooling flow filaments by Donahue & Voit (1993) who concluded on the presence of dust.

We have shown here that this sensitive method is also applicable to the conditions found in the EELR of radiogalaxies. In order to make more secure any inference about the presence of dust based on [CaII] lines, we have investigated alternative explanations for their absence: ionization of Ca^{+*} to Ca^{++} by $\text{Ly}\alpha$ photons and soft continuum photons from the metastable level of Ca^+ , thermal ionization of Ca^+ , ionization of Ca^+ due to either a very high U value (ionization bounded case) or to a hard continuum (with truncated clouds). Except for the highly excited EELR which might not possess any Ca^+ region due to their high ionization level, the results are negative: none of the alternative mechanisms or models studied can explain the absence of the [CaII] lines without dust depletion.

Our conclusion is that the dust content test appears generally valid for the EELR of radiogalaxies (unless the excitation level of the gas is extremely high). This will allow us to make important conclusions about the origin of such gas, discriminating between galactic debris and the standard cooling flow theory.

A BB ionizing continuum characterized by a temperature of $1.2 \times 10^5 \text{K}$ can reproduce the observed line ratios of the EELR at least as well as a PL of index $\alpha = -1.4$. On the other hand, the $\text{F1}/[\text{OI}]$ from a BB is higher than that of a PL so the case in favour of depletion is even stronger.

In a follow up paper, we will present long slit spectra of EELR, cooling flow filaments and Seyfert 2 NLR, all taken in the region of the [CaII] doublet. The goal will be to apply the test of the Calcium depletion described above in order to conclude whether or not the gas in these nebulosities is mixed with dust. This will be our starting point for deciphering the origin of the emitting gas.

References

- Anders E., Grevesse N., 1989, *Geochim. Cosmochim. Acta*, 53, 197
- Baum S.A., Heckman T., Bridle A., van Breugel W., Miley G., 1988, *ApJS*, 68, 643
- Binette L., Dopita M.A., Tuohy I.R., 1985, *Astrophys. J.*, 297, 476
- Binette L., Robinson A., Courvoisier T.J.L., 1988, *A&A*, 194, 65
- Bruzual A., Magris C.M., Calvet N., 1988, *Astrophys. J.*, 333, 673
- Buson L.M., Sadler E.M., Zeilinger W.W., Bertin G., Bertola F., Danzinger I.J., DeJonghe H., Saglia R.P., de Zeeuw P.T., 1993, *A&A*, 280, 409
- Clements, D.L., Andreani, P. and Chase, T., 1993, *Mon. Not. Roy Astr. Soc.*, 261, 299
- Crinklaw G., Federman S.R., Joseph C.L., 1994, *Astrophys. J.*, 424, 748
- di Serego Alighieri S., Fosbury R.A.E., Quinn P.J., Tadhunter C.N., 1989, *Nature*, 341, 307
- Donahue, M., Voit G.M., 1993, *Astrophys. J.*, 414, L17
- Draine B.T., Salpeter E.E., 1979, *Astrophys. J.*, 231, 77
- Fabian A.C., Johnstone R.M., Daines S.J., 1994, *Mon. Not. Roy Astr. Soc.*, 271, 737
- Ferland G.J., 1993, in Proc. Madrid Meeting on The Nearest Active Galaxies, ed. J.E. Beckman, H. Netzer & L. Colina, p. 75
- Forman W., Jones C., Tucker W., 1985, *Astrophys. J.*, 293, 102
- Fosbury R.A.E., di Serego Alighieri S., Courvoisier T., Snijders M.A.J., Tadhunter C.N., Walsh C.N., Wilson W., 1990, in Evolution in Astrophysics, Toulouse, ESA SP-310
- Goudfrooij P., 1994, Ph.D. Thesis, University of Amsterdam, The Netherlands
- Haniff C. A., Ward M.J., Wilson A.S., 1988, *Astrophys. J.*, 368, 167
- Heckman T.M., Baum S.A., van Breugel, W.J.M., Miley G.K., Illingworth G.D., Bothun G.D. & Balick B., 1986, *Astrophys. J.*, 311, 526
- Januzi B.T., Elston R., 1991, *Astrophys. J.*, 366, L69
- Jordan C., 1969, *Mon. Not. Roy Astr. Soc.*, 142, 501
- Kingdon J., Ferland G.J., Feibelman W.A., 1995, *Astrophys. J.*, 439, 793
- Morganti R., Robinson A., Fosbury R.A.E., di Serego Alighieri S., Tadhunter C.N. Malin D.F., 1991, *Mon. Not. Roy Astr. Soc.*, 249, 91
- Nulsen P.E., Stewart G.C., Fabian A.C., 1984, *Mon. Not. Roy Astr. Soc.*, 208, 185

- Quinn P.J., 1984, *Astrophys. J.*, 279, 256
- Robinson A., Binette L., Fosbury R.A.E., Tadhunter C.N., 1987, *Mon. Not. Roy Astr. Soc.*, 227, 97 (RBFT87)
- Sutherland R.S., Bicknell G.V., Dopita M.A., 1993, *Astrophys. J.*, 414, 510
- Tadhunter C.N., 1986, D.Phil. Thesis, University of Sussex
- Tadhunter C.N., Fosbury R.A.E., Quinn P.J., 1989, *Mon. Not. Roy Astr. Soc.*, 240, 255
- Tadhunter C.N., Robinson A., Morganti, R., 1989. In: *ESO Workshop on Extranuclear Activity in Galaxies*, p. 293, eds Meurs, E.J.A., Fosbury, R.A.E., ESO Conf. and Workshop Proc. No. 32, Garching
- Tadhunter C.N., Scarrot S.M., Draper P., Rolph C., 1992, *Mon. Not. Roy Astr. Soc.*, 256, 53p
- Thomas P.A., Fabian A.C., Arnaud K.A., Forman W., Jones C., 1986, *Mon. Not. Roy Astr. Soc.*, 222, 655
- Toomre A., & Toomre J., 1972, *Astrophys. J.*, 178, 623
- Viegas S.M., Prieto A., 1992, *Mon. Not. Roy Astr. Soc.*, 258, 483
- Villar-Martín M., Binette L., 1995, *submitted to A&A*
- Wallerstein G., Bolte M., Whitehill-Bates P., Mateo M., 1986, *Pub. Astr. Soc. Pac.*, 98, 330
- Whittet D.C.B., 1992, *Dust in the Galactic Environment* (Bristol:IOP)
- Wilson A.S., Tsvetanov Z., 1994, *Astron. J.* 107, 1227
- Wyse A.B., 1941, *Pub. Astr. Soc. Pac.*, 53, 184

Chapter 4

Calcium depletion and the presence of dust in large scale nebulosities in radio galaxies (II).

Villar-Martín & Binette 1995, A&A, submitted

Abstract

We investigate here the origin of the gas observed in extended emission line regions surrounding AGNs. We use the technique of calcium depletion as a test to prove or disprove the existence of dust in such a gas in order to discriminate between two main theories: (1) a cooling process from a hotter X-ray emitting phase surrounding the galaxy, (2) merging or tidal interaction between two or more components. We have obtained long slit spectroscopy of a sample of objects representative of different galaxy types although our main interest focus on radio galaxies. The spectral range always includes the [CaII] $\lambda\lambda 7291, 7324$ doublet. The faintness or absence of such lines is interpreted as due to the depletion of calcium onto the dust grains and, therefore, is a proof of the existence of dust mixed with the gas in the EELRs.

4.1 Introduction

In Chapter 3, we have demonstrated that the test of proof of the existence of internal dust based on the depletion of calcium is valid (and very sensitive) under the conditions found in EELR studied here. We studied in detail all the most plausible *alternative* mechanisms to that of internal dust for explaining the absence of [CaII] lines. No acceptable alternative solution was found and we concluded in favour of the validity of the method. The observational results and their interpretation are presented in this chapter. We have applied this test to a sample of objects of different types: radiogalaxies with extended emission line regions, cooling flows (hereafter CF) and starburst galaxies.

We describe the observations, data reduction and analysis of the spectra in §4.2. In §4.3 we present the results of the comparison between measurements and model predictions. The implications on the origin of the gas are discussed in §4.4. The conclusions compose section §4.5.

4.2 Observations and data reduction

The observations were carried out on the nights 21-23 August on 1993. All the spectra were obtained at La Silla Observatory, Chile, with the 3.6 m telescope, using the EFOSC 1 spectrograph with a CCD detector (TEK#26) of 512×512 pixels² of $27 \mu\text{m}^2$. The slit width was $1.5''$. The grism, R150, with a dispersion of $120 \text{ \AA} / \text{mm}$, a wavelength bin of $3.3 \text{ \AA} / \text{pixel}$ and covering a spectral range of $\sim 6870\text{-}8560 \text{ \AA}$. The observing conditions were photometric. Table 1 gives a log of the observations.

Table 1: Observing Log

Name	RA(1950)	Dec(1950)	z	Comment	Exp time (s)	PA
NGC1052	02 38 37.33	-08 28 09	0.005	Liner	1800	270°
NGC6215	16 46 47.0	-58 54 30	0.005	Liner	2700	240°
NGC7552	23 13 25.0	-42 51 24	0.005	Liner	1200	270°
NGC7714	23 33 40.59	01 52 42	0.009	Starburst	2700	270°
PKS1404-267 (nuc)	14 04 38	-26 46 51	0.021	RG	2700	270°
PKS1404-267 (5" S)					2700	270°
PKS2014-55	20 14 06	-55 48 52	0.061	RG	3600	190°
PKS2152-69 (nuc)	21 52 58	-69 55 40	0.028	RG	2700	270°
PKS2152-69 (cloud)					3600	290°
PKS2158-380	21 58 17	-38 00 51	0.033	RG	2700	270°
PKS2356-61	23 56 29	-61 11 42	0.096	RG	3300	285°
PKS2300-18	23 00 23	-18 57 36	0.129	RG	2700	240°
2A 0335+096	03 35 52	09 48 10	0.035	CF	5400	147°
A2029	15 08 30	05 57 00	0.077	CF	2700	270°
A2597	23 22 42	-12 23 00	0.085	CF+RG	2700	197°

a) Basic data reduction

The reduction of the data was done using standard methods in IRAF. The spectra were bias subtracted and divided by a flat-field frame (dome flat-field). Illumination corrections along the slit were found to be negligible.

In general, we obtained three frames for each object and each slit position, allowing the direct removal of cosmic ray events. For a given object, all the frames corresponding to the same slit position were averaged together. In the cases where only two frames were available, the cosmic rays were removed visually, replacing the affected pixels by the mean of the surrounding region. The spectra were calibrated in wavelength using comparison spectra of an HeAr arc taken at the beginning and end of each night, and additionally before and after each object. The wavelength calibration was done very carefully in order to later subtract the sky as accurately as possible. The IRAF routine “background” was used to subtract the contribution of the sky by interpolation of the background detected in windows close to and on both sides of the object. With this method the sky features were successfully subtracted.

b) Atmospheric extinction

The spectra were corrected for atmospheric extinction with the aid of mean extinction coefficients for La Silla. Molecular absorption bands of O₂ (the A band at 7620 Å and the H₂O bands, bands in the region 7100-7450 Å and 8100-8400 Å) were also evident in the spectra. They were removed separately from all of the observed spectra. These absorption bands are composed of many closely spaced absorption features, unresolved in our spectra. Many of the features which comprise the A band are optically thick and therefore nearly independent of zenith distance, but most of those in the H₂O bands are not independent of time and zenith distance. In principle, the best method to remove these lines is to observe standard stars as close as possible in zenith distance and in time to that of the program object to obtain the best correction (c.f. Osterbrock, Shaw & Veilleux, 1990) . But as these authors pointed out the star closest to the objects’s observing time and zenith distance is not always the one producing the best correcting spectrum.

The procedure we used was the following: we observed three different standard stars whose frames were reduced in the same way as described before. After modeling the atmospheric bands with them, we decided that the best results were obtained with Feige 110, a dwarf with no intrinsic absorption features in the spectral range observed. An 1-dimensional integrated spectrum of the standard star was obtained by adding all the light along the spatial direction. A smooth fit to the continuum was done and then the original spectrum was divided by this. The result was a normalized spectrum keeping the features due to the atmospheric absorption. Due to the dependence on zenith distance and time, we had to model the bands for each object, i.e. to construct an specific restoring spectrum for each

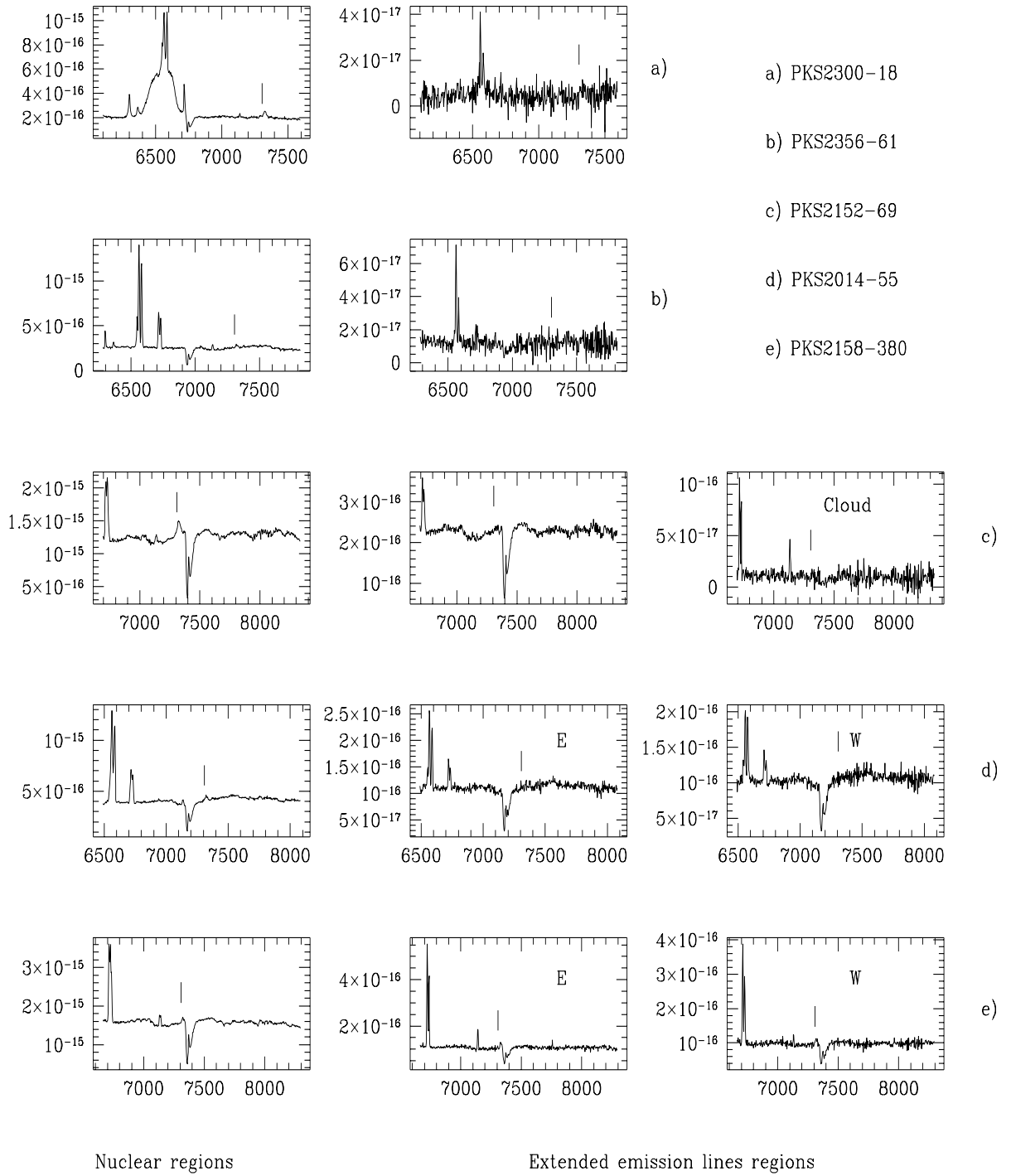


Figure 21:
Spectra of observed Radiogalaxies, nuclear (first column) and extended emission line regions (second and third columns). The expected position of the F1 line is indicated with | . Flux is given in units of $erg s^{-1} cm^{-2} \text{\AA}^{-1}$.

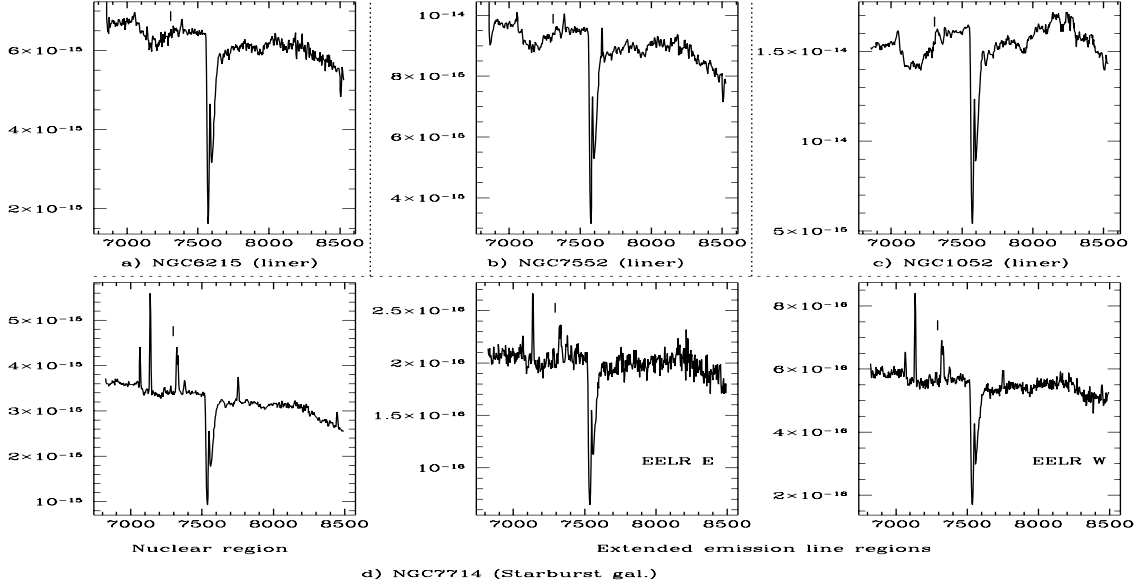


Figure 22:

Spectra of observed Liners and Seyfert 2 galaxies. The liner spectra have been extracted from the whole spatial extension of the object. The expected position of the F1 line is indicated with | . Flux is given in units of $erg\ s^{-1}cm^{-2}\text{\AA}^{-1}$.

object, multiplying the normalized spectrum by appropriate factors.

c) Flux calibration

The atmospherically corrected spectra of the standard stars were used to obtain the flux calibration. For each night we built a mean response curve from the two standard stars observed that night.

d) Template galaxy subtraction.

We checked that effects of stellar absorption features intrinsic to the galaxy could be neglected: the calcium doublet is on top of the raising part of a molecular band whose narrow line components are not resolved. Its only effect is to change the slope of the continuum under the doublet and we can easily correct for this effect, fitting a smooth continuum of certain slope in such region. $H\alpha$, a line that has been used as a reference to predict the flux in the F1 line, can be underestimated due to the underlying $H\alpha$ absorption line. But in our objects the $H\alpha$ emission is so strong that the difference is less than 5% of the emitted flux. This was computed by comparing the EW of the emission line in our objects and the EW of the absorption feature in a template elliptical galaxy.

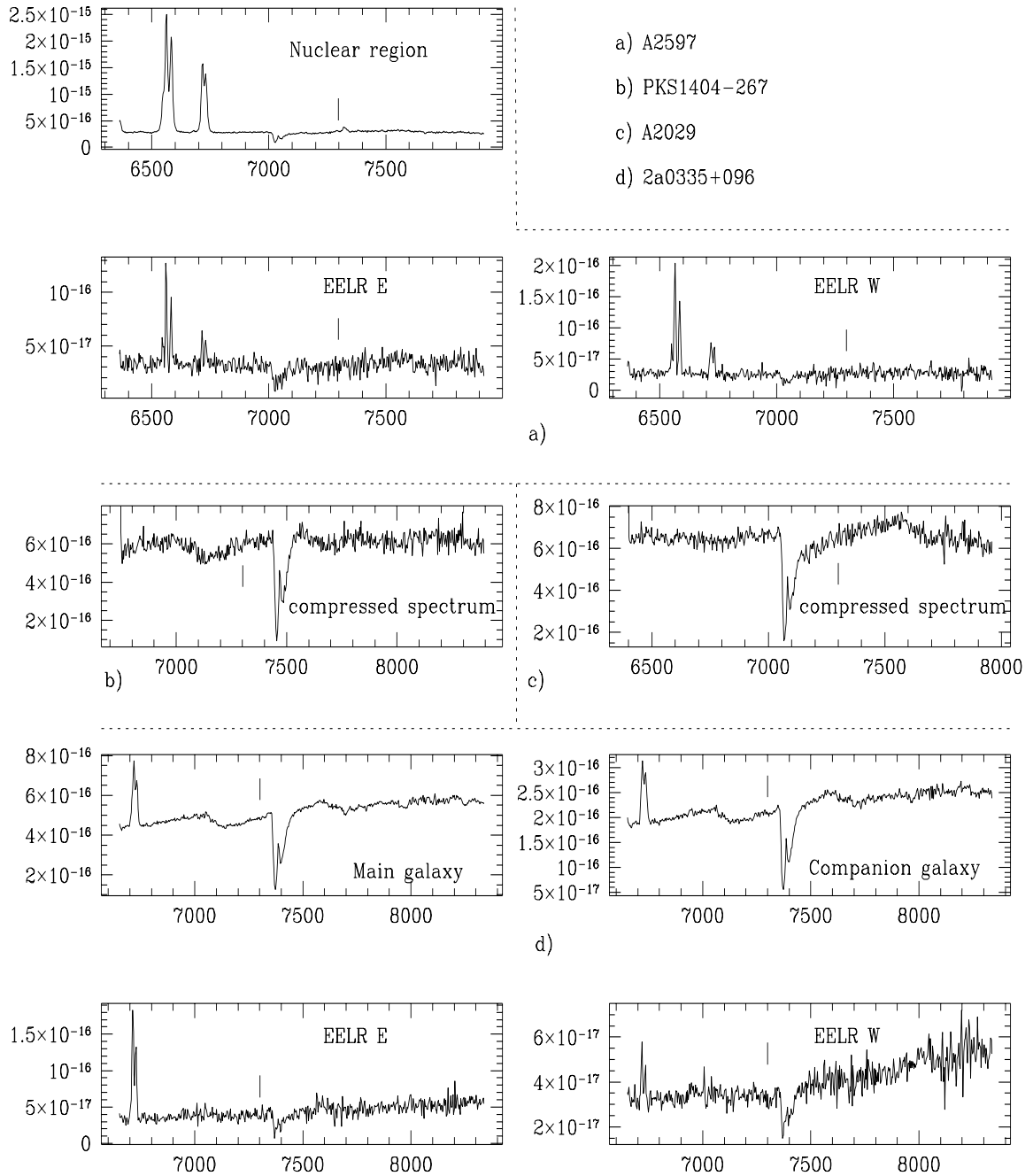


Figure 23:

Spectra of objects with properties associated with cooling flows. The spectra of PKS1404-267 and A2029 have been extracted from the whole spatial extension of the object. The expected position of the F1 line is indicated with |. Flux is given in units of $erg s^{-1} cm^{-2} \text{\AA}^{-1}$.

4.2.1 Data analysis

a) Extraction of the spectra

For those objects for which no extended emission lines were detected, we compressed the whole spatial extension to extract a 1-dimensional spectrum. For those objects showing extended emission lines, we separated it into two different components: the nucleus, and the extended emission line spectrum. In order to do this, we subtracted from the spatial profile in the brightest spectral line, the spatial profile in the nearby continuum. In this way, we are left with the spatial profile of the line emitting regions. In some cases blobs appear well detached from the nuclear emission. But sometimes the extended and nuclear emission were mixed. In order to avoid contamination of the EELRs by the nuclear spectrum, we fit a Gaussian (PSF) to the nuclear region. The residuals after subtracting this Gaussian were considered to be due to the EELR. The resulting spectra are shown in Fig. 21, 22 and 23.

It is possible that we may be venturing close enough to the nucleus to sample higher densities, more typical of the classical narrow line region (with densities higher than 10^3 cm^{-3}). To verify this, when it was possible, we used the [SII] doublet to estimate the density. The values were always below 100 cm^{-3} , which indicates that the spectra are dominated by low density gas. In any event, even if the NLR dominated the emission, as a result of its high critical density the line F1 (in the dustfree case) was calculated to remain stronger with respect to other emission lines (like $\text{H}\alpha$ or [ArIII]) than in the EELR. Our conclusions about inferring dust or not are therefore not affected by high densities. (Higher density models would imply a stronger calcium depletion).

b) Line measurements

IRAF routines were used to measure the emission line fluxes. For the blends, decomposition procedures were used, fitting several Gaussians at the expected positions of the components. The fluxes were the values estimated for the Gaussians that better fitted the given profile.

The upper limits on [CaII] emission were measured directly from the noise level in the data.

4.3 Observed and predicted F1 fluxes.

4.3.1 Prediction of F1 fluxes

The second component of the [CaII] doublet (F2) is the weakest and is blended with the [OII] $\lambda\lambda 7320, 7330$ multiplet. The first component is the strongest and lies

well aside, some 30 Å shortward of [OII]. It is straightforward to isolate it given a reasonable spectral resolution. Therefore, for simplicity, we have based our study on the measurement of this line. The observed values are compared with the flux that photoionization models predict. MAPPINGS (Binette et al. 1993a,b) is the multipurpose photoionization-shock code that we used for the modeling. It considers the effects of dust mixed with the ionized gas: extinction of the ionizing continuum and of the emission lines, scattering by the dust, heating by dust photoionization and depletion of heavy elements. The appropriate input parameters for the models were justified in Chapter 3.

The predicted value of the F1 flux has been computed in the following way: we used as a reference line (*ref line*), the strongest and/or the simplest to measure, like H α , [SII] $\lambda\lambda$ 6716,6731, the [OII] $\lambda\lambda$ 7320,7330 blend and/or [ArIII] λ 7136. The appropriate photoionization model allows the prediction of $R = \frac{F1}{ref\ line}$, from which we can easily deduct the F1 flux:

$$Predicted\ F1\ flux = R \times Measured\ flux\ in\ the\ reference\ line.$$

In table 2, we show the reference lines used for each object and for each spatial region, the measured flux, the predicted $R = \frac{F1}{ref\ line}$ ratio, the measured F1 flux and its theoretical value. We have used different lines for different objects and different zones. For the nuclear regions, we always base our predictions on the blend [OII] $\lambda\lambda$ 7320,7330. The density in the nuclear narrow line region spans a wide range up to $10^6\ cm^{-3}$. The critical density of the [CaII] forbidden lines is very high, and the flux of the lines under the nuclear conditions are predicted to be far stronger than the [OII] lines (Ferland 1993). [OII] can be de-excited due to high density so that if CaII remains much smaller than [OII], it is actually a more stringent test since high densities would have actually helped to increase the CaII/OII ratio. To measure the flux in the [OII] blend, we assume that there is a negligible contribution from the F2 component. This assumption is reasonable: it is fainter than F1 and this line is near or under the detection limit in all cases. We can therefore assume that the [OII] multiplet is not contaminated by F2.

4.3.2 Comparison with the observations

The comparison between the measured and predicted F1 flux values shown in table 2 demonstrates that, whenever the calculations were possible (sometimes there was no a reference line available, however), it is always fainter (non detected in most cases) than expected. This result is common to all the regions considered here: nuclear, EELRs and cooling flow filaments. It demonstrates that calcium is depleted and, therefore, *the gas is mixed with dust*, both in the nuclear as in the extended emitting gas in radio galaxies and cooling flow filaments.

Donahue & Voit applied this same test to emission line nebulae in cluster cooling flows (1993). They interpreted the observed lack of [CaII] emission as depletion of calcium onto dust grains in the ionized filaments. Our work support

Table 2: Emission line fluxes for the sample of galaxies observed (in units of $\text{erg s}^{-1}\text{cm}^{-2}$). The superscripts M and P indicate measured and predicted values respectively. The last two columns show the predicted and measured values for the $F1$ line. For those objects where the calculations were possible, the observed line is clearly fainter than photoionization models predict.

Name	Spatial reg.	ref line	$Flux^M$	$\frac{F1}{ref\ line}^P$	$Flux(F1)^P$	$Flux(F1)^M$
NGC1052	Total	None	—	—	—	$\leq 6.99\text{e-16}$
NGC6215	Total	None	—	—	—	$\leq 3.34\text{e-16}$
NGC7552	Total	None	—	—	—	$\leq 3.95\text{e-16}$
NGC7714	Total	[OII] λ 7325	1.59e-14	≥ 1.00	$\geq 1.59\text{e-14}$	$\leq 6.84\text{e-17}$
PKS1404-267	Nucleus	None	—	—	—	$\leq 1.79\text{e-16}$
	5" South	None	—	—	—	$\leq 5.23\text{e-17}$
PKS2014-55	Nucleus	[OII] λ 7325	1.54e-15	≥ 1.00	$\geq 1.54\text{e-15}$	$\leq 3.34\text{e-17}$
	EELR (E)	H α	1.47e-15	~ 0.45	6.62e-16	$\leq 2.60\text{e-17}$
	EELR (W)	H α	1.06e-15	~ 0.45	4.77e-16	$\leq 3.18\text{e-19}$
PKS2152-69	Nucleus	[OII] λ 7325	7.48e-15	≥ 1.00	$\geq 7.48\text{e-15}$	1.92e-16
	EELR	[SII] λ 6731	1.33e-15	~ 0.40	5.32e-16	$\leq 3.03\text{e-17}$
	Cloud	[ArIII] λ 7136	3.86e-16	~ 4.50	1.74e-15	$\leq 2.24\text{e-17}$
PKS2158-380	Nucleus	[OII] λ 7325	4.03e-15	≥ 1.00	$\geq 4.03\text{e-15}$	3.15e-16
	EELR (E)	[ArIII] λ 7136	7.28e-16	~ 5.0	3.64e-15	$\leq 2.55\text{e-17}$
	EELR (W)	[ArIII] λ 7136	3.00e-16	~ 5.0	1.5e-15	$\leq 5.00\text{e-17}$
PKS2356-61	Nucleus	[OII] λ 7325	9.39e-16	≥ 1.00	$\geq 9.39\text{e-16}$	2.78e-16
	EELR	H α	5.36e-16	~ 0.18	9.6e-16	$\leq 1.03\text{e-17}$
PKS2300-18	Nucleus	[OII] λ 7325	1.80e-15	≥ 1.00	$\geq 1.80\text{e-15}$	4.37e-16
	EELR	H α	3.61e-16	~ 0.40	1.44e-16	$\leq 1.97\text{e-17}$
2A 0335+096	cD galaxy	[SII] λ 6725	7.46e-16	~ 0.40	2.98e-16	$\leq 2.72\text{e-17}$
	EELR (E)	[SII] λ 6725	2.24e-15	~ 0.40	8.96e-16	$\leq 1.29\text{e-17}$
	EELR (W)	[SII] λ 6725	4.22e-16	~ 0.40	1.68e-16	$\leq 1.40\text{e-17}$
	companion	[SII] λ 6725	7.89e-15	~ 0.40	3.16e-15	$\leq 1.69\text{e-17}$
A2029	Total	None	—	—	—	$\leq 1.43\text{e-16}$
A2597	Nucleus	[OII] λ 7325	1.79e-15	≥ 1.00	$\geq 1.79\text{e-15}$	5.14e-16
	EELR	H α	2.32e-15	~ 0.50	1.16e-15	$\leq 5.86\text{e-17}$

these results, in a different sample of objects: the NLR in AGNs and the filaments in objects classified as 'cooling flows' are well mixed with dust.

The most important result is the confirmation that *dust exists mixed with the ISM in low z radio galaxies*.

4.4 Discussion

4.4.1 Implications on the origin of the gas

As explained in Chapter 3, there are some pieces of evidence indicative of dust *in the extended ionized gas* in active galaxies, mainly derived from polarization measurements that show the existence of scattered nuclear light over large spatial scales, although it is difficult to discriminate between dust and electrons as the scattering agent. Our results confirm that dust exists *mixed with the ISM in low redshift radio galaxies*.

As mentioned before, this produces discrepancies with the traditional cooling flow theory, which would now be required to explain the formation of dust in a shorter time than the cooling time! According to this theory (see Fabian 1994 for a review), the galaxies, groups and clusters of galaxies were formed out of gas that collapsed gravitationally. During this process, gravitational energy was released which heated the clouds and a hot X-ray atmosphere would remain. Inhomogeneities in the gas would cause matter from the hot atmosphere to cool down and fall towards the center of the galaxy or cluster. The resulting filaments would eventually be visible at optical wavelengths and would emit strong lines. For massive galaxies and cluster, the cooling process would have been slower than for normal galaxies and the hot atmosphere would still exist, with typical temperatures of several million K and emitting strongly in the X-ray band.

If this is actually the origin of the gas in the EELRs (and cooling flow filaments), it should clearly be devoid of dust. Any dust introduced in the hot intra-cluster medium would be sputtered and rapidly destroyed (time scale of the order of 10^7 years) (Draine & Salpeter 1979), much before the filaments cooled down and became visible. Is there a way to introduce dust in the filaments during the cooling process? The common place where dust is formed is stellar atmospheres. Do stars exist in the accreted gas? Such gas must be deposited in some form and it has been generally thought that the more plausible fate for most of the gas is the formation of new stars (e.g., O'Connell & McNamara 1989; Fabian, Nulsen & Canizares 1991). Although there are some indications of star formation in cooling flow galaxies, the latter seems to be taking place in the inner parts (over the central few kpc) (Cardiel, Gorgas & Aragón Salamanca 1995, Fabian 1994). There is a lack of evidence of star formation (or any kind of stars) at large distances, out of the main body of the galaxies, where the EELRs filaments are still visible.

In high z RG there is an extended blue continuum aligned with the radio axis that has often been interpreted as due to young stars. However, as I mentioned already before, further results (e.g., Tadhunter, Fosbury & di Serego 1988; Cimatti et al. 1993) proved that this continuum is polarized and the contribution of a hidden quasar continuum scattered by dust and/or electrons in the ISM can well be an important component (in fact, this extended polarized UV continuum has been used as a proof of the existence of dust in the EELRs of high z radio galaxies). This effect has also been detected in some radio galaxies at low z (Cimatti & di Serego Alighieri S. 1995). Although young stars may exist, we don't have a clear idea about their overall contribution.

There is another mechanism which can form dust: if most of the cooled gas from a flow does not form stars with normal IMF, maybe it remains as cold clouds or as low-mass stars. There are evidences of X-ray absorption (White et al. 1991; Mushotzky 1992; Allen et al. 1993) in cooling flows in cluster of galaxies. The absorbing material could be in the form of cold gas embedded in the hot intra-cluster medium of the cooling flow (White et al. 1991; Daines, Fabian & Thomas 1994). This cold gas, very slightly photoionized by X-rays from the surrounding hot corona, can become molecular (Ferland, Fabian & Johnstone, 1994). Fabian, Nulsen & Canizares (1994) propose that the conditions suitable for dust to form may occur in this cool gas, through the condensation of gaseous particles. The authors propose that the gas which is cooling towards the center could be a mixture of both the molecular gas and the very hot gas and, therefore, could contain the existing dust. However, even if such a scheme was possible, the dust grains will not remove the calcium which already existed in the hot gas; the temperature is too high for the condensation of calcium onto the dust grains. Therefore, we should observe the CaII lines from the hot gas when it cools down, even if it contains dust.

On the other hand, the interaction scenario (gas accreted from outside the galaxy, as a result of recent tidal interactions or mergers between two or more components) predicts the existence of dust mixed with the gas, the one already existing in the interacting objects. Some morphological evidences and theoretical ideas (see Chapter 3) support this scene. Heckman et al. (1986) showed that a large fraction of powerful radio galaxies have morphological features (shells, tails, loops, etc) similar to those produced in numerical simulations of galaxy interactions (e.g., Toomre and Toomre 1972, Quinn 1984). Kinematic measurements show that the radio galaxy EELR generally have a high specific angular momentum which is difficult to reconcile with the cooling flow picture (Tadhunter, Fosbury & Quinn 1989).

Therefore, if there is a common origin for the EELRs of all radio galaxies, our results suggest that it is mergers or tidal interactions. However, we don't exclude the possibility of an origin which is *not* universal, that is, which may differ from object to object.

4.5 Conclusions.

We have confirmed that the gas in extended emission line regions in radio galaxies at low z is mixed with dust.

Our results support the existence of dust mixed with the gas in the Narrow Line Region and in the cooling flow filaments.

If there is an universal origin for the EELRs, the existence of internal dust favours mergers or tidal interactions as the most plausible scenario.

References

- Allen S.W., Fabian A.C., Johnstone R.M., White D.A., Daines S.J., Edge A.C., Stewart G.C., 1993, *Mon. Not. Roy Astr. Soc.*, , 262, 901
- Cimatti A., di Serego Alighieri S., Fosbury R.A.E., Salvati M., Taylor D., 1993, *Mon. Not. Roy Astr. Soc.*, 264, 421
- Cimatti A., di Serego Alighieri S., 1995, *Mon. Not. Roy Astr. Soc.*, 273, L7
- Cardiel N., Gorgas J., Aragón-Salamanca A., 1995, *Mon. Not. Roy Astr. Soc.*, 277, 502
- Daines S.J., Fabian A.C., Thomas P.A., 1994, *Mon. Not. Roy Astr. Soc.*, 268, 1060
- Donahue, M., Voit G.M., 1993, *Astrophys. J.*, 414, L17
- Draine B.T., Salpeter E.E., 1979, *Astrophys. J.*, 231, 77
- Fabian A.C., Nulsen P.E.J., Canizares C.R., 1991, *ARA&A*, 2, 191
- Fabian A.C., 1994, *ARA&A*, 32, 277
- Ferland G.J., 1993, in Proc. Madrid Meeting on The Nearest Active Galaxies, ed. J.E. Beckman, H. Netzer & L. Colina, p. 75
- Heckman T.M., Baum S.A., van Breugel, W.J.M., Miley G.K., Illingworth G.D., Bothun G.D. & Balick B., 1986, *Astrophys. J.*, 311, 526
- Mushotzky R.F., 1992, in Fabian A.C., ed., Clusters and Superclusters of Galaxies. Kluwer, Dordrecht, p.91
- O'Connell R.W., McNamara B.R., 1989, *Astron. J.* 98, 2018
- Osterbrock D.E., Shaw R.A., Veilleux S., 1990, *Astrophys. J.*, 352, 561
- Quinn P.J., 1984, *Astrophys. J.*, 279, 256
- Tadhunter C.N., Fosbury R.A.E., di Serego Alighieri S., 1988, in Maraschi L., Maccacaro T. & Ulrich M.H., eds., "BL Lac Objects", Springer-Verlag, Berlin, p.79

Tadhunter C.N., Fosbury R.A.E., Quinn P.J., 1989, *Mon. Not. Roy Astr. Soc.*, 240, 255

Toomre A., & Toomre J., 1972, *Astrophys. J.*, 178, 623

White D.A., Fabian A.C., Johnstone R.M., Mushotzky R.F., Arnaud K.A., 1991, *Mon. Not. Roy Astr. Soc.*, 252, 72

Chapter 5

Effects of dust and resonant scattering on the UV spectrum of radio galaxies.

Villar-Martín, Binette & Fosbury 1995, A&A, submitted

Abstract

In the powerful, high redshift radio galaxies, it is believed that the dominant source of ionization for the gas is the hard radiation field associated with the active nucleus. The photon source is generally external to the clouds being ionized and so the geometrical perspective from which the gas is observed and the presence and distribution of dust must be properly accounted for in the diagnostic process. In this paper, we examine the formation of three strong lines, CIV λ 1549, Ly α and CIII] λ 1909 which are often observed in the nuclear and extended emission from these sources. We find that the observed trends, in particular the high CIV λ 1549/Ly α ratio, are often better explained by geometrical (viewing angle) effects than by the presence of large quantities of dust either within or outside the excited clouds. We show that condensations of neutral gas along the line-of-sight can increase the observed CIV/Ly α ratio, by reflecting photons near the wavelength of Ly α . The existence of HI absorption clouds (i.e., mirrors) external to the emission region leads also to the presence of large, diffuse haloes of what appears to be pure, narrow Ly α emission.

5.1 Introduction

The strong, spatially extended, rest-frame ultraviolet emission lines observed in high redshift radio galaxies provide one of the principal diagnostics in establishing the state of the interstellar medium in galaxies at early epochs. The presence of a blue continuum and emission lines from regions aligned with the radio axis (McCarthy et al. 1987; Chambers, Miley & van Breugel 1987) warned us that much of the observed optical radiation might be associated with the nuclear activity and so may not be giving us a clear picture of the stellar processes which are of great interest in studies of galaxy formation and evolution. Subsequent work has shown, indeed, that much of the blue light is scattered, polarized nuclear radiation (e.g., Tadhunter et al. 1989; di Serego Alighieri et al. 1993; Cimatti et al. 1993) and that the emission lines have a high ionization state and cannot result from photoionization by normal stars (McCarthy 1993). It is clearly necessary, therefore, to reach a clear understanding of the physical processes involved in the formation of the various lines and continua to be able to disentangle the stellar and the AGN-related sources.

For objects at high z , the UV rest-frame lines are shifted into the optical band and the spectrum is generally dominated by $\text{Ly}\alpha$, $\text{CIV}\lambda 1549$, $\text{HeII}\lambda 1640$ and $\text{CIII}\lambda 1909$. The strength of the high ionization lines suggests the presence of a hard photoionizing continuum which could originate at the AGN itself (Robinson et al. 1987) or be associated with fast shocks generated in extranuclear regions by the radio jets (Sutherland, Bicknell & Dopita 1993). The strong radio/optical asymmetries observed in these objects which exhibit the ‘alignment effect’ (McCarthy, van Breugel & Kapahi 1991) may simply result from a one-sidedness in the distribution of material. It is clear, however, that correlated line and continuum asymmetries could be produced by dust scattering and line fluorescence for sources where the radio axis falls significantly away from the plane of the sky.

In this work, we concentrate on modeling the high excitation lines for which rather extreme ratios relative to $\text{Ly}\alpha$ have recently been reported. The presence of dust has been universally invoked to explain the weakness of $\text{Ly}\alpha$ which is a resonance line and therefore, due to multiple scattering, more susceptible to absorption. We explore the fact that any resonance line will be extremely sensitive to geometrical factors, an aspect of the problem which has so far been overlooked in modeling the UV lines. If in radio-galaxies the distant gas clouds are photoionized from the outside by partially collimated UV radiation emitted by the nucleus, the line formation process — particularly for the resonance lines — is very different from that of the internally ionized HII regions. The escape of resonance line photons is strongly influenced by the presence of voids between the line emitting clouds.

We have collected from the literature the observed line ratios for a number of radio-galaxies at high z ($z > 1.5$) in which no contribution from any nuclear BLR is apparent. We have built a diagnostic diagram consisting of the lines

CIV λ 1549/Ly α vs. CIV λ 1549/CIII] λ 1909, in which we compare the position of the objects with photoionization models which not only consider the effects of internal dust but also those of the viewing perspective — the angle between the incoming ionizing radiation and the observer’s line of sight. Our concentration on the particular class of radio galaxies is purely for pragmatic reasons. It is these objects, which we presume to harbour a powerful quasar which is hidden at optical/ultraviolet wavelengths to our line of sight, which are most readily found and studied at high redshifts where we have access to the ultraviolet spectrum from groundbased observations. Our conclusions should be equally applicable to other classes of AGN.

For some objects, Ly α is observed to be fainter with respect to CIV than predicted by dust-free photoionization models. The explanation previously proposed to explain the weakness of Ly α with respect to H α or H β has been dust destruction of resonant Ly α photons. This is *not* borne out by our calculations in which we have used arbitrary amounts of dust and found that this cannot simultaneously weaken Ly α while leaving the CIV/CIII] ratio relatively unchanged since resonant CIV suffers also from dust absorption. Alternatively, by varying the proportions of the illuminated and the shadowed cloud faces which contribute to the observed spectrum, we are better able to match the data.

As we find that geometry alone (with or without internal dust) can in principle explain most of the specific line ratios observed (fainter Ly α compared with either CIV or HeII), we also discuss the possibility of a patchy outer halo of neutral gas to account for the diffuse Ly α seen in some cases to extend much beyond the CIV emitting region and even the outermost radio lobes. Reflection by cold gas of the brighter Ly α emitting side of the ionized clouds would lead to a narrower profile for such a diffuse component. Another possibility is that part of the beamed nuclear *continuum and BLR* radiation might be reflected at the wavelength of Ly α by thin matter-bounded photoionized gas at very large distances from the nucleus leading to a diffuse Ly α component aligned with the radio axis. It appears to us that geometrical perspective effects are an essential component of the interpretation of the UV spectrum of radio-galaxies whether or not dust is present. Furthermore, a spectrum in which only Ly α appears does not necessarily imply starburst activity, other lines must be observed before the existence of HII regions can be inferred.

5.2 Data sample and modeling procedure

5.2.1 The data

We have constructed a data sample containing galaxies at high z for which the CIV, Ly α and, in most cases CIII], emission lines have been measured. Since very high densities such as those encountered in the BLR alter significantly the line formation and transfer processes, we have excluded those objects which show evidence of a BLR. In Table 3, we list the object names, the line ratios of interest to us here, the redshift and the reference to the observations. The larger fraction of the data are taken from the recent thesis by van Ojik (1995) which includes objects selected on the basis of a very steep radio spectrum. Probably by virtue of the radio selection, these sources populate the region of the line ratio diagram (Fig. 29) with lower CIV/CIII] ratios (lower ionization parameter) than the previously published objects. The line measurements refer to the integrated emission from the object collected with a long slit aligned with the major axis.

5.2.2 The model and its parameters

The data are compared to photoionization models computed using the code MAPPING. The version described in Chapter 2 is particularly suited to this study since it considers both the effects of the observer's position with respect to the emitting slab and the ionizing source (see Fig. 4, Chapter 2), distinguishing between the spectrum seen from the back and from the front of the slab. Phenomena related to dust are also properly considered. The treatment of the escape of resonant CIV and Ly α photons in a dusty medium (a fundamental process that needs to be well understood) is described in Appendix B of Binette et al. (1993a) and is based on the results of Hummer & Kunasz (1980). The presence of dust implies depletion of refractory trace elements and this effect has also been considered, as described in Appendix A. The calculations consider the gas pressure to be constant (isobaric models) and so the density behaviour with depth in the cloud is determined by the behaviour of the temperature and the ionization fraction of the gas.

5.2.3 Adopted physical conditions

The detailed studies of the optical emission lines of low z radio galaxies provide our basic reference for the properties of the emitting gas and the ionizing continuum (e.g., Robinson et al. 1987, hereafter RBFT87). As a guide in choosing the input parameters, we have assumed that the excited gas of *very* high z radio galaxies ($z > 2.5$) has similar properties to that of the low redshift ($z < 0.1$) objects. As explained in Chapter 3, for the extended (EELR) as well as the (narrow) nuclear emission lines, photoionization by a hard continuum appears to best explain the various line ratio diagnostic diagrams: a power law of index $\alpha \simeq -1.4$ ($f_\nu \propto \nu^{+\alpha}$),

Table 3: Observed UV line ratios for several high z RG with not apparent broad component

Name	CIV/CIII]	CIV/Ly α	z	ref.
Average RG	2.054	0.118	$0.1 < z < 3$	McCarthy (1993)
MG1019+0535A	2.12	1.24	2.76	Dey et al. 1995
F10214+4724	3.68	8.75	2.29	Elston et al. 1994
TX0211-122	3.33	0.91	2.34	van Ojik et al. 1994
3C294	0.83	0.10	1.79	McCarthy et al. 1990a
0902+34	–	0.11	3.40	Lilly 1988
3C256-3C239	1.90	0.14	1.82 & 1.78	Spinrad et al. 1985
0200+015	1.05	0.241	2.23	van Ojik 1995
0214+183	1.67	–	2.13	”
0355-037	1.17	0.24	2.15	”
0417-181	–	0.40	2.73	”
0448+091	0.44	0.10	2.04	”
0529-549	0.22	0.05	2.58	”
0748+134	1.29	0.29	2.42	”
0828+193	0.95	0.14	2.57	”
0857+036	–	0.39	2.81	”
0943-242	1.70	0.19	2.92	”
1138-262	0.62	0.06	2.16	”
1357+007	–	0.19	2.67	”
1410-001	1.58	0.16	2.36	”
1545-234	0.61	0.17	2.76	”
1558-003	2.25	0.18	2.53	”
2202+128	–	0.25	2.71	”
2251-089	2.20	–	1.99	”
4C23.56	3.40	–	2.48	”
4C24.28	–	0.23	2.88	”
4C26.38	3.71	–	2.61	”
4C28.58	0.17	–	2.89	”
4C40.36	1.05	–	2.27	”
4C41.17	–	0.05	3.80	”
4C48.48	2.18	–	2.34	”
4C60.07	–	0.27	3.79	”

that has produced remarkably good agreement with the optical line ratios at low z , will be adopted as ionizing energy distribution.

Concerning metallicity, RBFT87 indicated that the abundances cannot be much higher than solar values. They could however be lower by a factor of a few, a distinct possibility in the case of the extranuclear gas in very high z galaxies. Unless specified otherwise, we have adopted $Z = 1$ in our calculations and have verified that lower abundances do not in any way affect the conclusions reached here.

The red [SII] doublet ratio in low z radio galaxies indicates densities for the extended emission line regions which are lower than 100 cm^{-3} . We therefore adopt the low density regime, specifically $n_H = 100 \text{ cm}^{-3}$, since the *extranuclear* gas generally dominates the line luminosities.

5.3 Models and comparison with observed UV lines

In this section we first extend the assumption of photoionization to modeling the line emission in the ultraviolet rest-frame of high z radio galaxies. We distinguish the effects of having a back and a front view of an externally photoionized slab (section 5.3.2). In 5.3.3, we introduce internal dust and discuss how, alone, it is insufficient to explain the low value of the $\text{Ly}\alpha/\text{CIV}$ ratio in some objects. In 5.3.4 we distinguish between the resonance line ‘mirror’ intrinsic to our photoionized slab and the possibility of having external cold gas — which is shadowed from the ionizing source — acting as a reflector of $\text{Ly}\alpha$ photons.

5.3.1 The photoionization assumption at low and high z

At very high redshift, observational access to the normal optical plasma diagnostic lines is restricted and the available data set is small. Also, where measurements are available, few lines are measured in any given source. It is nevertheless interesting to compare the $[\text{OIII}]\lambda 5007/\text{H}\beta$ value observed at very high z to that of low z radio galaxies as plotted in Figure 24. The curved line corresponds to the sequence of photoionization models of RBFT87 which reproduce reasonably well the optical (rest frame) line ratios of the extended emission line regions and their associated narrow nuclear line emission. The range in U is $[10^{-4}, 10^{-1}]$. The three lower horizontal lines correspond to high z radio galaxies while the upper one corresponds to the “average” radiogalaxy spectrum as defined by McCarthy (1993). The high z objects are not substantially different from the low z sample although the apparent trend towards weaker $[\text{OIII}]/\text{H}\beta$, if confirmed, might indicate substantially lower metallicities: low enough to overcome the higher ratios produced by the higher kinetic temperatures in moderately underabundant objects. Such an effect could

also be produced by insufficient spatial resolution at high z to separate the high from the low excitation regions.

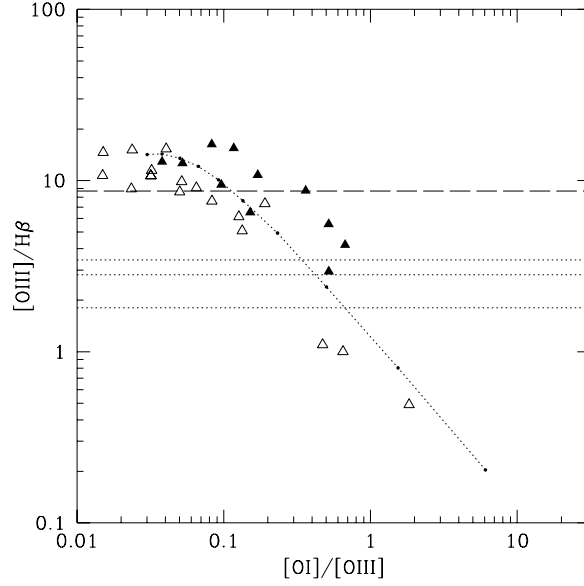


Figure 24: Excitation diagnostic for the ionized gas in low z radio-galaxies ($[\text{OIII}]\lambda 5007/\text{H}\beta$ vs. $[\text{OI}]\lambda 6300/[\text{OIII}]\lambda 5007$). Open triangles correspond to extended emission line regions (EELR) while solid triangles correspond to nuclear regions. The three lower horizontal lines indicate the observed $[\text{OIII}]\lambda 5007/\text{H}\beta$ ($[\text{OI}]$ is not measured) ratio of very high z radiogalaxies (Eales & Rawlings 1993) while the long-dash line corresponds to the “average” radiogalaxy spectrum as derived by McCarthy (1993). The dotted line correspond to the sequence of photoionization models of RFBT87. $\log U$ is in the range $[-4,-1]$.

5.3.2 Effects of viewing direction on the UV lines

To see if these models reproduce the observed $\text{CIV}/\text{Ly}\alpha$ and $\text{CIV}/\text{CIII}]$ ratios, we have presented the observed and predicted values in Fig. 25. The line ratios shown correspond to calculations in which the ionization parameter is varied, generating a sequence in U . The three sequences differ in density or metallicity and $\log U$ is in the range $[-4,-1]$.

We find that somewhat higher values of U than are typically used in the optical are required to reproduce the $\text{CIV}/\text{CIII}]$ ratio observed. We have investigated possible effects due to variations in metallicity and density (see Fig. 25), but none of them is able to explain the high values of the line ratios, unless a higher ionization parameter than in the optical is considered. This is most probably a consequence of the different way in which the objects at high and low z are selected: the distant sources are all very powerful radio sources with luminous AGN. For a power law of index -1.4 , the optimum value is $U \simeq 0.1$. Hereafter, diagrams will only cover the range of $[0.01,0.1]$ in U .

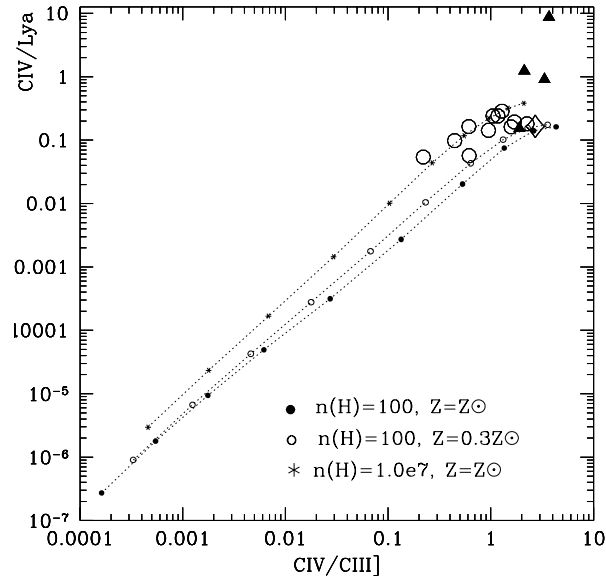


Figure 25: Observed and predicted UV line ratios. Filled triangles are the ratios of objects observed by several authors. Open circles correspond to data taken from van Ojik’s thesis, selected on the basis of a very steep radio spectrum. The open diamond is the average radiogalaxy spectrum of McCarthy (1993). Dotted lines represent models in which the front and back spectra have been summed. $\log U$ is in the range $[-4, -1]$, as in Fig. 24. It is clear that high values of the ionization parameter U are required to reproduce the high $\text{CIV}/\text{CIII}]$ value observed.

A notable observation is the distribution of observed points above the model loci in Fig. 25 even at the highest value of U . In the extreme objects at least — like F 10214+4724 and TX 0211-122 — this results from a weakening of $\text{Ly}\alpha$ rather than from atypical values of $\text{CIV}/\text{CIII}]$. It is usually claimed that the destruction of $\text{Ly}\alpha$ photons by resonance scattering in the presence of dust is the explanation for its faintness, but why does *not* the same process reduce CIV which is also a resonance line? Is there an alternative explanation for this selective dimming of $\text{Ly}\alpha$?

To answer this question, we examine the geometrical aspects of the line formation process. Each emitting cloud is approximated as a plane parallel slab which contains a fully ionized region and a partially ionized zone where low ionization species co-exist (e.g., O^0 , S^+ , etc) with a mixture of H^0 and H^+ . In principle there can be an additional neutral zone which does not contribute to the emission line intensities (see Fig. 4, Chapter 2).

In this section we consider the dust-free case. For most lines (like $\text{CIII}]$, HeII , $\text{H}\beta$, $[\text{OIII}]$, etc) line opacity is negligible and the line is emitted isotropically with photons escaping freely in all directions. However, when the line opacity is important as it is for CIV and $\text{Ly}\alpha$, line scattering occurs which increases the path length. Another important effect of large optical depths is that the line photon will not escape isotropically. A resonance line photon following many scatterings must statistically escape in the direction of highest escape probability which can

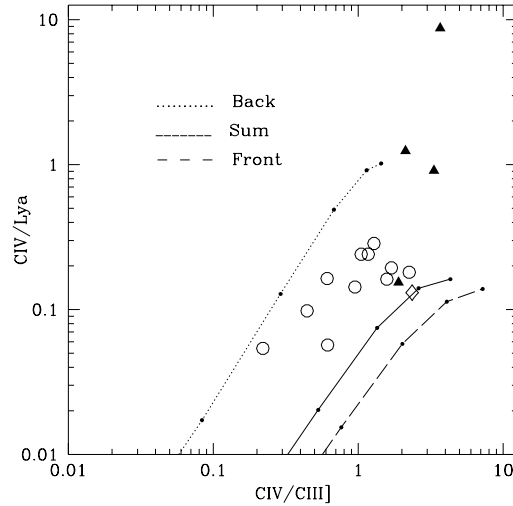


Figure 26: Influence of viewing geometry on the UV line ratios. The dotted line corresponds to the line spectrum seen from the *back* of the slab (cf, Fig 4, Chapter 2) while the dashed line corresponds to the spectrum seen from the *front* (UV irradiated face). It is apparent that perspective plays a very important role on the CIV/Ly α ratio. The solid line represents models obtained by summing the back and front spectra which would represent symmetric case where equal numbers of clouds are observed with shadowed and illuminated faces. The data are the same as in Fig. 25.

be shown to be the front for the photoionized slab depicted in Fig. 4 (Chapter 2). In the case of Ly α , the reason is that — while Ly α photons are generated more or less uniformly within the slab (except within the PIZ) by recombination — the neutral fraction and therefore the incremental line opacity $d\tau_L/dx$ increases monotonically as a function of depth as discussed in more detail by Binette et al. 1993b (BWVM3). This means that for an *open* geometry like that shown in Fig. 4 (Chapter 2), the zone of equal escape probability of front *vs* back occurs far beyond the point where half the luminosity of Ly α is produced. For the collisionally excited CIV line, the tendency to escape from the front also exists although it is less pronounced. It arises mainly because the emissivity of CIV is larger towards the front due to the temperature gradient across the C⁺³ zone. Note that while CIV is emitted and scattered within the rather limited zone containing C⁺³, Ly α remains subject to scattering outside the region where it is produced. While most Ly α emission is produced in the fully ionized zone, most of the line opacity occurs within the PIZ. The presence of a layer of neutral gas beyond the PIZ will increase the anisotropy of Ly α escape.

The effects described qualitatively above are shown in Fig. 26 using detailed photoionization calculations. We present the same sequence of dust-free models as in Fig. 25 but distinguish between the spectrum seen from the *back* — equivalent to observing the clouds through the PIZ — from that seen from the *front* — equivalent

to seeing the UV irradiated side. The differences are striking: both Ly α and to a lesser extent CIV are fainter when seen from the back. The CIII] line is isotropic in the dust-free case. The fact that Ly α is more affected by perspective is due to the significant amount of neutral hydrogen (i.e., large line opacity) in the PIZ which acts as a mirror. Although we have considered a very simplified geometry in our calculations, the method nevertheless treats properly the essential physical effects and indicates how important the viewing direction is in this open geometry.

Fig. 26 suggests that perspective effects alone (*without any dust*) are sufficient to explain the weak Ly α seen in some objects. Ionization bounded calculations with $U = 0.1$ imply total hydrogen column densities (H⁺ region + PIZ) $N_H \sim 10^{22} \text{ cm}^{-2}$ (of which about 60% is ionized). Adding a modest neutral zone beyond the PIZ of $\simeq 4 \cdot 10^{21} \text{ cm}^{-2}$ would double the CIV/Ly α ratio without affecting in any way the CIV/CIII] ratio. It seems, therefore, that a geometry where we see preferentially the ionized gas from the side of the PIZ gives us an explanation for the weakness of Ly α .

How would this apply to the EELR of powerful radio galaxies? In a very simplified scheme, we can imagine (see Fig. 27) that the clouds seen from the nearside cone are seen from a direction which we approximate as the back perspective in our slab calculations while clouds on the far side would be seen from the front. The studies of McCarthy, van Breugel & Kapahi (1991) which emphasized the one-sidedness of the line brightness distribution suggest that the observer with limited spatial resolution at very high z will be biased towards either a back or front dominated perspective depending on whether it is the near or the farside illuminated cone which is intrinsically brighter. Our proposed interpretation of the high CIV/Ly α ratio of some objects in Fig. 26 is that they correspond to the case where the brightest clouds are seen from behind. Note that, because of the intensity weighting, there is rather little difference between the pure front perspective and the sum of equal numbers of front- and back-clouds, a small effect which is not easily distinguished from that of slightly reducing the value of U .

Our conclusion from this section is that perspective effects in an open — externally illuminated cloud — geometry go a long way towards explaining the behaviour of the CIV, Ly α , CIII] line ratio diagram which implies that, when spatially resolved spectra become available, marked asymmetries in the CIV/Ly α ratio could arise when the axis of the illuminated cones forms a large angle with the sky plane.

5.3.3 The effects of internal dust

There is evidence for the existence of dust in some high z radio galaxies. The detection of 4C41.17 ($z = 3.8$) and B2 0902+34 ($z = 3.5$) (Chini & Krügel 1994; Dunlop et al. 1994) and 8C1435+635 ($z = 4.26$) (Ivison 1995) in the mm spectral range is attributed to warm dust. Also, the IRAS galaxy F10214+4724 ($z = 2.29$) has been shown, from the far infrared flux, to contain $\sim 10^8 M_\odot$ of dust,

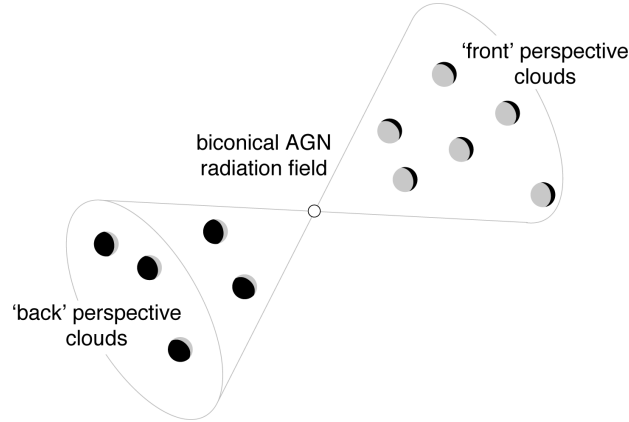


Figure 27: *Front* and *back* clouds within the ionized cones of a radio galaxy.

although this figure may be reduced by the gravitational lensing amplification factor (e.g. Eisenhardt et al. 1995; Serjeant et al. 1995). In addition, the mid- to far-infrared measurements at intermediate z are explained as emission from warm dust (Heckman, Chambers & Postman 1992). We should emphasize, however, that we have no direct measurement of how this dust is spatially distributed. In the event that this infrared emission arises from the reprocessing of higher energy photons from the AGN by a dusty torus, it has no direct bearing on our modeling of ionized gas at tens of kpc. However, there is considerable evidence that aligned blue polarized continuum is the result of scattering of the anisotropic nuclear radiation field by dust (e.g., Cimatti et al. 1993). In this case it is very likely that at least some of the dust is internal to the extended line emission regions. In this section we consider the effects of including dust within the gas clouds which emit the UV lines.

We illustrate the effects of dust mixed with the emitting gas in Fig. 28 where we plot sequences of models which correspond to the front perspective for three different dust-to-gas ratios: $\mu = 0, 0.3$ and 1 . The effects on the line ratios are evident. The resonance scattering suffered by CIV and Ly α increases their pathlengths many times and, therefore, the probability of their being absorbed by dust grains is much higher than for CIII]. In the case of Ly α , however, the geometrical thickness of the H $^+$ region exceeds greatly that of the C $^{+3}$ since we observe more than one stage of ionization of metals (e.g. C $^{+2}$). Any reasonable parameters for the ionization structure of a photoionized slab with $Z \sim 1$ indicates that the opacity in Ly α greatly exceeds that of CIV, which implies a larger pathlength increase for Ly α than for CIV. This results in relatively more Ly α absorption by dust. This effect explains how the ratio CIV/Ly α increases somewhat with increasing μ . Dust absorption of resonant CIV on the other hand causes a comparable decrease in CIV/CIII]. What is important in these results is that, even with a concentration of internal dust as high as $\mu = 1$ (equivalent to that in solar neighbourhood cold clouds), it is not possible to reproduce the high ratio CIV/Ly $\alpha \geq 1$ which is

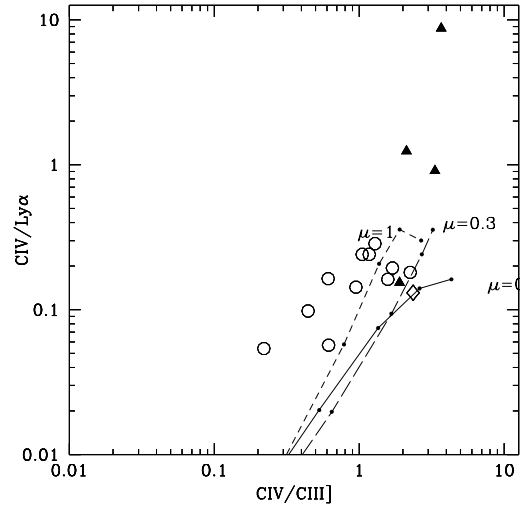


Figure 28: Effects of varying the amount of internal dust as seen from the front perspective. As in the previous figures, the various lines correspond to sequences in U . Short-dashed line corresponds to models with $\mu = 1.0$, the long-dashed to models with $\mu = 0.3$ and solid line to dust free models.

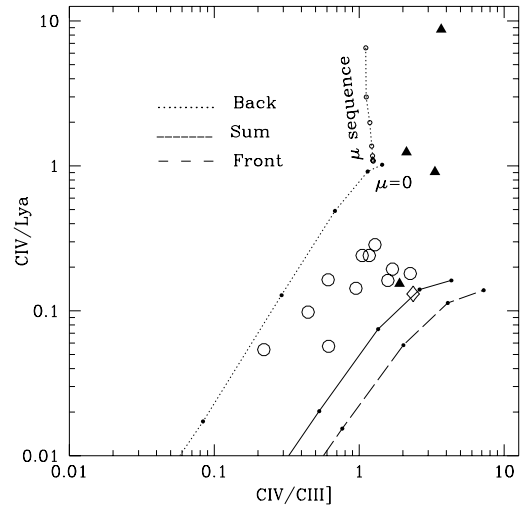


Figure 29: Effects of perspective combined with small quantities of internal dust. The dust-free U sequences of Fig. 26 are repeated in this figure. The dotted line connected by open circles corresponds to the last model with $U = 0.1$ (but with metallicity $Z = 0.3$ in which the dust content is increased in proportion up to $\mu = 0.017$). Larger quantities of dust do not improve these results because dust severely extinguishes both the CIII] and CIV lines which are produced in the front layers.

observed in some objects and has been attributed to dust.

When the clouds are viewed from behind, even with $\mu = 0.3$ they are sufficiently opaque that all the UV lines are severely absorbed. With $\tau_V = 5 \cdot 10^{-22} \mu N_H \sim 5$ and $\mu = 1$, all of the high excitation UV lines become absorbed within the PIZ. To produce an acceptable spectrum, without reddened CIV/CIII] and CIV/HeII ratios, as seen from the back of an ionization bounded slab with $U = 0.1$, we have to use much smaller amounts of dust like $\mu \simeq 0.017$ (2% of local ISM) in models. In Fig. 29, we plot the back and front sequences for such models. These can reproduce the weak Ly α objects although this result is obtained only for the back spectrum, emphasizing that perspective is the dominant factor. It should be noted that the amount of extinction within the ionization bounded slab implied by $\mu = 0.017$ (i.e., $A_V \simeq 0.1\text{--}0.2$) is consistent with the quantity of small dust grains needed to explain the extremely blue continuum of the “detached” ionized cloud in PKS 2152-69 (di Serego Alighieri et al. 1988; Magris & Binette private communication), supposing that the continuum energy distribution is the result of dust scattering of the nuclear radiation.

Note that because the scattering/absorbing dust is locally kinematically linked to the emission line gas, we require much smaller column densities of HI than the absorbing screen proposed by van Ojik et al. (1994) ($\sim 10^{23} \text{ cm}^{-2}$) to explain CIV/Ly $\alpha \sim 1$. The line widths and centroids of the PIZ and of the fully ionized gas are expected to be quite similar within each of the emitting clouds, the ensemble of which could have a greater ‘turbulent’ velocity dispersion.

To reproduce the extreme case of the IRAS galaxy F10214+4724 with CIV/Ly $\alpha \sim 10$, we need additional neutral gas beyond the PIZ. For instance, it requires only a column density of $N_{H^0} \sim 1.5 \cdot 10^{21} \text{ cm}^{-2}$ assuming $\mu = 0.017$. Alternatively we might consider that μ within the PIZ increases with depth as the degree of ionization decreases. In this case, no additional HI gas would be required. If this IRAS galaxy is indeed an extreme Seyfert 2 as argued by Elston et al. (1994), then a closed, dust enshrouded geometry as proposed by BWVM3 to explain the Lyman and Balmer decrements in Seyfert 2 would be more appropriate than the open geometry adopted here which may be applicable only to the truly extended large scale gas. It is likely that objects with unusually strong NV λ 1240 emission (such as in F10214+4724 and TX0211-122) are cases where the NV originates predominantly from the inner NLR. A high NV/CIV ratio indicates very enriched gas which is not unexpected within the inner parts of an AGN (Hamman & Ferland 1993) and is consistent with the lack of convincing evidence that NV is spatially resolved in any of these objects.

5.3.4 Neutral gas mirrors

So far we have considered the effects of scattering by gas which forms part of the line emitting clouds: we refer to this as an ‘intrinsic’ process. Similar effects could be produced by a large-scale distribution of predominantly neutral material

surrounding the emitting regions: we will refer to this as the ‘extrinsic’ case. Any extrinsic neutral gas component with a non-negligible covering factor could affect the observed spectra in a way which mimics that of the back perspective described earlier. Let us suppose that this outer material is broken up into cold gas clumps which are randomly distributed. In such a case, some Ly α photons which leave the ionized cones will escape the region through the holes between the external clumps while others will strike the neutral clumps and be immediately scattered away to escape eventually through another hole in a different direction (see Fig. 30). If observed with sufficient spatial resolution, such a geometry would result in holes in the Ly α brightness distribution due to reflection by intervening clumps as well as diffuse sources corresponding to reflection from clumps on the far side of the source. The bulk of the Ly α luminosity would be preserved but redistributed on an apparently larger scale than the true line emitting clouds. Only a more closed geometry would result in a significant destruction of Ly α , assuming that the interclump space does not contain pure dust segregated from the gas phase.

The reflection efficiency of clouds will, of course, depend strongly on the relative velocity fields of the emitting and the cold regions. If the extended gas has a large scale ordered motion but small ‘microturbulence’, the reflection effects would be localized. Broad Ly α emission and continuum from the AGN could, however, be scattered by any of the extranuclear clouds (see below, 3C294). In general, we would expect the diffuse, scattered Ly α to show a narrower line profile than the integrated emission profile.

We will review the observational evidence for the existence of such large scale mirrors.

The radio galaxy PKS2104-242

PKS2104-242 (McCarthy et al. 1990b) shows very extended emission lines of Ly α , CIV and HeII associated with continuum knots which lie between the radio lobes and are aligned with the radio axis. The Ly α image shows emission resolved into three distinct clumps, two of them corresponding roughly with the two continuum knots. In addition, there appears to be a low surface brightness halo of emission surrounding the entire object. Is this halo a consequence of reflection by neutral material of either Ly α emission or of the intense nuclear *continuum*, or are these photons emitted locally by H⁺ recombination? A way of discriminating between these two possibilities is to look for the detection of any other emission line in the halo. If Ly α is the result of reflection by cold HI, there will be *no* other lines (except possibly resonant MgII). If it is instead produced by recombination, other lines should be detected in the rest-frame optical band like H α , [OIII] λ 5007, etc.

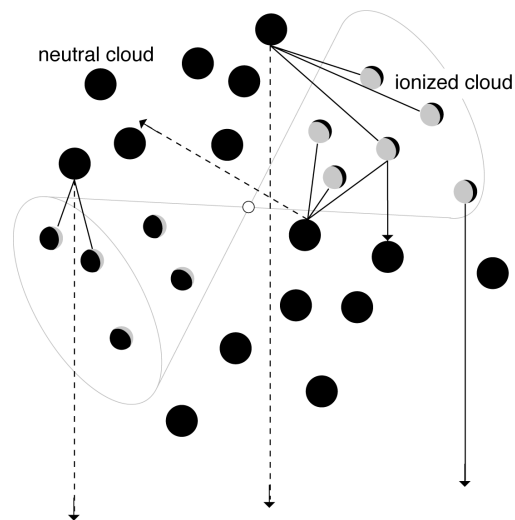


Figure 30: The extrinsic case. Neutral material external to the ionized regions can strongly influence the appearance of the object in $\text{Ly}\alpha$. In this figure, the neutral clumps (black clouds) cover a significant fraction of the ionized regions (grey+black clouds). The solid arrows represent $\text{Ly}\alpha$ photons emitted directly in the ionized regions. Dashed arrows represent $\text{Ly}\alpha$ photons that after striking neutral clumps are then reflected in other directions. The reflection by the neutral H atoms is so effective that the dust has little chance to interact with the photons before they find a hole to escape.

The radiogalaxy 3C 294

From images of this object, McCarthy et al. (1990a) report the existence of Ly α emission extending over a region covering 170kpc. The Ly α emission is elongated and well aligned with the inner radio-source. An intriguing aspect of the observations is the one-sidedness of the CIV emission (obtained with a long slit aligned with the axis of elongation). The decreasing linewidth of Ly α on the side where CIV is absent (South) suggests to us the possibility that Ly α in the south corresponds to scattered *continuum and BLR Ly α photons* by HI clumps lying along this direction provided the ionizing radiation has already been reprocessed (filtered out) within the nuclear regions into NLR or BLR emission.

Failing that (scattering by HI clumps), an alternative possibility resides in very thin matter-bounded photoionized sheets of gas which can be very efficient at reflecting the intense (beamed) nuclear continuum as well as BLR Ly α photons. Due to its large scattering cross section, very small column depths of H⁰ (a trace specie within the ionized phase) are sufficient to scatter effectively the impinging flux within the core of the Ly α thermal profile. If we suppose the existence within the cone of ionization of the radio-galaxy of a population of clouds of similar physical conditions to that thought to apply to Ly α forest clouds, the energy reflected due to resonant scattering by HI typically exceeds that generated within the clouds by reprocessing of the ionizing radiation (i.e. by recombination). In effect, adopting $N_{H^0} = 10^{13.8} \text{ cm}^{-2}$ as a typical column density of such cloud, we derive an equivalent width in absorption (i.e. the scattered intensity) of

$$EW_{Ly\alpha}^{abs} \approx 0.15 \sqrt{\ln(4.2 \cdot 10^{-14} N_{H^0})} \text{ \AA} = 0.15 \text{ \AA}$$

which corresponds to the saturated part of the Ly α curve of growth. Adopting for definiteness $U = 0.1$ and $\alpha = -1.4$, we obtain that the fraction of reprocessed ionizing photons, F_{MB} , within a very thin photoionized sheet¹ is given by

$$F_{MB} \approx 1.8 \cdot 10^{-18} N_{H^0} = 1.1 \cdot 10^{-4}$$

The equivalent width of Ly α in emission as a result of recombination is simply

$$EW_{Ly\alpha}^{em} \approx 390 F_{MB} C_f \text{ \AA} = 0.04 C_f \text{ \AA}$$

where C_f is the covering factor. If we integrate the absorbed intensity over the same area as that given by C_f , the ratio of scattered versus emitted Ly α is ~ 4 (the ratio between the above two equivalent widths). Allowing for the fact that the cloud will be exposed not only to the nuclear continuum but to the BLR Ly α which typically peaks at twice the continuum level, the ratio can be expected to increase up to 8 times the Ly α emitted by recombination. To account for the

¹With these parameters, the total column density is given by $N_H = N_{H^+} \approx 2.3 \cdot 10^4 N_{H^0}$.

observed FWHM $\leq 1000 \text{ km s}^{-1}$ in 3C294 (South), one must rely on a turbulent velocity field for the Ly α clouds.

We ought to consider seriously the possibility that Ly α on the southern knot of 3C294 corresponds to large scale scattered light by either HI or even ionized gas unless other bona fide emission lines were detected. So far, no lines other than Ly α are observed and this is consistent with our suggestion. The only certain way of discriminating between reflection and *in situ* emission would be the detection at this radius of *any* non-resonance line in either the optical ([OII], [OIII], H β etc.) or the UV (CII], CIII]). To conclude, we believe that HII regions or starbursts should not be considered the default emission mechanism in cases where only Ly α is present, especially along the axis where the AGN supposedly collimates its intense nuclear continuum + Ly α (BLR) light.

Ly α absorption in 0943-242

The radio galaxy 0943-242 shows a Ly α profile with several absorption features which cover the whole spatial extent of the Ly α emission (Röttgering et al. 1995). The strongest of the absorbers is at least as extended spatially as the emitting region ($\sim 13 \text{ kpc}$) and its HI column density is 10^{19} cm^{-2} . The absorption line is blue-shifted 250 km s^{-1} with respect to the emission peak. The ‘screen’ is kinematically distinct from the emitting gas and therefore clearly external to the emitting clouds). This is a clear demonstration that HI screens — or mirrors depending on the perspective — exist on galaxy scales at these early epochs. From Fig. 5 of Röttgering et al., we estimate that this cloud would reflect $\sim 30\%$ of the Ly α . Thicker clouds could exist around other objects but would be hard to detect when only the faint wings at the extremities of the emission profile were transmitted. In the case of 0943-242, even if the screen contained dust, its effects would be negligible. The reason, as stated before, is that Ly α photons (seen by the cloud) are incident from the exterior and will be very effectively scattered away before being absorbed by the dust. Even the photons getting through (i.e., without any scattering) to us because they are sufficiently far in the wings of the profile would not see much dust in this particular cloud. With such low column densities, $\tau_V \sim 5 \cdot 10^{-22} \mu N_H = 7.5 \cdot 10^{-5}$ for $\mu = 0.015$ and $\tau_V \sim 0.005$ for $\mu = 1$. Much thicker clouds may result in some non-negligible extinction but again this does not arise because of the multiple scattering of Ly α .

5.4 Conclusions

If the large-scale extended emission line regions (EELR) in radio galaxies are photoionized predominantly by the collimated UV radiation emitted by a hidden AGN, the line emission and transfer processes are characterized by what we call an ‘open’

geometry with externally illuminated clouds. This produces an emission line spectrum which is distinctly different from an internally ionized HII region, especially in the ultraviolet.

Our principal conclusion is that internal dust, even in proportions as large as that found in the solar neighbourhood, does not satisfactorily explain the large CIV/Ly α ratios commonly seen in groundbased observations of high redshift radio galaxies. We have demonstrated that geometrical effects can, in most cases without invoking any dust, explain the observed trends in the data. While internal dust can quite effectively kill the Ly α luminosity, it is essential to examine also its effects on the other UV lines, especially CIV which is also a resonant transition. Although some internal dust within the ionized gas is allowed by our modeling and is required in a few cases, we find that the effects of geometrical perspective dominate the observed decrease of Ly α without affecting excessively the other lines. This implies that the faintness of Ly α cannot necessarily be used as an argument to demonstrate the existence of dust in these objects.

The influence of these geometrical factors on the line spectrum gives us, potentially, a natural explanation for some of the emission line asymmetries seen in the 'alignment effect' radio galaxies.

We have also investigated the effects that material external to the ionized cones will have on the appearance of the objects in the light of Ly α . We suggest that the existence of diffuse Ly α halos observed in some high z radio galaxies could be due to the reflection of Ly α photons by neutral clumps lying outside the ionization cones. In addition to reflecting Ly α , such neutral clouds could be responsible for the spatially extended absorption seen within the Ly α emission profile. Pure Ly α emission clouds need not, therefore, necessarily be identified as star-forming regions.

References

- Binette L., Wang J.C.L., Zuo L., Magris C.M., 1993a, *Astron. J.* 105, 797
- Binette L., Wang J.C.L., Villar-Martín M., Martín P.G., Magris C.M., 1993b, *Astrophys. J.*, 414, 535 (BWVM3)
- Chambers K.C., Miley G.K., van Breugel W.J.M., 1987, *Nature*, 329, 604
- Chini R., Krügel E., 1994, *A&A*, 288, L33
- Cimatti A., di Serego Alighieri S., Fosbury R.A.E., Salvati M., Taylor D., 1993, *Mon. Not. Roy Astr. Soc.*, 264, 421
- di Serego Alighieri, S., Binette, L., Courvoisier, T. J- L., Fosbury, R.A.E. & Tadhunter, C.N., 1988. *Nature*, 334, pp. 591-593
- di Serego Alighieri S., Cimatti A., Fosbury R.A.E., 1993, *Astrophys. J.*, 404, 584
- di Serego Alighieri S., Cimatti A., Fosbury R.A.E., 1994, *Astrophys. J.*, 431, 123

- Dey A., Spinrad H., Dickinson M., 1995, *Astrophys. J.*, 440, 515
- Dunlop J.S., Hughes D.H., Rawlings S., Eales S.A., Ward M.J., 1994, *Nature*, 370, 347
- Eales S.A., Rawlings S., 1993, *Astrophys. J.*, 411, 67
- Eisenhardt P., Soifer B.T., Armus L., Hogg D., Neugebauer G., Werner M., 1995, *BAAS*, 186, 5202
- Elston R., McCarthy P.J., Eisenhardt P., Dickinson M., Spinrad H., Januzzi B.T., Maloney P., 1994, *Astron. J.* 107, 910
- Fosbury R.A.E., di Serego Alighieri S., Courvoisier T., Snijders M.A.J., Tadhunter C.N., Walsh C.N., Wilson W., 1990, in *Evolution in Astrophysics*, Toulouse, ESA SP-310
- Hamman F., Ferland G., 1993, *Astrophys. J.*, 418, 11
- Heckman T.M., Chambers K.C., Postman M., 1992, *Astrophys. J.*, 391, 39
- Hummer D.G., Kunasz P.B., 1980, *Astrophys. J.*, 236, 609
- Isaak K.G., McMahan R.G., Hills R.E., Withington S., 1994, *Mon. Not. Roy Astr. Soc.*, , 269, L28
- Iverson R.J., *Mon. Not. Roy Astr. Soc.*, 275, L33, 1995
- Lilly S.J., 1988, *Astrophys. J.*, 333, 161
- McCarthy P.J., van Breugel W.J.M., Spinrad H., Djorgovski S., 1987, *Astrophys. J.*, 321, L29
- McCarthy P.J., Spinrad H., van Breugel W.J.M., Liebert J., Dickinson M., Djorgovski S., Eisenhardt P., 1990a, *Astrophys. J.*, 365, 487
- McCarthy P.J., Kapahi V.K., van Breugel W.J.M., Subrahmanya C.R., 1990b, *Astron. J.* 100, 1014
- McCarthy P.J., van Breugel W.J.M., Kapahi V.K., 1991, *Astrophys. J.*, 371, 478
- McCarthy P.J., Elston R., Eisenhardt P., 1992, *Astrophys. J.*, 387, L29
- McCarthy P.J., 1993, *ARA&A* 31, 639
- van Ojik R., Röttgering H.J.A., Miley G.K., Bremer M.N., Macchetto F., Chambers, K.C., 1994, *A&A*, 289, 54
- van Ojik R., 1995, Ph.D.thesis, Rijksuniversiteit te Leiden
- Robinson A., Binette L., Fosbury R.A.E., Tadhunter C.N., 1987, *Mon. Not. Roy Astr. Soc.*, 227, 97 (RBFT87)
- Röttgering H.J.A., Hunstead R.W., Miley G.K., van Ojik R., Wieringa M.H., 1995, *Mon. Not. Roy Astr. Soc.*, in press
- Serjeant S., Lacy M., Rawlings L.J., King L.J., Clements D.L., 1995, *Mon. Not. Roy Astr. Soc.*, 276, L31

Spinrad H., Filippenko A.V., Wyckoff A., Stocke J.T., Wagner R.M., Lawrie D.G., 1985, *Astrophys. J.*, 299, L7

Sutherland R.S., Bicknell G.V., Dopita M.A., 1993, *Astrophys. J.*, 414, 510

Tadhunter C.N., Fosbury R.A.E., Quinn P.J., 1989, *Mon. Not. Roy Astr. Soc.*, 240, 255

Tadhunter C.N., Robinson A., Morganti, R., 1989. In: *ESO Workshop on Extranuclear Activity in Galaxies*, p. 293, eds Meurs, E.J.A., Fosbury, R.A.E., ESO Conf. and Workshop Proc. No. 32, Garching

Chapter 6

Discussion

The projects developed in this thesis, although selfcontained, provide results relevant, not only to the individual class of objects or gaseous regions considered, but also to the nature of active galaxies in general. In this concluding chapter, I want to summarize what we have learned about the family of active galaxies and connect our results with the current ideas on this field.

Active galaxies have been subdivided into several subgroups defined according to the strength and breadth of their emission lines and their luminosity over the entire electromagnetic spectrum. Sometimes, different physical conditions and emission mechanisms are responsible for the differences between subgroups. In some cases, however, objects pertaining to distinct groups can be intrinsically similar, the differences being due to pure geometrical effects. This statement summarizes the basic ideas of the so called “unified scheme models” (e.g., Lawrence & Elvis 1982, Lawrence 1987, Barthel 1989), mentioned several times in this work. Such model propose that different classes of AGNs are the same kind of object but seen from different directions. The directionality is taken to be due to an anisotropic distribution of absorbing or scattering matter and a simple geometry which would produce this situation involves an absorbing torus around the nucleus (the proposed “molecular torus”). In such scenario, the continuum produced in the central, hidden nucleus is emitted anisotropically into two wide, oppositely directed ionized cones, as a result of the collimation by the torus.

Where does the unified scheme enter our discussion? It is represented in the kind of geometry assumed in all our calculations, in which a hard ionizing continuum illuminates the gas *externally*: a different situation from the one existing in HII regions, or planetary nebulae, where the continuum source (the stars) is embedded within the gaseous region. In AGNs, numerous pieces of evidence indicate that the main ionization mechanism of the EELRs is photoionization by a hard continuum, which is produced in the central engine (shocks could also play a role, see section 6.2). Such situation is better described by an open geometry.

The resulting models are able to explain the observed data which suggests

that the scene is basically correct. However, the relatively high number of input parameters necessary to construct the models allows an apparent high degree of freedom to fit the observational results. One might argue that, using another geometry, the same strategy would have driven us to the same results. The question is, how unique is the scheme that can reproduce the observed data?

Different observational pieces of evidence restrict the n-dimensional space of valid input parameters, to a much smaller space than that of all the models able to reproduce the observed emission line ratios. In this thesis, each chapter where theoretical models are presented, justifies in detail the assumed input parameters, based on our own or other authors' knowledge. We select the input parameters in accordance with the nature of the objects and regions under study.

This chapter is divided into several sections, each one referred to a specific aspect of the nature of active galaxies: dust, ionization mechanisms and geometry. Every section is completed with a brief overview of the current state of the field, as well as a comparison between other authors' results and ours.

6.1 Dust in the ionized regions.

Dust has been the main object of investigation in this thesis. We have provided a detailed analysis of the interaction between the dust grains and the radiation impinging on the gaseous component. We have also studied its effects on the line emission from the ionized gas like changes on the ionization structure of the gas, electronic temperature, metallicity, etc. Taking these effects into account is necessary in order to interpret more correctly what is observed.

This understanding is useful, for instance, to distinguish when dust must be considered and when its effects can be neglected, allowing a simplification in the interpretation. Robinson et al. (1987, hereafter RBFT87) showed that in several diagnostic diagrams involving optical lines, the observed position of the EELR of radio galaxies at low z were well represented by a sequence in which one simply varies the ionization parameter, U (a measurement of the excitation level of the emitting gas, see Chapter 2). Using the observed values of the line ratios, they inferred that the EELR spectra were not reddened and presented models which did not include dust effects.

I used the same set of data employed by these authors in order to investigate how dust mixed with the ionized gas would influence the predicted line ratios and, therefore, the positions within the diagnostic diagrams (Villar-Martín, 1993). The models showed that internal dust does not affect severely the optical line ratios (unless species susceptible of depletion are considered!). The influence is negligible for low U values and increases with this parameter. For highly excited EELR, like a few of the objects in RBFT87's sample, we should be more careful. At such high U , the effects of dust are stronger (see Chapter 2) and it might be necessary to consider them when interpreting their observed ratios. However, for typical EELRs at low redshift, where the ionization parameter is in the range $[-4, -3]$ in the logarithm, dust effects on the optical line ratios are not relevant. The absence of reddening effects does not imply that dust is *not* present, instead is probably indicative of an open geometry for the gaseous ionized regions, where the clouds are externally illuminated. In a closed geometry, dust effects are stronger and the high reddening of some NLR line ratios of Seyfert 2 suggests a much higher covering factor than previously assumed (see Chapter 2).

The situation described in the previous paragraph has advantages and disadvantages. On the one hand, if dust effects are negligible, we can simplify enormously our modeling when interpreting the optical line ratios or the diagnostic diagrams that have been traditionally used to learn about the nature of the ionizing source and the physical conditions of the ionized gas. We are therefore confident that our diagnostics are not wrong because of dust effects which we did not take into account. On the other hand, these same optical line ratios, easy to measure, do not tell us about the properties of the dust in the EELR, not even whether dust exists or not. As explained in Chapter 3, we need to develop other strategies and tools which are highly sensitive to dust, like observations of emission lines

emitted by species *susceptible to depletion*, as shown in detail in Chapters 3 and 4. In these chapters we have studied (theoretically + observationally) the emission of the [CaII] $\lambda\lambda 7291, 7324$ lines, which are appropriate because 1) calcium is an element very sensitive to depletion, and 2) as our models demonstrate, these lines should be strong and easy to detect under the physical conditions of EELR whose the gas does not contain dust. Their weakness demonstrates that *dust does exist in the EELR of low z RGs*. This favours the idea that the origin of the EELR is interaction or merging of two or more galaxies rich in gas, rather than cooling from a hotter corona, a scenario which is difficult to reconcile with the existence of dust mixed with the emitting gas (see section 4.4.1).

6.1.1 Dust at high z .

The subsequent question is: *can we extrapolate our conclusion to high z EELRs? Can we affirm that they also contain dust?* The answer is *NO*. The techniques applied in this thesis, do not demonstrate the existence of internal dust mixed with the ionized gas of high z radio galaxies. However, as explained in Chapter 5 and below, there is strong evidence that dust exists in objects at redshifts as high as 2 and even more. Our work does not contradict this, but demonstrates that the line diagnosis based on UV (or optical) line ratios does not help us to infer the presence of dust because other factors, like geometry, dominate what we see. We have studied the UV emission line spectrum of a sample of high z radio galaxies analyzing the position in the diagnostic diagram CIV $\lambda 1549$ /Ly α vs. CIV $\lambda 1550$ /CIII] $\lambda 1909$. Both line ratios are very sensitive to geometry and dust due to the resonance character of the CIV $\lambda 1549$ and Ly α lines. We have demonstrated that dust, even in proportions as large as the one found in our ISM, can not explain the observed data, unless the influence of geometry is considered. In fact, our study shows that geometrical effects can in most cases, without invoking any dust, explain the observed data. Our models allow some internal dust but it must be in very little amounts ($\sim 2\%$ of the dust/gas ratio in our ISM) in order to not contradict other line ratios, like CIV/CIII, which is not reddened. Effects of geometrical perspective, and not dust, dominate the observed line ratios.

This can have important implications. As explained in Chapter 5, the weakness of Ly α has been used as an argument to demonstrate the existence of dust at high z but we have shown that there is an alternative explanation based on purely geometrical effects. The resonance character of the Ly α line makes neutral hydrogen a very efficient mirror for the Ly α photons which, depending on the *geometry*, prevent photons from reaching the observer. In this case the line becomes much fainter than expected while no photons have actually been destroyed but rather deflected from our line of sight. Conversely this same effect can be responsible for the apparent strength of Ly α emitted from regions associated with neutral hydrogen and which reflects Ly α photons back towards the observer. This could explain the huge Ly α halos observed around some objects, where the line originates from

zones which seem to be located out of the ionizing cones (like PKS0943-242, see section 5.3). This reflection effect is very efficient, whether dust is present or not, which means that Ly α can even be stronger than predicted in the absence of dust, if the geometry is favourable.

We have shown that the Ly α line (its intensity or ratio with other emission lines) is *not* a reliable indicator of dust, but, on the contrary, a good tool to learn about the gas distribution (ionized as well as neutral) and, thus, about the geometry of the object. I will discuss further this point in section §6.4.

The existence of dust at high z is indicated by other observational pieces of evidence like the extended polarized blue continuum mentioned several times in this work. Also, as explained in Chapter 4, there are several objects at high z detected in the millimeter spectral range, like 4C41.17 ($z=3.8$) and B2 0902+34 ($z=3.5$) (Chini & Krügel 1994; Dunlop et al. 1994). Their fluxes imply the presence of dust masses of the order of $10^8 M_{\odot}$. Also high z quasars have been detected in the millimeter region by Andreani et al. (1993), McMahon et al. (1993) and Isaak et al. (1994).

The paragraphs above refer to objects where the UV line emission is dominated by the EELR. There can also be objects where the unresolved *nuclear emission dominates* over the extended emission (EELR). In such cases, as demonstrated in Chapter 2, a rather closed geometry would be more appropriate. A good example is the IRAS source F10214+4724 ($z=2.3$) (Downes et al. 1992), a galaxy where the emission lines seem to reveal a very strong reddening. IR measurements indicate the existence of large quantities of dust, due in part to the amplification effects of a gravitational lens (e.g. Eisenhardt et al. 1995, Serjeant et al. 1995) which amplifies the IR luminosity. We know that dust is present, also from polarization measurements (Lawrence et al. 1993; Goodrich et al. 1996). But is its emission line spectrum as reddened as some authors claimed (e.g. Elston et al. 1994)? Our results indicate rather little reddening (or a very patchy distribution) while Elston et al. (1994) reported strong line reddening by measuring $H\alpha/H\beta \geq 20$, which would imply $A_V \geq 5.4$. However, according to these same authors, the CIV/CIII ratio is quite high (~ 3.6) (~ 3.4 according to Goodrich et al. 1996). Also, the HeII/CIII ~ 1.7 and CIV/HeII ~ 2.0 ratios (Goodrich et al. 1996) are similar to the values observed for other high z objects (see Chapter 5 and Villar-Martín, Binette & Fosbury 1995). Why is $H\alpha/H\beta$ so reddened and not the UV line ratios? Goodrich et al. (1996) for instance detect broad components of several UV lines in the polarized flux. For CIII, however, a broad component can be seen in direct unpolarized light. Maybe $H\alpha$ has similarly a broad component in direct unpolarized light while the fainter $H\beta$ has none. This would result in an *apparent* higher Balmer decrement. By themselves, the UV line ratios do not indicate high quantities of dust and as explained in Chapter 5, if this object is a Seyfert 2 (Elston et al. 1994), a more closed geometry might be more appropriate for describing the emitting gas. And, as shown in Chapter 2, only small amounts of dust are required to strongly weaken the Ly α emission.

In the near future, I want to combine what we have learned from our photoionization models, with the knowledge that the powerful polarization techniques have already provided. Much of what is known nowadays about the nature of the alignment effect observed at $z > 0.7$ (see Chapter 4, Introduction) is the result of polarization studies, which distinguish between the scattered and the “in situ” continuum emission and tell us about the nature and distribution of the scattering material. In this way, for instance, di Serego Alighieri, Cimatti & Fosbury (1994) were able to exclude the possibility of scattering in two radio galaxies as due to *hot electrons* in a gaseous halo.

Comparisons of our models with the observations do not allow a precise estimation of the amounts of dust existing in the EELRs, both at high and low z . Studying the depletion of calcium, we have demonstrated that dust exists, but we can not say how much. Calcium is so sensitive to depletion that very tiny amounts of dust will deplete it completely: a dust /gas ratio (μ) =0.1 decreases the abundance of calcium in the gaseous phase by a factor of ~ 24 and if $\mu=1$, by a factor of 5000! (see chapter 3). On the other hand, although polarization measurements set strong constraints to the nature and distribution of scattering material, it is still difficult to distinguish between cool electrons and dust as the origin of the scattering (Dey, Spinrad & Dickinson, 1995 and di Serego Alighieri et al. 1996). It could be interesting to investigate if the low dust/gas ratios which we deduce, are able to explain the level of polarization and the polarized flux observed in some objects.

6.2 The ionization mechanism.

There is strong evidence which support photoionization by the hard continuum emitted by the central AGN as the main ionization mechanism of the EELRs (and NLRs) of most radio galaxies and Seyferts, at least at low redshift. At higher z the uncertainties due to the lower spatial resolution and sensitivity of our instrumentation makes such study much more difficult. Moreover, at high z , most objects have been observed in the UV rest frame, a spectral range that is not well known, and still not often used for diagnosis. The optical line ratios that have provided so much information about the nature of low z objects, are redshifted into the IR where the observations are still difficult. The existing IR instrumentation (MIRACLE MPE/ROE camera, UKIRT CGS4 spectrometer, the 3D Near Infrared Imaging Array Spectrometer (MPE), etc) has already allowed the study of the rest-frame optical wavelengths of a few objects at high z (≥ 1) (e.g. Eales & Rawlings 1993, McCarthy, Elston & Eisenhardt 1992), but much more effort needs to be dedicated.

Our models support that photoionization by the hard continuum produced in the central engine is the main ionization mechanism both for the NLR and the EELR line ratios of radio galaxies and Seyferts. However, there is an important

limitation of the optical line ratios as a diagnostic: with photoionization models it is possible to diagnose the mean ionizing photon energy (RBFT87), but not to distinguish between hard power laws and hot black bodies. Ionization by normal stars is ruled out, but a cluster of superhot stars, so called ‘Warmers’ could also explain the optical line ratios.

At this point, I want to center this discussion around shocks, which have not been discussed yet in this thesis and deserve special attention.

6.2.1 Shocks in active galaxies

In many active galaxies radio jets have been detected. Very likely the energy which triggers them is originated in the central AGN. The jet contains relativistic particles accelerated to near the speed of light which propagate through the gas of the host galaxy. In its way out the jet will interact with the external gas and the shocks produced during such an interaction will disturb the kinematics and morphology of that gas. The hot gas behind a fast shock emits cooling radiation and this could also ionize the gas. However, as explained before, we expect that the central AGN plays also an important role in the ionization of the gas. But, which is the dominant process? Do shocks only alter the morphology and density of the gas or do they also modify its ionization state? Jets in AGNs are still surrounded by many mysteries and a clear understanding of the jet/cloud interaction phenomena is needed.

At least for most low z objects, AGN photoionization has had better agreement with the observations. Beautiful evidence supporting this point came from the ionization *cones* imaged in several nearby Seyfert galaxies, like NGC5252 (Tadhunter & Tsvetanov 1989; Acosta-Pulido et al. 1996; see also the clearly defined ionization cones in the WFPC images of NGC5728, Fig. 31). Wilson, Ward & Haniff (1988) suggested a possible broad trend for the radio axis to be aligned with the axis of the extended emission line regions in Seyfert galaxies on a similar spatial scale. Wilson and Tsvetanov (1994) confirmed this tendency, pointing towards a common collimation mechanism of the radio plasma and the ionizing radiation.

In many objects, spectroscopic evidence favours AGN against shock photoionization. For instance, the already mentioned trend defined by the EELRs line ratios in the diagnostic diagrams of RBFT87, which is well explained if they are ionized by the central AGN allowing for a different ionization state (i.e. U) in each object. It is difficult to understand this behaviour with the excitation parameter in the frame of the shock theory.

On the other hand, there have been also problems with photoionization models that shocks were able to explain, at least partially. Three were the main discrepancies: a) too weak high excitation lines, b) too low electronic temperatures, and c) too small range in HeII/H β . A recent work by Binette, Wilson & Storchi-Bergmann (1995) demonstrates that a mixture of matter- and radiation-bounded

Figure 31:

An HST WFPC (1992) image of the core of the barred spiral Seyfert galaxy NGC5728. The bi-conical structure of the ionized gas indicates that ionizing continuum emitted in the central AGN is beamed in two opposite cones (Wilson et al. 1993).

clouds (proposed earlier by Viegas and Prieto, 1992; although not successfully) can solve these discrepancies, without the need of additional heating sources, like shocks. Moreover, from comparing U at different positions within the EELR in many RG (e.g., the radio galaxy 3C227, Prieto et al. 1993), the observations indicate that, in general, the ionization (U) does not change dramatically with radius, as we would expect if photoionization is due to the central AGN. This is a difficult question with no answer yet within the frame of pure AGN photoionization.¹

There are some objects, where the presence of shocks is clear: a clear example is the intermediate redshift ($z=0.310$) radiogalaxy PKS 2250-41 which shows an emission line arc circumscribing the western radio lobe (Tadhunter et al. 1994), which strongly indicates the influence of the radio jet on the distribution and, possibly also on the ionization of the warm gas. Also, the highly disturbed kinematics and the low ionization state near the radio structures is indicative of the presence of shocks. However, the source of ionizing energy is not clear: are the shocks dominating over the AGN continuum and ionizing the gas or are they just compressing the clouds in the arc, which are then ionized by the AGN?

Although at low redshifts, the line emission spectra of most active galaxies are well explained by photoionization by the central AGN it is important to understand the jet/cloud interaction physics to disentangle on a case by case basis which effects are dominant.

In our models we have also assumed photoionization by a hard continuum to explain the UV line ratios of high z radio galaxies. The trend in U shown by the data in the diagnostic diagram $CIV/Ly\alpha$ vs. $CIV/CIII$, is indicative of this kind of excitation. But the possibility that shocks could also play an important role in the ionization of the gas can not be excluded. At high redshifts, radio galaxies show a strong alignment between the optical and the radio structures. One interpretation, well supported by polarization studies, has already been mentioned here: scattering of continuum emitted by the hidden AGN. Another interpretation is that the propagation of the radio jet through the ISM of the host galaxy compresses the gas and triggers intense star formation (e.g. Rees 1987, de Young 1989, Begelman & Cioffe 1989). In fact the optical structures revealed by ground based and HST images (Longair, Best & Röttgering 1995; see Fig. 33) point towards shocked gas, with much narrower spatial distribution than the expected diffuse photoionized cone. High z radio galaxies have been selected on the basis of their powerful radio emission and line spectra. At such high z we are biased towards very powerful objects, where the jet-cloud interaction might be very strong. Moreover, the shocked material, more concentrated, emits stronger lines than the surrounding gas. This could mean that due to the lack of sensitivity of our instrumentation, we are only detecting the material that is interacting with the radio plasma.

In order to reach a clear understanding of the jet/cloud interaction physics,

¹ If shocks are strongly influencing the spatial distribution of the excited gas, even if they do not ionize it, the variation of U may be different than that expected from the pure AGN presence, as often assumed.

Figure 32:
WFPC2 HST images of gaseous jets from three newly formed stars.

it is necessary to use low and intermediate z objects as laboratories, or even more local events, like the jets ejected from stars. HST WFPC2 images of jets originated by newly forming stars (e.g. Stapelfeldt et al. 1995) show the complicated interactions that take place when the ejected gas collides with the interstellar medium (see Fig. 32). The general picture which could describe this scenario is a new star surrounded by a dusty disk, which feeds material onto the star. When the star is hot enough, it will blow away much of the disk. The high speed material will collide with the slower gas in the interstellar medium and a bow shaped shock wave is created. In this way, a cavity is formed surrounding the star. If the shock wave encounters an obstacle (denser isolated clouds), a bow shaped shock wave is formed around the obstacle. Such a process will not only influence the ISM surrounding the star, but also the future of the star itself. The jet can, for instance, modify the mass accretion rate.

The geometry in this scene is quite similar to that which describes the AGN phenomena, where the central source (presumably a black hole) is surrounded by an accretion disk that feeds it. What we learn from stellar jets can be very useful in understanding the role jets play in active galaxies.

6.3 Geometry

This thesis provides a tool for the understanding of the geometrical effects which influence the emission line spectrum radiated by an “open” geometry appropriate for the AGN phenomenon. This study demonstrates how important it is to take perspective effects into account; the narrow line emission depends on the orientation of the ionized cones with respect to the observer. Such geometrical effects, studied in detail by us for the first time, have been used to explain some observational effects, like the UV spectrum of high z radio galaxies and the discrepancies between the predicted and the observed HI line ratios emitted by the Narrow Line Region of Seyfert 2 galaxies (and, therefore, indirectly of Seyfert 1s according to the unification schemes). As explained in section 6.1, we have studied how neutral material external to the ionized cones can influence the “appearance” of an object in the Ly α light.

The excited gas that we see does not necessarily map the distribution of material in the galaxy, but rather, the distribution of *excited* gas. Outside the radiation cones, there must be important reservoirs of neutral material. The work on NGC5252 by Prieto & Freudling (1993) shows that the neutral hydrogen surrounds the nucleus but is located outside the radiation cones of ionized gas. Also, in many high z radiogalaxies, the Ly α profile shows absorption features due to absorption of Ly α photons by intervening hydrogen gravitationally bound to the radio galaxy and spatially extended over a region of ~ 50 kpc in some cases (van Ojik 1995). The HI absorption systems might be due to neutral gas located outside the ionized cones. It is therefore very important to distinguish between excitation and matter

distribution.

As explained in Chapter 5, the rest-frame UV spectral range constitutes a powerful tool for exploring the 3-dimensional structure of active galaxies in general: the existence of resonance lines in this spectral range which are so sensitive to geometry has made this study possible. In the “open geometry” that describes the EELRs, the two opposite cones, with apex in the nucleus which are ionized by the central AGN will most often be forming a non negligible angle with the plane of the sky in such a way that one of the cones will be closer to the observer. It is not a trivial task to distinguish which is closer and which is farther from the observer: only when there is some kind of observable asymmetry is this distinction possible. For instance, in high luminosity FR II sources, one-sided jets are detected, while two-sided jets are detected only in low luminosity (FR-I type) radio galaxies. This jet asymmetry can be explained by an illusion caused by a doppler-boosting effect due to the bulk relativistic motion of the jet. This effect makes the nearest side (to the observer) brighter than the other one. Moreover, in powerful radio galaxies with one-sided jets, the depolarization is systematically stronger on the counter-jet side (Laing 1988). Garrington & Conway (1991) interpreted this effect as produced by an external halo of ionized gas (identified by the authors with the extended X-ray emission often observed in clusters). The depolarization asymmetry is a geometrical effect, due to the different column densities of hot gas that the radio emission from both sides has to cross, the counter-jet side being seen through a longer path length of gas.

When these asymmetries are present, we can readily distinguish which cone is closer *to the observer* and which one is further. However, it is not often easy to find these. For radio galaxies with no visible jets (or which are symmetric) or with the radio emission from both lobes too faint for the polarization to be measured, the distinction must be based on another strategy.

We have proposed a new method to solve this problem using the strong emission lines that are expected in the UV rest frame domain. Our models (Chapter 5) demonstrate that the line ratios involving resonance lines (like Ly α and CIV λ 1550) should be different on both sides of the nucleus, with the differences increasing with the inclination angle with respect to the plane of the sky. This suggested us a test to distinguish between the cone closest to the observer and the furthest one: the cone which emits the spectrum resembling our “back” clouds will be the nearest one, while the furthest one should emit line ratios more similar to our “front” models.

In this way, we expect to be able to describe the 3-dimensional structure of the objects. Furthermore, this will also help to understand some of the anisotropies that are observed in radio galaxies (some of them, in fact, expected from the unified schemes). For instance, the 3C256 radio galaxy (Dey, Spinrad & Dickinson 1995) has different levels of polarization in different regions. The optical images obtained with the Keck 10m telescope, show two clumps of emission in the south and a fainter more diffuse component extending to the north west. Both regions

Figure 33:
WFPC2 HST images of three high z radiogalaxies 3C265 ($z = 0.81$), 3C324 ($z = 1.21$), 3C368 ($z = 1.13$) (left to right). VLA data are superimposed on the images of 3C324 and 3C368. The alignment between the radio axis and the UV rest-frame structures is clear in these two cases. The radio axis is marked by lines in the case of 3C265. The rest-frame UV continuum of this object has an elongated morphology misaligned by about 35° from the radio axis.

have rather different polarization levels. As the authors suggest, maybe there is a different contribution of diluting radiation. However, we have to be careful with this interpretation. It could also be a geometrical effect. The cross sections for forward and backward scattering of dust grains are different. This means that the dust scattering produced in both cones (when they are not in the plane of the sky) is asymmetric, and, therefore, the relative polarization measured will also be different. I plan to develop this study in the near future.

McCarthy, van Breugel & Kapahi (1991) showed that in essentially all radio galaxies the extended optical line emission is brightest at the cone closest to *the nucleus*. The most plausible explanation that the authors propose is inhomogeneities in densities and distribution of dense clouds. which means that one of the cones is intrinsically brighter than the other. Assuming this to be the situation, in some cases, the brightest cone must be nearer *the observer* and in other cases, it will be further away. Therefore, (independently of which side is brighter) some objects can be expected to be dominated by a “back” type spectrum and others by a “front” type spectrum. We find that this effect could explain the high dispersion observed in the Ly α /CIV ratio in very powerful radio galaxies at very high z , while CIV/CIII remains nearly constant from one object to another.

As we see, there is evidence to support our view. A very strong test will be provided by spatially resolved UV spectroscopy of active galaxies with extended emission on both sides of the nucleus (objects devoid of any broad components will simplify enormously the study). The data that we have used for our modeling were extracted from the literature and correspond to high redshift radio galaxies where the spatial resolution is generally insufficient to separate clearly the extended from the nuclear emission. A project for the near future is to obtain long slit spectroscopy (UV rest frame) of high z radio galaxies with extended Ly α already reported in the literature and where other strong UV lines (like CIV, III and HeII) have also been detected. The aim is to analyze the spatial distribution of the different lines and how the line ratios vary on both sides of the nucleus. So far, the spectra have generally been presented in the literature with no spatial information, compressing the objects in the spatial direction. Moreover, there has not been an attempt to obtain narrow band image in other UV lines but Ly α . Quotient maps, like Ly α /CIV will describe the geometry of the ionized gas and will reveal regions of pure Ly α emission probably indicative of the existence of neutral hydrogen.

But, of course, the best tool for this research, available nowadays is the HST, that, with the Faint Object Spectrograph, makes possible UV spectroscopy at high spatial resolution for low z objects, where the distinction between the nuclear region and the extended ionized gas is much easier. This is one of the main goals of our HST project (section 6.6).

6.4 Our HST project

I have mentioned the HST project in which I am involved and which got observing time for the next observing cycle. I will describe it in more detail in this section.

We plan to obtain spatially resolved UV spectroscopy with the Faint Object Spectrograph (FOS) covering the observed frame Ly α -CIII] λ 1909, of four low z radio galaxies with clear extended emission line regions already observed from the ground in the optical spectral range. With the data to be obtained, we will apply our newly developed ultraviolet line diagnostic and should be able to describe the 3-dimensional geometry of the objects as well as study the dust effects on the measured lines. We will be able to distinguish between the material on the near and far side of the AGN and compare our results with other observed asymmetries (see section 6.4). The main goal is, therefore, to elucidate the nature of the geometrical effects which influence the line spectrum radiated by the “open geometry” (externally ionized clouds) that describe the EELRs.

In order to understand the nature of these objects, a clear separation between the different components contributing to the spectral energy distribution is needed: AGN + stars + scattered continuum + additional sources (like nebular continuum). There are many phenomena that are a direct, or indirect consequence of the AGN activity, like the extended scattered continuum or the line emission (both if the ionization is directly by the AGN or indirectly by shocks induced by the radio jet crossing the ISM). The study of these phenomena will provide information, not only on the AGN, but also on the stellar populations. Once we have a clear understanding of how the AGN influences its environment, it will be easier to separate the different components. What we learn will be very useful to interpret phenomena observed at very high z , where powerful radio galaxies are good laboratories to study the formation and early evolution of galaxies. So far, it has been very difficult to establish the state of evolution due to the difficulties in interpreting the observations with a non clear understanding of the AGN influence. If we knew the age of the oldest stars we could constrain the formation redshift and test even the current cosmological models.

When we were choosing our targets we searched for objects with known anisotropies and for which we could distinguish which cone is on the near or far side. This will provide a strong constraint to test the validity of the diagnostic method that we have proposed. A practical limitation appeared when we realized that not many objects exist in which the aforementioned distinction between cones has been possible. We looked for targets with a clear one-sided jet, indicative of the cone nearer to *the observer*. However, objects containing jets are rather better candidates of classes strongly influenced by shocks produced by the interaction of the said jet with the cooler gas of the galaxy, while our models are more appropriate and intended for objects where photoionization by the central AGN is (more clearly) the main ionization mechanism of the gas. Therefore, we decided

to prepare a more complete proposal which would allow us the study of both phenomena: the influence of geometry *and* the jet/cloud interaction. We chose one target (PKS2152-69) which presents clear evidence of interaction between the radio and optical plasmas. Moreover, we selected one source (PKS0349-27) which show EELR on both sides of the nucleus and with no evidences of shocks. A new UV line diagnosis to distinguish between shock and AGN photoionization will be developed. With our newly developed diagnostic method, we expect to infer important clues on the geometry of the ionized gas.

References

- Acosta-Pulido J.A., Vila-Vilaró B., Pérez-Fournón I., Wilson A.S., Tsvetanov Z.I., *Astrophys. J.*, 1996, *in press*
- Andreani P., La Franca F., Cristiani S., 1993, *Mon. Not. Roy Astr. Soc.*, , 261, L35
- Barthel P.D., 1989, *Astrophys. J.*, 336, 606
- Begelman M.C., Cioffe D., 1989, *Astrophys. J.*, 345, L21
- Binette L., Wilson S.W., Storchi-Bergmann T., *A&A*, *in press*
- Cimatti A., di Serego Alighieri S., Fosbury R.A.E., Salvati M., Taylor D., 1993, *Mon. Not. Roy Astr. Soc.*, 264, 421
- Cimatti A., di Serego Alighieri S., Field G.B., Fosbury R.A.E., 1994, *Astrophys. J.*, 422, 562
- Chambers K.C., McCarthy P.J, 1990, *Astrophys. J.*, 354 L9
- Chini R., Krügel E., 1994, *A&A*, 288, L33
- Dey A., Spinrad H., Dickinson M., 1995, *Astrophys. J.*, 440, 515
- de Young D.S., 1989, *Astrophys. J.*, 342, L59
- di Serego Alighieri S., Cimatti A., Fosbury R.A.E., 1994, *Astrophys. J.*, 431, 123
- di Serego Alighieri S., Cimatti A., Fosbury R.A.E., Pérez-Fournón, 1996, *Mon. Not. Roy Astr. Soc.*, *submitted*
- D'Odorico S., Cristiani S., Fontana A., Giallongo E., 1995, ESO PR 11/95; 15 Sept.
- Downes D., Radford S.J.E., Greve A., Thum C., Solomon P.M., Wink J.E., 1992, *Astrophys. J.*, , 398, L25
- Dunlop J.S., Hughes D.H., Rawlings S., Eales S.A., Ward M.J., 1994, *Nature*, 370, 347
- Eales S.A., Rawlings S., 1993, *Astrophys. J.*, 411, 67
- Eisenhardt P., Soifer B.T., Armus L., Hogg D., Neugebauer G., Werner M., 1995,

BAAS, 186, 5202

Elston R., McCarthy P.J., Eisenhardt P., Dickinson M., Spinrad H., Januzzi B.T., Maloney P., 1994, *Astron. J.* 107, 910

Garrington S.T., Conway R.G., 1991, *Mon. Not. Roy Astr. Soc.*, 250, 644

Goodrich R.W., Miller J.S., Martel A., Cohen M.H., Tran H.D., Ogle P.M., Vermeulen R.C., 1996, *Astrophys. J.*, 456 L9

Isaak K.G., McMahan R.G., Hills R.E., Withington S., 1994, *Mon. Not. Roy Astr. Soc.*, , 269, L28

Laing R.A., 1988, *Nature*, 331, 149

Lawrence A., Elvis M., 1982, *Astrophys. J.*, 256, 410

Lawrence A., 1987, *Pub. Astr. Soc. Pac.*, 99, 309

Lawrence A. et al., 1993, *Mon. Not. Roy Astr. Soc.*, 260, 28

Lilly S.J., 1988, *Astrophys. J.*, 333, 161

Lilly S.J., 1989, *Astrophys. J.*, 340, 77

Longair M.S., Best P.N., Röttgering H.J.A., 1995, *Mon. Not. Roy Astr. Soc.*, 275 L47

McCarthy P.J., van Breugel W.J.M., Kapahi V.K., 1991, *Astrophys. J.*, 371, 478

McCarthy P.J., Elston R., Eisenhardt P., 1992, *Astrophys. J.*, 387, L29

McCarthy P.J., 1993, *ARA&A* 31, 639

Macchetto F.D., Lipari S., Giavalisco M., Turnshek D.A., Sparks W.B., 1993, *Astrophys. J.*, , 404, 511

McMahon R.G., Omont A., Bergeron J., Kreysa E., Haslam C.G.T., 1993, *Mon. Not. Roy Astr. Soc.*, 267, L9

Prieto A., Walsh J., Fosbruy R.A.E., di Serego Alighieri S., 1993, *Mon. Not. Roy Astr. Soc.*, 263, 10p

Prieto A., Freudling W., 1993, *Astrophys. J.*, 416 668

Rees M.J., 1987, *Mon. Not. Roy Astr. Soc.*, 239, 1p

Robinson A., Binette L., Fosbury R.A.E., Tadhunter C.N., 1987, *Mon. Not. Roy Astr. Soc.*, 227, 97 (RBFT87)

Serjeant S., Lacy M., Rawlings L.J., King L.J., Clements D.L., 1995, *Mon. Not. Roy Astr. Soc.*, 276, L31

Stapelheldt K.R. et al., 1995, *BAAS*, 185, 1802

Tadhunter C., Tsvetanov Z., 1989, *Nature*, 341, 422

Tadhunter C., Shaw M., Clark N., Morganti R., 1994, *A&A*, 288, L21

van Ojik R., 1995, Ph.D.thesis, Rijksuniversiteit te Leiden

Viegas S.M., Prieto A., 1992, *Mon. Not. Roy Astr. Soc.*, 258, 483

Villar-Martín, 1993, Proyecto de tesis: “Influencia del polvo en modelos de fotoionización aplicados a núcleos activos de Galaxias”. Ito. de Astrofísica de Canarias y Universidad de La Laguna.

Villar-Martín M., Binette L. & Fosbury R.A.E, 1995, in Proc. for the Workshop ”Cold Gas at high z ”, Hoogeveen, August 1995 (in press)

Wilson A.S., Ward M.J., Haniff C.A., 1988, *Astrophys. J.*, 334, 121

Wilson A.S., Braatz J.A., Heckman H.M., Krolik J.H., Miley G.K., 1993, *Astrophys. J.*, , 419, 61

Wilson A.S., Tsvetanov Z., 1994, *Astron. J.* , 107, 1227

Chapter 7

Conclusions

We have considered for the first time the combined effects of geometrical perspective and dust on the narrow emission line spectra of active galaxies. This is necessary to make a more correct interpretation of the observations. The kind of geometry determines strong differences on the emission line ratios when dust is present, due to the much more destructive effects of dust when we approach a close (spheric) geometry. Moreover, when we study the line emission from the EELRs or objects dominated by such extended emission, the influence of perspective must be considered if resonant lines are involved, both if dust is or is not present. In general the ionized cones have an inclination angle with respect the plane of the sky, which results on different viewing perspectives for both cones. This implies strong asymmetries on the UV line ratios of regions at both sides of the nucleus, due to the resonant character of Ly α and CIV and therefore, their strong dependence on perspective.

We have demonstrated that the NLR HI line ratios of Seyfert 2 galaxies points towards a significantly self-covered distribution of gas mixed with dust which is very patchy. The combination of line scattering and dust absorption effects can explain the observed ratios. Therefore, for those objects where the line emission is dominated by the unresolved Narrow Line Region, a more close geometry than previously assumed is appropriate. On the other hand, when the extended emission is dominant (EELR), an open geometry is more realistic. If such close geometry is valid for the NLR, we expect the central continuum source to be also reddened. We claim that the apparent deficit of ionizing photons seen in many Seyfert 2's could in part be due to dust extinction of the ionizing continuum, and not only to the presence of a circumnuclear torus that collimates the ionization radiation along its axis, as proposed by other authors.

Our studies on the UV emission line spectra of high z radio galaxies demonstrate that the UV line ratios are strongly determined by geometrical perspective, rather than dust effects. Internal dust, even in proportions as large as that found in the solar neighbourhood, can not explain the UV line ratios measured for high z radio galaxies, unless perspective effects are taken into account.

We claim that Ly α is not a good indicator of dust but rather a good tool to understand the geometry of the emitting gas. Moreover, the influence of geometrical factors could give a natural explanation for some of the emission line asymmetries seen in the ‘alignment effect’ radio galaxies. The reflection of Ly α photons by neutral material can determine the morphology of the object in the light of Ly α . We suggest that the diffuse Ly α halos observed in some high z radio galaxies could be due to the reflection of Ly α photons by clumps lying outside the ionization cones.

We have demonstrated that the gas in Extended Emission Line Regions in low z radio galaxies is mixed with dust. The faintness of the [CaII] $\lambda\lambda$ 7291,7324 lines indicates that calcium is depleted onto dust grains. We have used this result to discriminate among the current theories about the origin of the extended ionized gas. If there is an universal origin, the existence of internal dust favours debris from mergers or tidal interactions as the most plausible scenario.

Apendix A

Binette, Wang, Villar-Martín, Martín & Magris 1993, ApJ, 414, 535

The term depletion refers to the underabundance of gas phase elements with respect to the solar standard abundances as a result of their assumed presence in dust. References to the studies of depletion in the local ISM can be found in Whittet (1992). We describe here a *theoretical* algorithm which attempts to deplete in a meaningful way the trace element abundances when computing line diagnostic for a plasma of arbitrary *gas* metallicity Z_{gas} and dust content μ . Both quantities Z_{gas} and μ ($\propto Z_{dust}$; see eq.[A5]) are known to depart significantly from solar neighborhood values in low-mass extragalactic systems or as a function of galactic radius in the Galaxy. For the purpose of modeling plasma conditions in a nonsolar environment, we defined an algorithm which scales in a self-consistent manner the depletion of the gas phase in proportion to the quotient μ/Z , where Z is the *total* metallicity of the plasma ($Z = Z_{dust} + Z_{gas}$) expressed *relative* to local ISM values:

$$Z = \frac{\sum m_X(\{n_X\}_{dust} + \{n_X\}_{gas})_{plasma}}{\sum m_X\{n_X\}_{\odot}}, \quad [A1]$$

and μ is the dust content of the plasma expressed *relative* to that of the standard ISM dust-to-gas mass ratio. The reference solar abundances set which we adopt is taken from the compilation of Anders & Greveese (1989) and is listed in Table 4 (see entry $\{n_X\}/\{n_H\}_{\odot}$). We define $D(X)$, the depletion index of element X, as

$$D(X) = \left[\frac{X}{H}\right] = \log\left\{\frac{n_X L}{n_H L}\right\}_{ISM} - \log\left\{\frac{n_X}{n_H}\right\}_{\odot} \quad [A2]$$

where $\{n_X L/n_H L\}_{ISM}$ represents the ratio of the column densities of the gaseous element X (measured along various lines of sight of path length $L[\leq 6 \times 10^{20}$ cm]) over the corresponding measured column densities of H. In the local ISM, the number density of atoms n_X of element X which are found either in gas form (or depleted into dust grains) is given relative to n_H by $\{n_X/n_H\}_{\odot} 10^{D(X)}$ (or $\{n_X/n_H\}_{\odot}(1 - 10^{D(X)})$). The adopted set of local ISM depletion indices $D(X)$ is listed in Table A1 and was derived from Table 2.2 of Whittet (1992) except for carbon for which the value -0.5 was adopted as suggested by some authors. This value is also consistent with our dust model which includes graphite grains.

For the local ISM, for which $\mu \equiv 1$ (and $Z = Z_{dust} + Z_{gas} = 1$), the gas phase abundances are derived directly from the depletion indices of Table A1. As we are often interested in modeling line emission plasma with $Z \neq 1$, we could assume

Table 4: Solar Abundances, ISM Depletion Indices and Correlation Coefficient Ratios.

Element	$\{n_X/n_H\}_\odot$	$D(X)_{ISM}$	$\{r_n/r_N\}_X^{ISM}$
H	1.000
He	0.1	0.0	...
C	3.6×10^{-4}	-0.5	0.88
N	1.1×10^{-4}	-0.1	0.46
O	8.5×10^{-4}	-0.2	0.42
Ne	1.2×10^{-4}	0.0	...
Mg	3.8×10^{-5}	-0.7	1.11
Si	3.5×10^{-5}	-1.6	1.19
S	1.9×10^{-5}	-0.2	0.94
Ar	3.6×10^{-6}	0.0	...
Ca	2.2×10^{-6}	-3.7	1.42

that the dust content μ scales linearly with Z . That this is approximately true is supported by the results of Issa, MacLaren, & Wolfendale (1990) and Sauvage & Vigroux (1991) who compared the metallicity and extinction in the Galaxy with those of the Magellanic Clouds or of nearby spirals. In our calculations, if we adjusted the dust content such that always $\mu/Z = 1$, assuming that the depletion indices of Table A1 remain approximately valid, the procedure for depletion is straightforward and the gas phase abundance by number of element X is simply given by

$$\{n_X/n_H\}_{gas} = Z\{n_X/n_H\}_\odot 10^{D(X)}, \quad [A3]$$

This is equivalent to saying that when $\mu/Z = 1$ both the dust grains as well as the gas phase are made up of the same relative proportion of trace elements.

For the more general case where $\mu \neq Z$, we have no observational basis as to how the depletion indices might vary. If we use the local ISM indices as a guess of the depleted abundances, and then simply renormalize the whole abundance set by a constant factor until the depleted mass match the value implied by μ (see. eq. [A5] below), we obtain, in the case $\mu \ll Z$, rather implausible gas abundances for some elements. To alleviate this problem, we have chosen instead to vary the depletion indices in some proportion to the ratio μ/Z before linearly renormalizing the total mass of the depleted metals. An indication of the relative variation of the depletion indices $D(X)$ with the ratio μ/Z can be intuitively inferred from the measured quantities $\{r_n/r_N\}_X^{ISM}$ which represents the ratio for element X of the correlation coefficient of $D(X)$ with density, r_n , over the correlation coefficient of $D(X)$ with column density, r_N . The merits of the measured $\{r_n/r_N\}_X^{ISM}$ ratios is that they sample regions of somewhat different dust content μ . The algorithm we devised for each case $\mu \neq Z$ is the following: we first define modified depletion indices $D(X, \mu/Z)$ which are dependent on μ/Z as follows

$$D(X, \mu/Z)' = D(X) \left(\frac{\mu}{Z}\right)^{\gamma \{r_n/r_N\}^X}, \quad [A4]$$

By trial and error, we established that $\gamma = 0.25$ gave a reasonable behaviour of the depleted elements even when $\mu/Z \rightarrow 0$. The values we adopted for $\{r_n/r_N\}_X^{ISM}$ (see Table 4) were derived from Figure 2.9 of Whittet (1992). Linear renormalization of the abundances implied by the modified indices $D(X, \mu/Z')$ is required in order that the mass of the elements depleted onto dust grain remains consistent with the value of μ . This is done in an iterative fashion by determining the value of $\delta (\approx 1)$ until the following dust mass equation is satisfied

$$Z_{dust} \sum m_X \{n_X\}_\odot = 0.0089 \mu \frac{m_H \{n_H\}}{\sum m_X \{n_X\}} =$$

$$Z \sum \left\{ \frac{m_X n_X}{m_H n_H} \right\}_\odot [1 - \kappa \min(1, \delta 10^{D(X, \mu/Z')})], \quad [A5]$$

where the constant 0.0089 represents the dust-to-gas mass ratio relative to H (i.e., ρ_{dust}/ρ_H) of any of the extinction curves computed by P.G. Martin (this number is consistent with the ISM value if our dust composition within the grain model is valid). The constant $\kappa = 1.123$ is a small correcting factor to allow for the fact that the summation is limited to the elements of Table 4 (considered by MAPPINGS) which does not include all the depleted elements (e.g., Fe). Once δ is determined, the gas phase abundance of any element X is

$$\{n_X/n_H\}_{Z, \mu}^{gas} = Z \{n_X/n_H\}_\odot \min(1, \delta 10^{D(X, \mu/Z')}), \quad [A6]$$

The value of κ is such that δ becomes unity if $\mu/Z = 1$ in which case equation (A5) reduces to equation (A3). With the above depletion algorithm, as $\mu/Z \rightarrow 0$, the uncertainty in the absolute abundances of the highly depleted elements (e.g., Ca) is probably quite high but since no observational depletion data for $\mu/Z \ll 1$ is available, this situation cannot be helped. The main purpose of our algorithm was that it gave a cumulative depletion of the gas phase elements always consistent with the dust content μ . Furthermore, as $\mu/Z \rightarrow 0$ it also has the property of giving for *all* the elements concerned much more plausible values than any alternative linear scheme which we could devise. The need for a depletion algorithm even if imperfect is called for in any photoionized gas model since it is quite conceivable that the dust content is lower than in the ISM as a result of destruction of dust grains by sputtering (although the timescales are relatively long compared to the lifetime of an HII region; see Osterbrock 1989) or as a result of segregative acceleration away from the cloud of much of the smaller grains' population due to radiation pressure.

References

- Anders E., Grevesse N., 1989, *Geochim. Cosmochim. Acta*, 53, 197
- Issa M.R., MacLaren I., Wolfendale, A.W., 1990, *A&A*, 236, 237
- Osterbrock D.E., 1989, *Astrophysics of Gaseous Nebulae and Active Galactic Nuclei* (Mill Valley: University Science Books)
- Sauvage M., Vigroux L., 1991, in *IAU Symp. 148, The Magellanic Clouds*, ed. R. Haynes & D. Milne (Dordrecht: Kluwer), 407
- Whittet D.C.B., 1992, *Dust in the Galactic Environment* (Bristol:IOP)

Appendix B

Binette, Wang, Villar-Martín, Martín & Magris 1993, ApJ, 414, 535

1. CALCULATIONS OF N_{HI}^{critic}

We assume a slab geometry for the screen. For an isothermal screen with HI column density N_{HI}^{screen} , the optical depth for Ly α resonant scattering is

$$\tau(x) = N_{HI}^{screen} \sigma_0(T) \phi(x), \quad [B1]$$

where $x = (\omega - \omega_0) \omega_D$, $\sigma_0(T) \phi(x)$ is the thermally averaged resonant scattering cross section,

$$\sigma_0(T) = 5.9 \times 10^{-14} (T/10^4 K)^{-1/2} \text{ cm}^{-2}, \quad [B2]$$

$$\phi(x) = \frac{a}{\pi} \int_{-\infty}^{+\infty} \frac{e^{-y^2} dy}{a^2 + (x - y)^2}, \quad [B3]$$

$a = \Gamma/2\omega_D = 4.7 \times 10^{-4} (T/10^4 K)^{-1/2}$ is the damping constant with Γ^{-1} the radiative lifetime of the excited state, and $\omega_D = \omega_0 (2\kappa_B T/m_H c^2)^{-1/2}$ is the thermal Doppler width with $\omega_0/2\pi = 2.47 \times 10^{15}$ Hz the line center (Ly α frequency (Bonilha et al. 1979). For photons of frequency ω_i and direction cosine \mathbf{n}_i injected into a screen moving at velocity \mathbf{v} , we evaluate the optical depth (a Lorentz scalar) in the cloud (comoving) frame to obtain

$$\tau(\omega_{cloud}) = N_{HI}^{screen} \sigma_0(T) \phi(\omega_{cloud}, T), \quad [B4]$$

where $\omega_{cloud} = \gamma \omega_i (1 - \mathbf{v} \cdot \mathbf{n})$ and $\gamma = (1 - v^2)^{-1/2}$. For line center injection, $\omega_i = \omega_0$, and the column density at which $\tau(\omega_{cloud}) = 1$, N_{HI}^{crit} , is given by

$$N_{HI}^{crit} = \frac{1}{\sigma_0(T) \phi(\omega_{cloud}, T)} = N_{HI}^{crit}(v). \quad [B5]$$

2. CALCULATIONS OF f

Let $N(x)$ be the flux of Ly α photons impinging on a screen which we model as a plane parallel slab. The width of the impinging line feature is δV_s (in km s $^{-1}$ so that $x = (\omega - \omega_0)/(\omega \delta V_s)$). Let the width of the Ly α resonant scattering line profile in the screen be given by δV_a (in km s $^{-1}$). The probability that a line photon will suffer an interaction when traversing the screen is $1 - e^{-\tau(x')}$, where $\tau(x')$ is given

by equation (B1), and $x' = (\omega - \omega_0)/(\omega_0\delta V_a) = \kappa x$ with $\kappa \equiv V_s/\delta V_a$. The fraction of Ly α photons that suffer interactions when traversing the screen is then

$$f = \frac{\int_{-\infty}^{+\infty} dx N(x) [1 - e^{-\tau(x')}]}{\int_{-\infty}^{+\infty} dx N(x)} = f(N_{HI}^{screen}, \kappa). \quad [B6]$$

Taking $N(x) \propto e^{-x^2}$ gives

$$f = \pi^{-1/2} \int_{-\infty}^{+\infty} dx e^{-x^2} [1 - e^{-\tau(x')}] \quad [B7]$$

Equation (B6) also gives the fraction of the impinging Ly α energy flux that interacts with the HI gas in the screen since the impinging energy flux of Ly α is approximately $\hbar\omega_0 N(x)$.

References

Bonilha J.R.M., Ferch R., Salpeter E.E., Slater G., Noerdlinger P.D., 1979, *Astrophys. J.*, 233, 649

Appendix C

Binette, Wang, Villar-Martín, Martín & Magris 1993, ApJ, 414, 535

The transfer of the UV continuum across an arbitrary thick slab of dust which is discussed in §2.4.4 was carried out using the numerical solution described in detail by Magris (1985; see also Bruzual et al. 1988). Let us consider an arbitrary frequency with its corresponding absorption (σ_{abs}) and scattering (σ_{sca}) dust cross sections. We are interested in solving the following transfer equation

$$\mu \frac{dI(\tau, \mu)}{d\tau} = I(\tau, \mu) - S^S(\tau, \mu), \quad [C1]$$

where $d\tau = (\sigma_{sca} + \sigma_{abs})dx$ is the differential optical depth of the medium. This equation which takes into account scattering as well as absorption by homogeneously distributed dust particles is appropriate to the plane parallel geometry case. The scattering source function due to the dust grains is given by

$$S^S = \frac{a}{4\pi} \int I(\tau, \mu) - S^S(\tau, \mu), \quad [C2]$$

where $a = \sigma_{sca}/(\sigma_{sca} + \sigma_{abs})$ is the albedo and $\Phi(\theta) = (1 - g^2)/(1 + g^2 - 2g \cos\theta)^{3/2}$ is the scattering phase function. The phase function is characterized by the asymmetry parameter $g = \langle \cos\theta \rangle$ with θ the scattering angle and g the Henyey-Greenstein asymmetry parameter characterizing our dust grain models and tabulated by P.G.Martin as a function of frequency along with σ_{abs} and σ_{sca} (see grain model in Martin & Rouleau 1991). The transfer equation was solved by using the finite difference solution method of Milkey, Shine, & Mihalas (1975) with the following boundary conditions:

$$I(\tau, \mu) = 0 \quad \text{for} \quad \tau = 0, \quad \mu < 0 \quad [C3]$$

$$I(\tau, \mu) = I_c \quad \text{for} \quad \tau = T_{ext}, \quad \mu > 0,$$

where T_{ext} is the optical depth of the slab and I_c is the intensity of the incident continuum radiation which illuminates *isotropically* one side of the dust slab. To obtain the numerical solution, we use a logarithmically uniform mesh that is symmetric about slab points. In order to test the accuracy of our numerical solution, we have compared our results with the analytical solution of Roberge (1983). In particular, we could reproduce very well the behavior of the mean intensity versus optical depth inside the slab when illuminated isotropically on both surfaces.

References

- Bruzual A., Magris C.M., Calvet N., 1988, *Astrophys. J.*, 333, 673
- Magris C.G, 1985, in senior physics thesis, Universidad Simón Bolívar and CIDA, Venezuela
- Martin P.G., Rouleau F., 1991, in Extreme Ultraviolet Astronomy, ed. R.F. Malina & S. Bowyer (Oxford: Pergamon), 341
- Milkey R.W., Shine R.A., Mihalas D., 1975, *Astrophys. J.*, 202, 250
- Roberge W.G., 1983, *Astrophys. J.*, 275, 292

Apendix D

Villar-Martín & Binette 1995, A&A, in press

By comparing the estimated photoionization rates from the excited level 3d of Ca^{+*} , Π_{3d} , to that from the ground state 4s of Ca^+ , Π_{4s} , we show that photoionization of excited Ca^{+*} is a negligible process.

A fundamental parameter which determines the importance of the ionization rate from the metastable level is its relative population with respect to the ground state: $\frac{n_{3d}}{n_{4s}}$, being n_{4s} the density of Ca^+ ions in the ground level and n_{3d} the density of Ca^+ ions in the metastable level, 3d. To evaluate this fraction, we have solved analytically the statistical equilibrium equations. To simplify the calculations we have considered a three level atom, reducing the two 4p sublevels (see Fig. 16, Chapter 3) to a single level and the same for the 3p sublevels. We have taken into account all the processes (collisional and radiative) which can populate or depopulate each of the levels.

The resolution of the system of three equations gives us the ratios $\frac{n_L}{n_{\text{Ca}^+}}$, with $L=3d,4s,4p$, being n_{Ca^+} the total density of Ca^+ ions. The density and temperature we considered were 300cm^{-3} and 10000K , respectively. From this we deduced the relative population with respect the ground state. The results turn out to be:

$$\frac{n_{3d}}{n_{4s}} \sim 10^{-7}$$

and

$$\frac{n_{4p}}{n_{4s}} \sim 0$$

The negligible population of the upper 4p level prevents any contribution by cascade to the population of the 3d level, therefore collisional excitation is the only important mechanism populating the metastable 3d level. This is consistent with the fact that we do not observe the triplet of Ca^+ (8498,8542,8662) (4p to 4s) in any EELR although it is observed in the broad line region of AGN where densities are higher by many order of magnitudes.

a) Ionization of Ca^{+*} by soft continuum photons.

The soft UV counterpart of the ionizing continuum provides a source of ionization for both Ca^+ (IP: 11.9eV) and Ca^{+*} (IP: 10.2eV). To estimate the photoionization rates, we will make the following approximations:

1) At the fairly large depth in the cloud where the specie Ca^+ becomes abundant, we only need to consider photons with energies $< 13.6\text{eV}$, the ionization potential (IP) of H^0 , because photons just above this energy have already been absorbed

and also because of the rapid decrease of the photoionization cross section with increasing energies.

2) The ionizing continuum which reaches the PIZ is considered to be the soft UV counterpart of an ionizing PL of index -1.4 (but unattenuated since the opacity due to dust or trace elements below 13.6eV is relatively small). The continuum impinging the cloud is described by $F_\nu = F_s \nu^{-1.4}$. In number of photons this is $F_\nu/h\nu = F_s/h\nu^{-2.4}$. The constants F_s/h will cancel out when taking the ratio Π_{3d}/Π_{4s} .

The atomic data was taken from Osterbrock (1987) for H^0 and from Shine & Linsky (1975) for Ca^+ and Ca^{+*} . Tables 1, 2, 3 where we define $a'_\nu = a_\nu * 10^{18}$ and $\nu' = \nu/10^{16}$ show the relevant atomic data. The threshold ionizing frequency of H^0 is labeled ν_0 .

We estimate the quotient Π_{3d}/Π_{4s} as follows:

$$\frac{\Pi_{3d}}{\Pi_{4s}} = \frac{n_{3d} \nu_{3d} \int_{\nu_0}^{\nu_0} \nu^{-2.4} a_\nu(Ca^{+*}) d\nu}{n_{4s} \int_{\nu_{4s}}^{\nu_0} \nu^{-2.4} a_\nu(Ca^+) d\nu}, \quad [D1]$$

If we define $a'_\nu = a_\nu * 10^{18}$ and $\nu' = \nu/10^{16}$, we have

$$\begin{aligned} \frac{\Pi_{3d}}{\Pi_{4s}} &= \frac{n_{3d} \nu'_{3d} \int_{\nu'_0}^{\nu'_0} \nu'^{-2.4} a'_\nu(Ca^{+*}) d\nu'}{n_{4s} \int_{\nu'_{4s}}^{\nu'_0} \nu'^{-2.4} a'_\nu(Ca^+) d\nu'} \\ &= \frac{n_{3d} I_1}{n_{4s} I_2}, \quad [D2] \end{aligned}$$

The values of $a'_\nu(Ca^{+*})$ at ν'_0, ν'_{4s} and $a'_\nu(Ca^+)$ at ν'_0 and ν'_{4s} have been obtained by interpolation from (see Tables 2 and 3). Using the rule of the rectangle to approximate a given integral:

$$\begin{aligned} \int_{x_0}^{x_1} f(x) dx &\sim (x_1 - x_0) f(x_0) + (x_2 - x_1) f(x_1) + \dots \\ &\quad + (x_n - x_{n-1}) f(x_{n-1}) \end{aligned}$$

[D2] reduces to

$$\frac{\Pi_{3d}}{\Pi_{4s}} \sim \frac{n_{3d}}{n_{4s}} \frac{10.06}{0.156}, \quad [D3]$$

If we take into account that $\frac{n_{3d}}{n_{4s}} \sim 10^{-7}$ we obtain

Table 5: H^0 photoionization cross section

ν'	$a'_\nu(H^0)$	$\nu'^{-2.4}a'_\nu(H^0)$
0.3	6.4	115.1
0.4	2.5	22.54
0.6	1.15	3.919
0.8	0.6	1.025
1	0.3	0.3
1.2	0.2	0.1291
1.4	0.15	0.06689
1.6	0.1	0.03237
1.8	0.07	0.01708
2	0.05	0.009473
2.2	0.04	0.006029
2.4	0.03	0.00367
2.6	0.02	0.002019
2.8	0.015	0.001267
3	0.015	0.001074
3.2	0.01	0.0006133
3.4	0.01	0.0005302
3.6	0.01	0.0004622

$$\frac{\Pi_{3d}}{\Pi_{4s}} \sim 6 \times 10^{-6}$$

which means that the ionization of Ca^+ into Ca^{++} originates overwhelmingly from the ground level 4s.

b) Ionization of Ca^{+*} by $\text{Ly}\alpha$ photons.

$\text{Ly}\alpha$ photons have energies slightly higher than the treshold energy of level 3d of Ca^{+*} and constitute undoubtedly an important source of ionization for this level. To compute the $\text{Ly}\alpha$ emissivity, we assume the low density regime whereby $\simeq \frac{2}{3}$ of recombinations of H^+ lead to the emission of a $\text{Ly}\alpha$ photon. Since $\text{Ly}\alpha$ is a resonance line of large line scattering opacity, we consider that the density of $\text{Ly}\alpha$ photons within the Ca^+ region result from the production of $\text{Ly}\alpha$ either locally or from *deeper* regions. The justification for this is that resonance line photons generated from layers nearer the slab's surface would be reflected outward as a result of the increasing fraction of H^0 with depth (see Binette et al 1993b). Therefore the $\text{Ly}\alpha$ flux potentially available to ionize level 3d is a small fraction η of the total $\text{Ly}\alpha$ flux emitted by the cloud. This fraction is of order 0.2 corresponding to the fraction of ionizing photons of H^0 *not yet* absorbed at the typical depth where the Ca^+ specie is abundant.

We first compute the $\Pi_{3d}^{\text{Ly}\alpha}/\Pi_{4s}$ ratio taking into account that resonance scattering will increase the density of locally emitted line photons by a factor $\xi \sim 10^7$,

Table 6: Ca⁺ 4s photoionization cross section

$\lambda(\text{\AA})$	ν'	$a'_\nu(\text{Ca}^+)$	$\nu'^{-2.4}a'_\nu(\text{Ca}^+)$
1044	0.2873 (ν'_{4s})	0.2036	4.063
1000	0.3	0.2097	3.772
950	0.3158	0.2145	3.412
	0.3288 (ν'_0)	0.2157	3.114
900	0.3333	0.2170	3.031
850	0.3529	0.2172	2.644
800	0.375	0.2149	2.262
750	0.4	0.2103	1.896
700	0.4286	0.2033	1.554
650	0.4615	0.1942	1.242
600	0.5	0.1830	0.966
550	0.5455	0.1700	0.7282
500	0.6	0.1554	0.5295
450	0.6667	0.1394	0.369
400	0.75	0.1225	0.2443
350	0.8571	0.1049	0.1518
300	1	0.0870	0.08697
250	1.2	0.0691	0.0440
200	1.5	0.0519	0.0199
150	2	0.0352	0.00668
100	3	0.0199	0.001417
50	6	0.0198	0.0002685

Table 7: Ca⁺⁺ 3d photoionization cross section

$\lambda(\text{\AA})$	ν'	$a'_\nu(\text{Ca}^{++})$	$\nu'^{-2.4}a'_\nu(\text{Ca}^{++})$
1218	0.2462 (ν'_{3d})	6.148	177.70
1200	0.25	6.086	169.50
1150	0.2609	5.907	148.60
1100	0.2727	5.716	129.20
1050	0.2857	5.511	111.4
1044	0.2873 (ν'_{4s})	5.403	107.80
1000	0.3	5.295	95.22
950	0.3158	5.066	80.56
	0.3288 (ν'_0)	4.9465	71.39
900	0.3333	4.827	67.41
850	0.3529	4.576	55.72
800	0.375	4.315	45.43
750	0.4	4.044	36.46
700	0.4286	3.762	28.74
650	0.4615	3.47	22.19
600	0.5	3.168	16.72
550	0.5455	2.856	12.23
500	0.6	2.534	8.634
450	0.6667	2.202	5.827
400	0.75	1.862	3.714
350	0.8571	1.517	2.196
300	1	1.173	1.173
250	1.2	0.8424	0.5439
200	1.5	0.5401	0.2041
150	2	0.2865	0.05428
100	3	0.1051	0.007524
50	6	0.01471	0.0001995

the mean number of scatterings before escape. Such a high number of line scattering, however, characterizes only the locally produced Ly α photons. This accumulation (or slowing down) effect which we want to estimate is only effective within a zone of optical depth of order a few. Let's take $\tau_{scat} \sim 10 = \sigma_{scat} n(H^0) \delta X$ where δX is the geometrical depth and $n(H^0)$ the local density of H^0 . Adopting $\sigma_{scat} \simeq 6 \times 10^{-14} \text{cm}^2$ (cf Appendix B of Binette et al 1993b), the column density of recombining H^+ we should consider in generating Ly α is within a thickness $N(H^+) \sim N(H^0) = n(H^0) \delta X = 10/6 \times 10^{-14} = 1.7 \times 10^{14} \text{cm}^{-2}$.

Taking these considerations into account, the problem reduces to estimating the quotient

$$\begin{aligned} \frac{\Pi_{3d}^{Ly\alpha}}{\Pi_{4s}} &= \frac{n_{3d}}{n_{4s}} \frac{\frac{2}{3} \eta \xi a_{Ly\alpha}(Ca^{+*}) N(H^+) \int_{\nu'_0}^{\infty} \nu'^{-2.4} a'_{\nu}(H^0) d\nu'}{\int_{\nu'_{4s}}^{\nu'_0} \nu'^{-2.4} a'_{\nu}(Ca^+) d\nu'} \\ &= \frac{n_{3d}}{n_{4s}} \frac{2}{3} \eta \xi a_{Ly\alpha}(Ca^{+*}) N(H^+), \frac{I_3}{I_2} \quad [D4] \end{aligned}$$

where $a_{Ly\alpha}(Ca^{+*})$ is the photoionization cross section of Ca^{+*} at the Ly α energy ($\simeq 6 \times 10^{-18} \text{cm}^2$). Taking again $n_{3d}/n_{4s} \sim 10^{-7}$, we obtain

$$\frac{\Pi_{3d}^{Ly\alpha}}{\Pi_{4s}} \sim 1.36 \times 10^{-4} \frac{I_3}{I_2}, \quad [D5]$$

Using again the rule of the rectangle we obtain

$$\frac{\Pi_{3d}^{Ly\alpha}}{\Pi_{4s}} \sim 1.5 \times 10^{-2}.$$

The effect of slowing down of resonance line photons is interesting but appears insufficient as it involves too small a fraction of the Ly α photons generated within the nebula. Let's now estimate the importance of all the Ly α photons generated within the deeper zones which, after having scattered far enough in frequency to escape, must still cross the Ca^+ zone (without appreciable scattering in that zone). The effect on the photoionization of level 3d is given in this case by

$$\begin{aligned} \frac{\Pi_{3d}^{Ly\alpha}}{\Pi_{4s}} &= \frac{n_{3d}}{n_{4s}} \frac{\frac{2}{3} \eta a'_{Ly\alpha}(Ca^{+*}) \int_{\nu'_0}^{\infty} \nu'^{-2.4} d\nu'}{\int_{\nu'_{4s}}^{\nu'_0} \nu'^{-2.4} a'_{\nu}(Ca^+) d\nu'}, \quad [D6] \\ &= \frac{n_{3d}}{n_{4s}} \frac{2}{3} \eta a'_{Ly\alpha}(Ca^{+*}) \frac{I_4}{I_2} \quad [D7] \end{aligned}$$

(Note that a' is used here for Ca^{+*}). Using the rule of the rectangle we obtain

$$\frac{\Pi_{3d}^{Ly\alpha}}{\Pi_{4s}} \sim 2.43 \times 10^{-6}$$

In summary, Ly α emission and/or trapping are insufficient to ionize Ca⁺. As in the case of soft continuum photons, this is basically the result of the extremely small population characterizing the excited level 3d.

References

Roberge W.G., 1983, *Astrophys. J.*, 275, 292

Acknowledgements

I want to express my gratitude to Luc Binette, that, just a few months ago, became co-director of this thesis, because during these years he has oriented my thesis, sharing his knowledge and rigorous scientific method. Thanks to Bob Fosbury, my local supervisor at the ST-ECF (Space Telescope European Coordinating Facility, Garching-Germany) for his scientific support. I learned with him that the apparent complication of the Universe, is often the result of our too difficult questions. To Ismael Pérez, Reynier Pelletier y Jose Acosta who helped me with very constructive scientific discussions.

Very specially, thanks to my parents and sisters, who have always helped me to advance in my work with their permanent support. Also to Jacco van Loon because he has contributed so much to my professional and personal development, in the bad and good moments. And a special gratitude to Jesús A. Rodríguez (European Southern Observatory), who has supported me and followed step by step the evolution of my career towards the doctorate.

I want to thank the Deutsche-Forschung Gemeinschaft (DFG) for the grant I enjoyed during these years. Also, to the ST-ECF group that supported me, not only with money and computer facilities, but also with helpful scientific advices. Thanks to the Instituto de Astrofísica de Canarias (IAC, Tenerife-Spain) which provided me with appropriate tools to work in all my visits.

Agradecimientos

Quiero expresar mi agradecimiento a Luc Binette, que se convirtió en co-director de esta tesis hace tan sólo unos meses, porque durante estos años ha orientado mi trabajo, compartiendo sus conocimientos y su método científico riguroso. Gracias también a Bob Fosbury, mi supervisor en el ST-ECF (Space Telescope European Coordinating Facility, Garching-Germany), por su apoyo científico. Con él he aprendido que la complicación aparente del Universo es a menudo el resultado de nuestras preguntas demasiado difíciles. A Ismael Pérez, Reynier Pelletier y Jose Acosta que me ayudaron con discusiones científicas muy constructivas.

Muy especialmente, agradezco a mis padres y hermanas, que han empujado mi trabajo con su apoyo permanente. También a Jacco van Loon que tanto me ha aportado profesional y personalmente, en los malos y los buenos momentos. Y un agradecimiento especial a Jesús A. Rodríguez (European Southern Observatory) que me ha apoyado y ha seguido paso a paso la evolución de mi carrera hacia el doctorado.

Agradezco a la Deutsche-Forschung Gemeinschaft (DFG) por la beca que he disfrutado estos años. También al grupo ST-ECF que me proporcionó facilidades económicas y de ordenadores, así como útiles consejos para avanzar en mi trabajo. Agradezco al Itto. de Astrofísica de Canarias (IAC, Tenerife-Spain), que en mis visitas me proporcionó siempre medios adecuados para trabajar.

This figure "hst3c.jpeg" is available in "jpeg" format from:

<http://arxiv.org/ps/astro-ph/9605139v1>

This figure "jets.jpeg" is available in "jpeg" format from:

<http://arxiv.org/ps/astro-ph/9605139v1>

This figure "ngc5728.jpeg" is available in "jpeg" format from:

<http://arxiv.org/ps/astro-ph/9605139v1>